A NOVEL DIGITAL MICROMIRROR SPECTROMETER, SILANE EMISSION SPECTROMETRY IN A GLOW DISCHARGE, AND LASER EXCITED ATOMIC FLUORESCENCE SPECTROSCOPY

BY

EUGENE PAUL WAGNER II

A DISSERTATION PRESENTED TO THE GRADUATE SCHOOL
OF THE UNIVERSITY OF FLORIDA IN PARTIAL FULFILLMENT
OF THE REQUIREMENTS FOR THE DEGREE OF
DOCTOR OF PHILOSOPHY

UNIVERSITY OF FLORIDA

1996

UNIVERSITY OF FLORIDA LIBRARIES

ACKNOWLEDGMENTS

Obtaining my Ph.D. required much sacrifice and unselfish support by those individuals near to me. When deciding whether to continue my education at the University of Florida, Amy, my wife as of December 23, 1995, was in medical school at Northwestern University, which is over a 1000 miles away from UF! Without hesitation, she supported me and the decision to continue my formal education. It was very difficult being separated for three years, and we missed many special moments together. I hope and pray that we live a long life together so I can repay the love, sacrifice, and support she has given me during these years apart. I am grateful to my parents for their love and encouragement to continue my education, and I am very fortunate to have their guidance.

I would like to graciously thank Jim Winefordner for his guidance and wonderful support over the past three years. Working in his group has given me the unique opportunity to investigate and explore various research ideas and analytical techniques with a wide variety of instrumentation and equipment. The education and research facilities in the Winefordner laboratory are the best! My gratitude also goes to Ben Smith for his friendship, support, and always available assistance in the laboratory. He is the most valuable asset of the laboratory and an undiscovered treasure of the UF chemistry department. I am fortunate to be a JDW group member, and many thanks go to all the group members, past and present, who helped me with this research.

TABLE OF CONTENTS

ACKNOWLEDGEMENTS ii

ABSTRACT vi

CHAPTER

1 INTENT AND SCOPE OF DISSERTATION 1

2 CONSTRUCTION AND EVALUATION OF A VISIBLE SPECTROMETER USING DIGITAL MICROMIRROR SPATIAL LIGHT MODULATION 3

- Introduction 3
- Experimental 8
- Preliminary Results and Discussion 11
- Improvements to Experimental Design 15
- Results and Discussion 16
- Conclusions 24

3 PRINCIPLES OF A GLOW DISCHARGE 26

- Introduction and Basic Theory 26
- Theoretical Signal Considerations 32
- Recent Studies Utilizing Glow Discharge Atomic Fluorescence Spectrometry 37
- Recent Studies Utilizing Glow Discharge Atomic Emission Spectrometry 42

4 IMPROVEMENTS TO THE EXPERIMENTAL DESIGN AND EVALUATION OF A MAGNETICALLY-BOOSTED CATHODE AND A MICROSECOND PLUSED DISCHARGE 48

- Introduction 48
- Improvements to the Laser System 48
- Glow Discharge Chamber Design 52
- Evaluation of a Magnetically Boosted Cathode 57
- Evaluation of a Microsecond Pulsed Discharge System 62
- Conclusions 67

5 DETERMINATION OF SILICATE BY HOLLOW CATHODE GLOW DISCHARGE-ATOMIC EMISSION SPECTROMETRY WITH HYDRIDE GENERATION TECHNIQUE 69

Introduction 69
Instrumentation 70
Procedure 72
Results and Discussion 73

6 THREE-DIMENSIONAL DENSITY PROFILES OF SPUTTERED ATOMS AND IONS IN A DIRECT CURRENT GLOW DISCHARGE: EXPERIMENTAL STUDY AND COMPARISON WITH CALCULATIONS 80

Introduction 80
Theoretical Background of Fluorescence Measurements 81
Theoretical Background of Absorption Measurements 84
Experimental Setup 88
Mathematical Model 94
Results and Discussion 95
Conclusions 128

7 ULTRATRACE DETERMINATION OF LEAD IN WHOLE BLOOD AND AQUEOUS SOLUTIONS USING ELECTROTHERMAL ATOMIZATION LASER EXCITED ATOMIC FLUORESCENCE SPECTROMETRY 129

Introduction 129
Experimental Design 131
Experimental Results and Discussion 135
Theoretical Calculation of the Aqueous Lead Signal 145
    Atom Density Calculation 150
    Signal Processing Calculation 150
    Determination of the Number of Photons 151
Theoretical Results Compared to Experiment 151
Conclusions 152

8 FUTURE CONSIDERATIONS 154

APPENDICES

A ACRONYMS USED IN TEXT 159

B LIST OF PERSONAL PUBLICATIONS AND MANUSCRIPTS 160

REFERENCES 161

BIOGRAPHICAL SKETCH 170

Abstract of Dissertation Presented to the Graduate School
of the University of Florida in Partial Fulfillment of the
Requirements for the Degree of Doctor of Philosophy

A NOVEL DIGITAL MICROMIRROR SPECTROMETER, SILANE EMISSION SPECTROMETRY IN A GLOW DISCHARGE, AND LASER EXCITED ATOMIC FLUORESCENCE SPECTROSCOPY

By

Eugene Paul Wagner II

August, 1996

Chairman: Prof. James D. Winefordner
Major Department: Chemistry

Digital micromirror devices (DMDs) have been used to develop a visible spectrometer. A linear array of digital micromirrors at the focal plane of a monochromator are indexed individually and sequentially across the array directing the light of a specific wavelength onto the photomulitiplier tube. The spectral resolution of this system was calculated to be 11.5 nm (FWHM) and the effective spectral range of 360 nm and was determined to be from 340 to700 nm.

Glow discharge spectroscopy principles and theory that are of relevance to the projects presented are reviewed. Improvements to the copper vapor laser pumped dye laser system and glow discharge chambers, as well as incorporation and evaluation of a magnetically boosted cathode and a microsecond pulsed glow discharge, are also discussed.

Hollow cathode glow discharge atomic emission spectrometry has been applied to the determination of silicon coupled with a novel gaseous hydride generation technique, involving drying of an aqueous solution of silicate (sample) and mixing with powdered $LiAlH_4$. Sample introduction into the glow discharge chamber was performed *via* a pinhole at the center of the cathode which was connected to the hydride generator. The detection limit for silicon was 6 μg at 288.1 nm and 30 μg at 251.6 nm.

Complete three-dimensional density profiles of sputtered Ta atoms and ions have been measured in a direct current glow discharge, by laser induced fluorescence spectroscopy. Atomic absorption measurements were also performed to check the fluorescence results for the atom and ion densities. The experimental data have been compared with results of mathematical simulations for the same discharge chamber geometry. In general, satisfactory agreement was reached.

Laser excited atomic fluorescence coupled with a graphite furnace has been used to detect lead in whole blood and in aqueous solutions. The sample was electrothermally atomized and a copper vapor laser pumped dye laser was used to excite the lead. Excellent agreement for NIST & CDC certified whole blood reference samples was obtained with aqueous standards. A limit of detection in blood of 100 ag, and 6 ag in aqueous solutions, was achieved.

CHAPTER 1
INTENT AND SCOPE OF DISSERTATION

The scientific community has changed drastically over the past decade. After many years of fruitful expansion and funding of research programs in educational and industrial settings, the scientific community has started to feel the effects of a saturated market [1]. For the first time, this country has begun an attempt to decrease the production of graduates with advanced degrees in an attempt to maintain order over the new steady state of job opportunities [2]. The level of competition for the scarce number of corporate entry level research positions and entry level faculty positions at universities is both staggering and overwhelming [3,4]. In order for today's graduate student to be competitive for jobs, the student must possess the skills that are of importance to the future employer. One of the most sought after qualities in industry is the ability to be flexible, to think about projects from the perspective of multiple disciplines, and to be able to easily move from one project to another. The work presented in this dissertation describes many different projects I have worked on at the University of Florida in Jim Winefordner's laboratory. The objective was to develop a more broad and flexible knowledge base in spectrochemical analysis in a manner that provides the skills needed to succeed in the future work place. It is my belief that breadth of knowledge and practical application in chemistry as a discipline is important even at the advanced degree

Chapter 2 presents research on the construction of a visible spectrometer using a digital micromirror device supplied by Texas Instruments, Inc. Chapter 3 provides a general introduction on glow discharges. The next three chapters utilize this technique for an atom source. Each of these three projects, however, are distinctly different. Chapter 4 discusses the improvements that have been made to the copper vapor laser pumped dye laser system in order to obtain better laser power, and thus, greater sensitivity of detection in the glow discharge. Improvements to the glow discharge chamber are also discussed as well as the evaluation of a microsecond pulse discharge and a magnetically coupled cathode. Chapter 5 reports the results of a two week collaborative project with Kitao Fujiwara, a visiting professor from Hiroshima University, that utilized a hollow cathode glow discharge for the detection of silicon. Chapter 6 presents the results of a project which used glow discharge for production of tantalum atoms and ions for spatial atom and ion density determination in a glow discharge. These empirical results are compared with theoretical calculations developed by Annamie Bogaerts, a visiting graduate student from the University of Antwerp. Finally, Chapter 7 describes the analytical technique of laser excited atomic fluorescence in a graphite furnace for the ultratrace detection of lead in both aqueous solutions and whole blood. First approximation calculations for theoretical determination of the lead signal using this technique are developed and presented. The publications and submitted manuscripts that have resulted from this research are listed in Appendix B.

CHAPTER 2
CONSTRUCTION AND EVALUATION OF A VISIBLE SPECTROMETER USING DIGITAL MICROMIRROR SPATIAL LIGHT MODULATION

Introduction

Digital micromirror devices (DMDs), also known as spatial light modulators, have been produced in a wide variety of configurations specific to their applications such as joint-transform correlator systems [5], optical neural networks [6,7], and high definition televisions [8]. The characteristics of DMD technology and flexibility of design lends itself to a new application in optical spectrometers. Medium resolution optical spectrometers, with spectral bandwidth on the order of 1 nm, are widely used in instrumentation designed to record molecular absorption spectra in the ultraviolet and visible regions and are among the most widely used laboratory instruments. Modern UV-visible spectrometers usually are designed to use a multichannel detector, such as a photodiode array (PDA), in conjunction with a compact fixed resolution spectrograph and can record spectra with reasonable speed, ca. 30 ms. These spectrographs have no moving parts and are used for on-line detection of chromatographic eluents, routine analytical determinations, and industrial applications such as measurements made in process streams. However, diode array detectors are generally more expensive and are less sensitive than photomultiplier tubes (PMTs), particularly in the UV, and require cooling when a long integration time and low dark current are necessary. In addition, the diode array cannot acquire spectra fast enough for many kinetic studies. A medium resolution spectrometer which incorporates DMD technology and a PMT for detection has the potential of obtaining a complete spectrum on the order of a few milliseconds with high sensitivity at a low cost. Another advantage of the DMD spectrometer is that it possesses the capability of repetitively scanning a small portion of the spectrum without collecting the entire spectrum (random pixel access). The high sensitivity of a DMD spectrometer using a PMT also makes it ideal for fluorescence and phosphorescence detection.

From the viewpoint of the analytical chemist and spectroscopist, there are many attractive applications for a DMD. In their ultimate configuration, with large numbers of mirrors in two dimensions, there would be a great many applications in almost any instrument or device which manipulates light for some measurement purpose. The purpose of this research was to construct and evaluate a compact medium resolution spectrometer using DMD technology. A UV-visible spectrometer using this device would be unusually robust, more versatile than diode array instruments, and would be smaller in size. The deformable mirrors would allow selected spectral intervals to be directed to a PMT in any conceivable temporal sequence. Thus, a few wavelengths of particular interest could be examined with very high temporal resolution (on the 10 μs time scale) and an entire spectra recorded in a few hundred μs. The DMD would also not suffer the pixel "blooming" problems common to the diode array.

The general design of the DMD spectrometer, in this particular setup, positions a linear array of digital micromirrors at the focal plane of a monochromator. The mirrors, which are controlled by digital inputs programmed by spread sheet data files, are indexed individually and sequentially across the linear array directing the light of a specific wavelength onto the PMT. The DMD chip used in this project was originally designed to control the exposure of a photoconductor as part of an electrophotgraphic print but was the best choice for these feasibility studies. The DMD was the size of a standard 28 pin integrated circuit chip with a two row linear array of 840 mirrors (Figure 2-1). The 19 μm square mirrors are spaced 34 μm center to center, and the rows are in a staggered arrangement offset by 17 μm from each other to avoid mechanical interferences. The mirrors operate on a 45° torsion beam system suspended over an air gap which allows the mirrors to rotate on an axis through the diagonal of the mirror. Two electrodes pass under the mirror forming parallel plate capacitors with the mirror. When an address voltage is applied to one-half of the mirror, the torsion beam, and thus the mirror, rotate about the beam axis 10 ° from the plane of the chip due to electrostatic forces (Figure 2-2). Hornbeck provides a complete discussion on the operation and architecture of the torsion beam DMD developed by Texas Instruments, Inc. [9]. When a mirror was addressed, the light striking that particular mirror was sent to the PMT. In their neutral state, the mirrors are coplanar with a much larger, equally reflective surface. A spectrum was obtained by focusing the light from the grating onto the linear array of mirrors and then addressing the mirrors to toggle to +10 ° and back to -10 ° sequentially in pairs across the rows of mirrors.

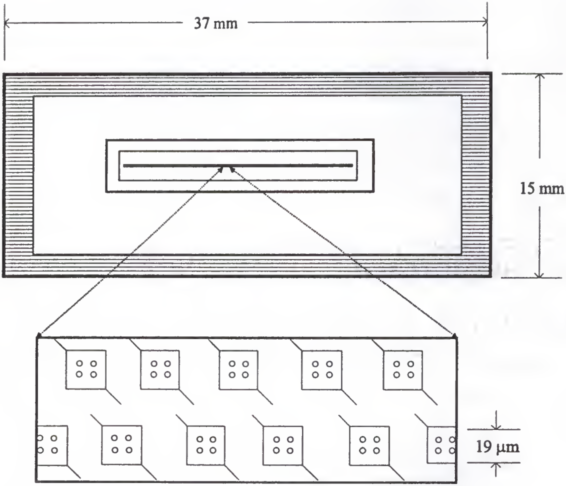

Figure 2-1. Diagram of the DMD used for the experimental setup. The enlarged portion shows the arrangement of the two rows of mirrors. Each mirror is 19 μm square and mounted on a torsion bar. The mirrors are separated by 34 μm center to center.

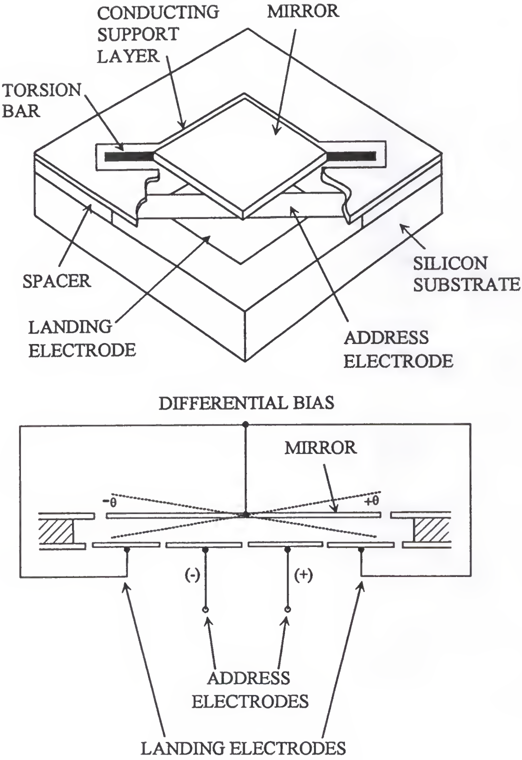

Figure 2-2. Detailed views of the torsion rod system used to toggle each mirror [6].

Experimental

Figure 2-3 shows a schematic diagram of the DMD spectrometer. The source for the spectrometer uses a 30 W variable voltage tungsten filament lamp. The lamp is connected to a DC power supply to eliminate AC frequencies and voltage drifts. The light was passed through a series of two lenses, a filter to eliminate the infrared region, and the sample cell before being focused on the entrance slit of an ISA Instruments USF-200 flat field spectrograph, a Rowland type spectrograph in which a curved grating collimated and focused the light. This type of spectrograph allowed each color of the spectrum to be focused on the plane surface of the DMD. The entrance slit width was 40 μm and the height was reduced to 100 μm so that the light at the focal plane focused only around the area of the mirrors on the DMD. The grating (200 grooves/mm) used gave an effective spectral range of 600 nm over 25 mm at the focal plane. A concave mirror was positioned to the upper left of the DMD in a manner to allow only light from an addressed mirror to be focused onto the photomulitiplier tube. Due to spatial constraints, the concave mirror was cut in half so that the light exiting the spectrograph was not obstructed. A PMT (Hamamatsu R928) with a spectral response of 185-900 nm was used for detection. The output of the PMT was fed into a transimpedence amplifier with a frequency band pass filter (30 Hz, low pass, 12 dB/octave). The DMD was supplied with the following DC powers; interface board +12 V, vcc +5 V, vcc2 +6 V, vreset -36 V, vbias -10 V. The final output was recorded on a Tektronix TDS 620A digital oscilloscope. A light tight box starting at the entrance slit of the spectrograph was made of black felt and construction board to surround all of the optical components. The software used to drive

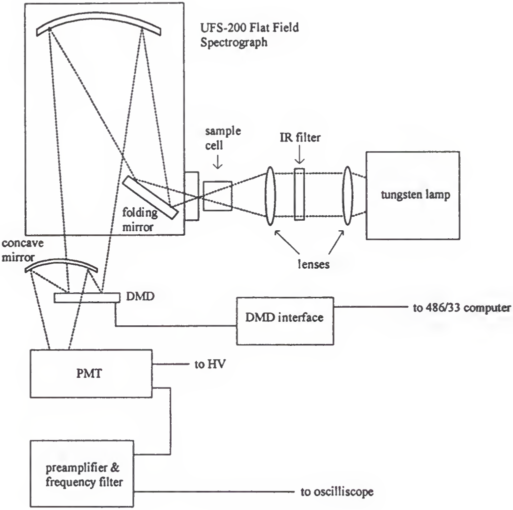

Figure 2-3. Schematic of the experimental setup. The concave mirror was positioned to the upper left of the DMD.

the interface and operate the chip supplied by Texas Instruments, Inc. only had the ability to download eight data files and index through four of them at a time. Each data file was capable of configuring the mirrors in one arrangement. For our purpose, we needed to index through all of the mirrors (or a specified range of mirrors) two at a time, sequentially. However, before any attempt was made to design a new program to index the mirrors, the existing program was used to determine the capabilities of this type of spectrometer. The following procedure was used to make executable files. Spread sheet files were made using Quattro Pro and consisted of columns of red, green, and blue colors for five DMD chips. Each row of the columns was for the corresponding mirror on the chip; 840 in all. The values for each column and row would position the corresponding mirror at an angle that would allow the light to be detected by the PMT. Each data file was configured to index two adjacent mirrors. These files were consecutively numbered and then printed to text files. Using the sstxtpak program, supplied by Texas Instruments, Inc., the text files were configured into readable files for the sharp.c program (Texas Instruments, Inc.) which operated the DMD chip. For this project, only one DMD chip was used and the control of color values was not needed. However, due to the programming of the software, it was still necessary to enter values for the other four DMD chips. Indexing between colors, which was controlled by the encolor and the enred BNC connectors on the interface, was disabled by connecting the encolor to ground and the enred to +5 V, respectively. The system was operated in the manner prompted by the sharp.c program.

Preliminary Results and Discussion

Observation of a signal for one addressed mirror was achieved by optimizing the positioning of the optical components. Figure 2-4 shows the difference in signal between background and one addressed mirror at various points on the DMD. The decrease in signal at both ends of the spectrum is most likely due to the limitations of the source. The decrease in signal at the UV end of the spectrum (low numbered mirrors) is also due to the glass cover slip on the DMD chip and possibly the range of spectral response of the PMT. At the sensitivity level needed for detection, it was difficult to achieve a steady baseline. This may have been due to the instability of the light source.

The time required to collect a spectrum was also investigated. Due to presence of high frequency spikes, the bandpass filter frequency must be set at a low value. As can be seen in Figure 2-5, the spikes become resolved when the filter was set at higher values . If the filter was set at too low of a value, then the resolution of the spectrum suffers due to a lower response time (Figure 2-6). It was found that the optimum settings were 30 Hz for the bandpass filter with the mirrors indexing at a rate of 66 ms/mirror. This correlates to a spectrum collection rate of approximately 55 s. However, these spikes were not observed when the DMD was operated by the blue test pattern box supplied by Texas Instruments, Inc. The source of these spikes was found to be generated by the computer interface hardware which allowed the mirrors to oscillate slightly in their specific position. If the oscillation of the mirrors, and thus the frequency spikes, can be eliminated from the spectrum, the speed of collecting an entire spectrum could be on the order of 1 ms.

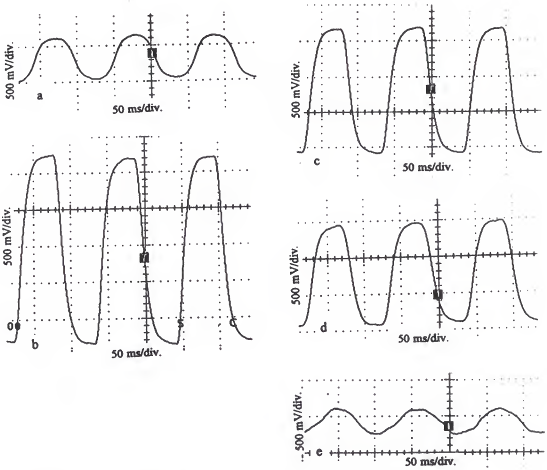

Figure 2-4. Signal magnitudes between baseline and one addressed mirror at a rate of 66 ms with the bandpass filter set at 30Hz. Individual mirror numbers addressed were 700, 600, 400, 300, and 196 for figures a-e, respectively. High numbered mirrors are at the red end of the spectrum.

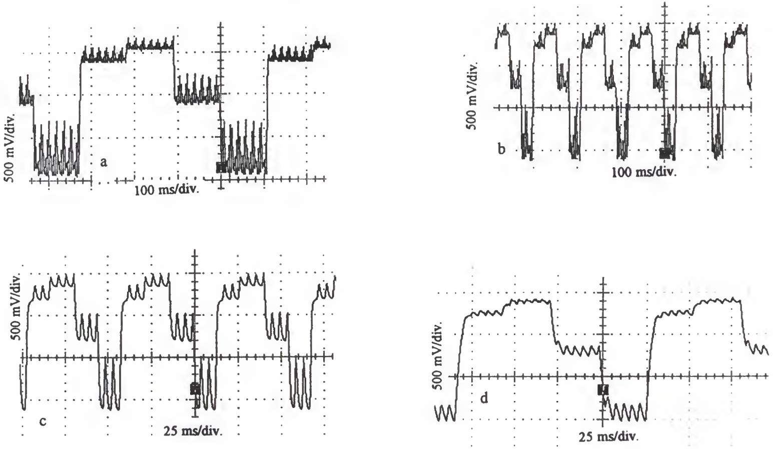

Figure 2-5. Figures a-c show the resolution of the spikes as the indexing rate of the mirrors is decreased from 133 ms to 33 ms and again to 16 ms respectively. The band pass filter was set at 300 Hz. Figure 3d shows a decrease in the spike resolution as the band pass filter was decreased to 100 Hz with an indexing rate of 33 ms. Each spectra shows the repeated pattern of four data files. Each file addressed 210 mirrors where the first file addressed mirror numbers 0-209, the second file addressed mirror numbers 210-409, etc.

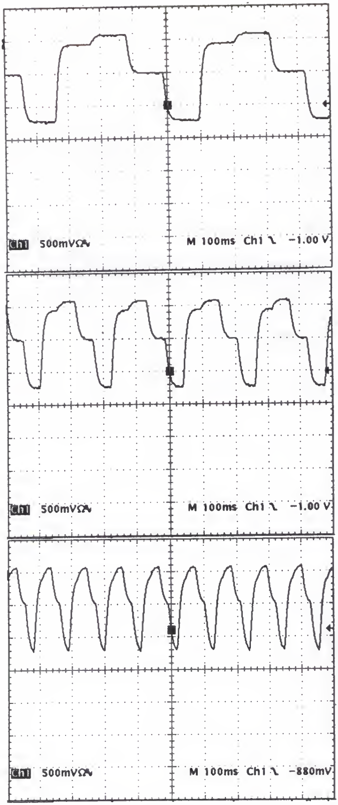

Figure 2-6. As the indexing rate was increased the resolution decreased for scans in which the band pass filter was set at 30 Hz. Indexing rates were a) 133 ms, b) 33 ms, and c) 16 ms.

Improvements to Experimental Design

From the preliminary experiments, it was believed that construction of a UV-visible spectrometer utilizing the DMD provided was possible. The experimental setup was changed by fitting the DMD chip with a quartz window and a more stable, greater intensity, 100 W tungsten lamp was used to improve the signal to noise ratio. The computer program that controlled the DMD was also redesigned to allow individual and sequential access to the mirrors. In order for a spectrum to be collected, this program was modified through a series of loops in which eight data files were downloaded at a time. Once these data files were indexed, they were dumped from the memory of the interface and the next eight data files were downloaded and indexed. The same procedure as before, was used to make executable files using Quattro Pro. Using the sstxtpak program, the text files were configured into readable data files for the new modified sharp.c program which operated the DMD chip. The system was operated by powering up the DMD in the manner prompted by the original sharp.c program. The modified sharp.c program was then executed with the range of mirrors (data files) to index, and the indexing rate which was picked from a list ranging from 16 ms to 8 s. The program would then automatically read in the first set of eight data files (0.dat - 7.dat) and index through them at the specified rate. Once this was complete, the next set of sequentially numbered data files were loaded into the interface. The repetitive process of loading and indexing through eight data files took approximately 5 s on the 486/33 computer and was continued until the specified range of mirrors was completed. This correlated to a complete spectrum collection rate, including the time to download the data files, of approximately 4.5 min. The vast majority of this time was occupied with downloading data from the computer to the interface. The final output was recorded on an IBM XT computer using the SRS 255 data acquisition program (Stanford Research Systems, Sunnyvale, CA).

The resulting spectrum obtained with the modifications to the experimental design is shown in Figure 2-7. The drastic repetitive change throughout the spectrum was due to recording the spectrum while the mirrors were in the off position during downloading of the next eight data files which toggled the next sequential group of mirrors. To eliminate this problem, the signal from the PMT was processed through a gated boxcar. Each time the DMD computer interface was executing the program commands for the DMD, a 5 V high level triggered the boxcar and the collection of data on the computer. When the DMD interface was in the process of downloading more data files, the triggering voltage was off (Figure 2-8).

Results and Discussion

The optical components were positioned to optimize the signal for two addressed mirrors at several places along the array of mirrors. The full scan of the tungsten lamp intensity across the array of mirrors is shown in Figure 2-9. Typically, the trigger switch would collect one to two data points when the mirrors were off. These points were eliminated from the data file. The large DC offset from the background scatter for these scans was typically eight times greater than the signal. Therefore the relative voltage was plotted with zero as the baseline. This large amount of scatter was almost completely due to stray radiation from the DMD light shield. As shown in Figure 2-1, this surface area was as large as the total surface area of all of the mirrors. The decrease in signal at both ends of the spectrum was due to the poor collection efficiency of the concave mirror. At

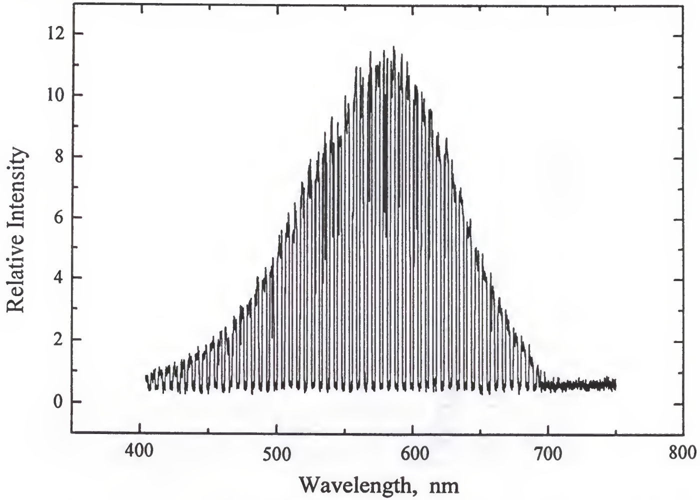

Figure 2-7. Tungsten lamp intensity profile obtained with the DMD spectrometer by indexing two adjacent mirrors at a time. The drastic repetitive change throughout the spectrum was due to recording the spectrum while the mirrors were in the off position during downloading of the next eight data files which toggled the next sequential group of mirrors.

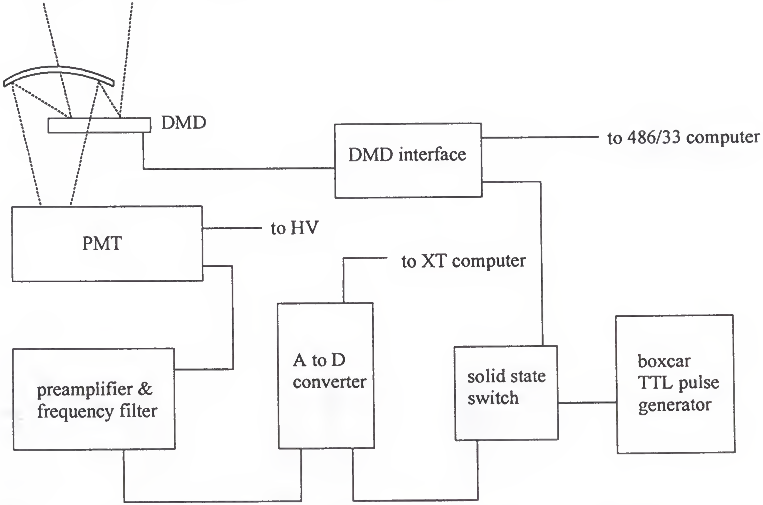

Figure 2-8. Schematic diagram of the final signal processing setup used to obtain spectra with the DMD spectrometer.

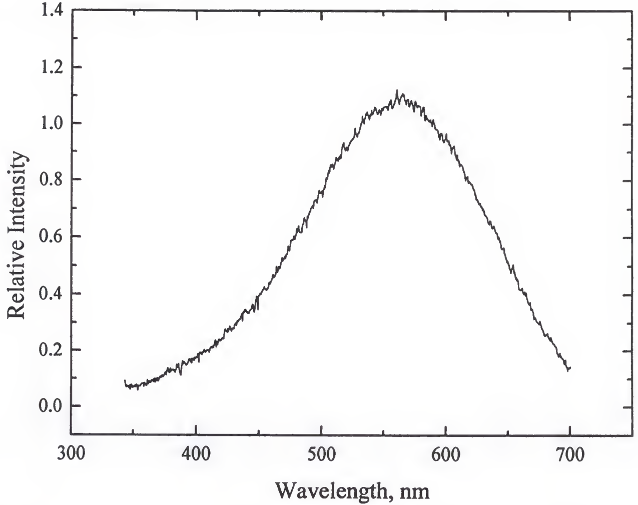

Figure 2-9. Tungsten lamp intensity profile obtained with the DMD spectrometer by indexing two adjacent mirrors at a time. Note that the baseline points were eliminated by using the triggering mechanism shown in Figure 2-8.

the UV end of the spectrum, the decrease in signal was also due to the decrease in light intensity output of the tungsten lamp. Because of this change in spectral response, the S/N ranged from 17.8 to 104.

The spectral resolution and range were determined using a 0.95 mW HeNe laser with a frosted lens to diffuse the light. The light was focused onto the entrance slit using the two plano convex lenses. From Figure 2-10, the resolution at FWHM was calculated to be 11.5 nm. Theoretically, the resolution should be less than 1.0 nm. The degradation in resolution as well as the rather poor spectral profile were caused by the severe background scatter from the DMD light shield. This light shield is a necessary part of this model DMD and is not removable. More recent designs of DMDs have improved light shields to reduce the scattering from the chip surface and the mirrors are placed closer together. Both of these improvement would decrease the background scatter and improve the resolution of this spectrometer. The spectral range was limited by the array of mirrors which spanned a distance of approximately 16 mm as compared to the focused spectrum from the monochromator which was 25 mm and spanned 600 nm. This gave an effective spectral range of 360 nm and was determined to be from 340 to 700 nm.

The absorption spectra of $K_2 CrO_4$ (3.0×10^{-7} M) and $KMnO_4$ (3.8×10^{-4} M) were recorded (Figures 2-11 and 2-12). Due to the large background scatter, the percent transmittance was calculated by:

$$\%T = (I_a - I_b)/(I_w - I_b) \qquad (2\text{-}1)$$

where I_a, I_b, and I_w are the signal intensities of the analyte, background, and water blank respectively. The transmittance curves are similar to those obtained with conventional

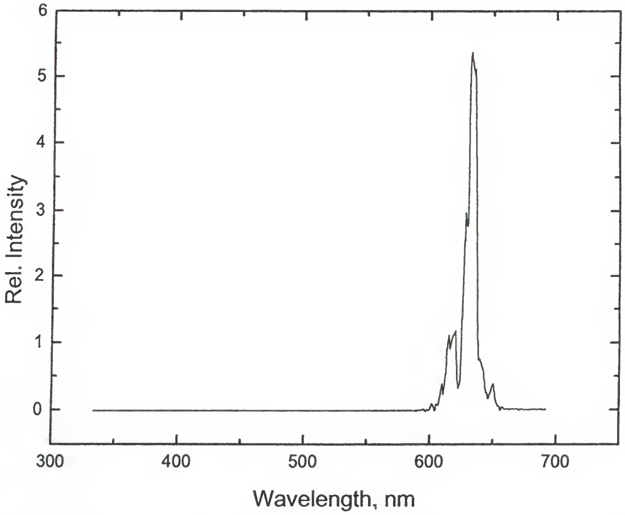

Figure 2-10. Spectrum of a 0.95 mW HeNe laser. The resonance line was adjusted to be at 632 nm. The FWHM resolution was 11.5 nm.

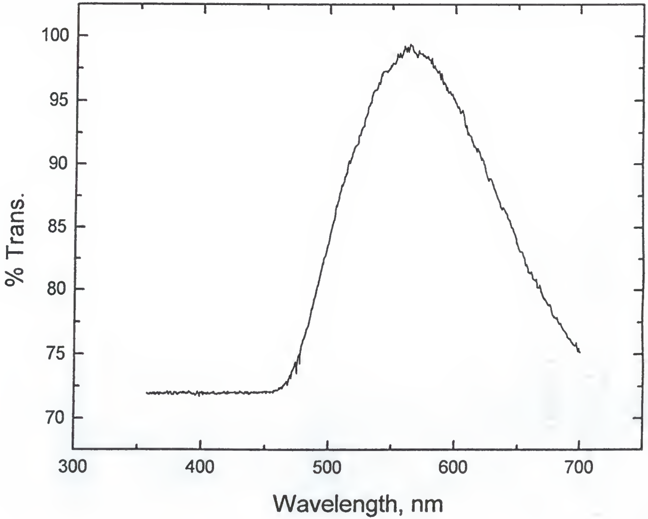

Figure 2-11. Transmittance spectrum of $K_2 CrO_4$ obtained using the DMD spectrometer.

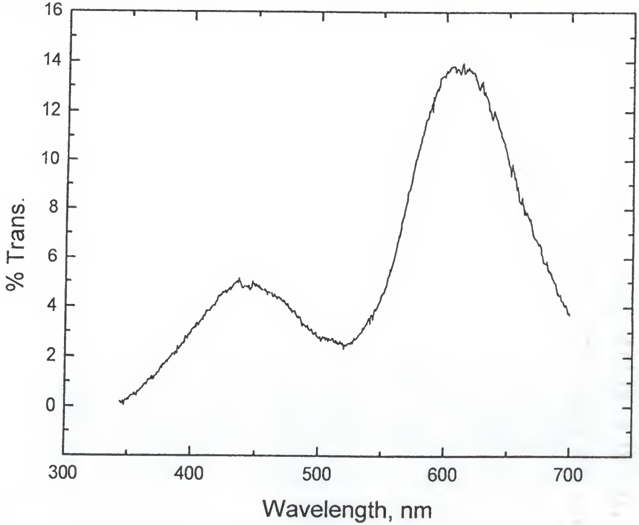

Figure 2-12. Transmittance spectrum of $KMnO_4$ obtained using the DMD spectrometer.

instrumentation but the absolute and relative scales of transmittance do not match [10]. The largest cause for this discrepancy was the large background scatter. At the edges of the spectrum, the ability of the DMD spectrometer to obtain an accurate measure of the transmittance sharply decreased due to poor source intensity and the light collection of the concave collection mirror.

Conclusions

From these experiments, it is believed that construction of a practical UV-visible spectrometer (resolution <1.0 nm) using DMD technology is possible. The current spectrometer design can be improved in several areas. The range of spectral response can be improved by using a light source with greater intensity at shorter wavelengths. Also, to increase the amount of light directed towards the PMT at either end of the array of mirrors on the DMD, a concave mirror with a design more appropriate for this application, such as a cylindrical mirror, is needed. The spectral range can be improved by matching the dimensions of the spectrum from the monochromator with the array of mirrors on the DMD. As previously stated, the DMD used in this setup was designed for another application. However, DMD design today is completely flexible in the height and width aspect ratio and in the number of mirrors that can be incorporated for an application. A DMD designed specifically for this application would have an aspect ratio similar to PDAs and CCDs to increase the capability of gathering light. All of the mirrors would be closer to each other with little dead space between them and the surface in which the mirrors are mounted should be made with the improved light shield. These improvements in the DMD would significantly reduce the background scatter as well as greatly improve the resolution. A short pass filter designed with a cut off wavelength greater than 800 nm will also improve this situation. Finally, to make this spectrometer practical, the DMD interface must be able to load all the data files simultaneously to avoid significant time interruptions during the scan. With these improvements, it is believed that a useful and practical DMD spectrometer with sub-nanometer resolution and millisecond scan rates could be achieved.

CHAPTER 3
PRINCIPLES OF A GLOW DISCHARGE

Introduction and Basic Theory

The next three chapters describe various research projects that utilized a glow discharge for the atom source. This chapter serves as a general introduction for the next three chapters and describes the principles of the glow discharge and how it is used as an atom source.

A glow discharge in the most simple of terms, is a plasma that is initiated by the application of a sufficiently high voltage between two separated electrodes in a low pressure inert gas. The applied potential causes free electrons to accelerate towards the anode and a low current, on the order of 10^{-6} A or less, is established between the electrodes. This is referred to as the breakdown voltage or Townsend discharge. At this point, the discharge is in a steady state relationship between the positive ions formed and the applied external current. This discharge is entirely dependent upon the applied voltage and is extinguished when the potential is removed from the electrodes [11]. The electrons possess sufficient energy to excite and ionize the fill gas (usually argon) and this collisional process produces more charged species until the discharge becomes self-sustaining with a continued application of a much lower external potential than the breakdown voltage [12,13]. Once the discharge becomes self-sustaining the current is much greater, approximately 10^{-4} A, although the current density remains the same since the area covered by the discharge grows proportionally with the increase in the current. At this point, a visible glow is produced from the emission and numerous spatial regions exist between the electrodes. The number of these zones is dependent upon the physical conditions of the discharge, but, from an analytical standpoint, only the cathode dark space and the negative glow are of interest (Figure 3-1). There are numerous types of collisions and electrical processes in a glow discharge as well [14]. Only those that occur in the dark space and negative glow and are of relevance to this research are described. Figure 3-2 shows many of the reactions and interactions occurring in a glow discharge.

Near the cathode surface, the electrons are accelerated in a strong potential field executing few ionizing collisions with the fill gas. Many of these electrons escape this cathode dark space and enter the bright negative glow area. The two types of electrons entering this region are fast electrons which retain their energy, and slow electrons, which are of low energy due to inelastic collisions. The fast electrons carry enough energy to ionize the fill gas. The energy of the slow electrons is insufficient to cause ionization of the fill gas but is adequate to excite these atoms upon collision causing the glow appearance. The positively charged ions resulting from these collisions are accelerated across the cathode dark space and strike the cathode. Ion bombardment energies typically range from 100 to 500 eV [15]. There are four possible results when the positively charged ions collide with the cathode surface; 1) reflection of the ion from the surface of the cathode, 2) implantation of the ion into the cathode, 3) ejection of electrons from the cathode, and the most analytically important process, 4) ejection of the atoms from the cathode, known as cathodic sputtering. If the cathode is a solid made of

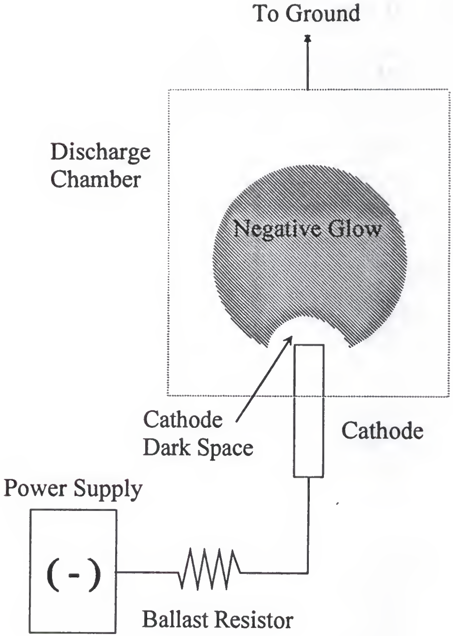

Figure 3-1. Schematic representation of a simple glow discharge. The body of the discharge is connected to ground.

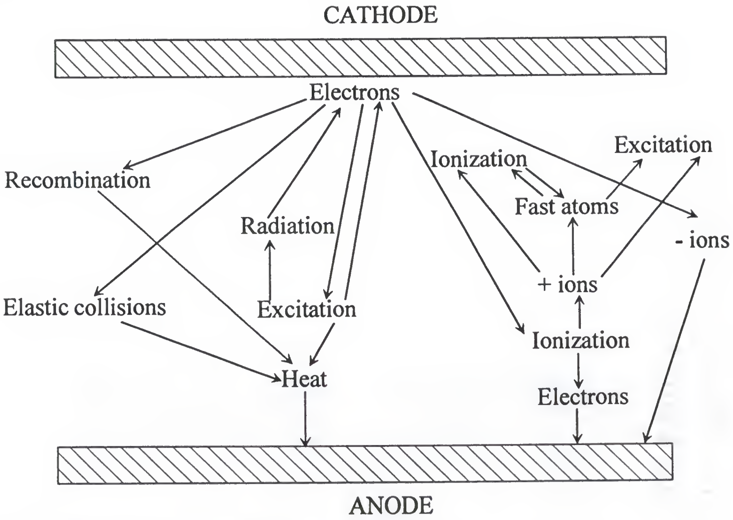

Figure 3-2. Elementary processes that occur in a glow discharge.

the analyte or a solution containing the analyte is dried on the surface of the cathode before the glow discharge is established, the analyte will be sputtered from the cathode and into the analytical volume (Figure 3-3). It has been shown that the impacting ion must possess a minimum threshold energy of 15 to 35 eV in order for the sputtering process to occur [16,17]. The sputtering yield is the ratio of the number of atoms sputtered from the surface to the number of incident sputtering particles, usually expressed as the number of atoms per ion. The yield increases proportionally with the impact energy, which is determined by the external applied voltage, up to approximately 100 eV. Since the ejected atoms usually originate from the first few angstroms of the cathode, the sputtering yield will level off at greater impact energies due to deeper penetration of the ion into the cathode material [15,18]. The sputtering yield is also dependent upon the masses of the impact ion and the analyte atom, and reaches a maximum when the two masses are equal [19]. The complete theoretical expression for the sputtering yield, S, is given below [20]:

$$S = \frac{3\sigma m_i m_t E}{\pi^2 (m_i + m_t)^2 U_o} \tag{3-1}$$

where E is the energy of the incident ion (eV), m_i and m_t are the masses (g) of the incident ion and the analyte atom respectively, U_o represents the surface binding energy (eV), and σ is a function of the relative masses and the angle of incidence of the incoming ion. Over 90% of the sputtered atoms remain in the ground state [21,22]. This sputtering process is used as the atom source in the research presented in chapters 4 and 6. As the sputtered analyte atoms leave the cathode surface, the atoms enter into the analytical volume which is defined by the monochromator slit dimensions and the laser beam spot size where laser induced fluorescence is used as the detection technique. In chapter 5, a

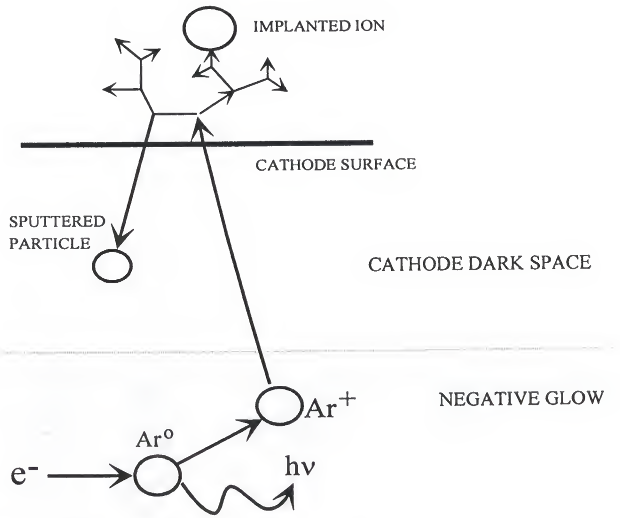

Figure 3-3. Representation of the sputtering process.

hollow cathode system is used to introduce the gaseous silicon analyte. The analyte is introduced at the base of the hollow cathode and is collisionally excited by the impacting ionized fill gas as the analyte enters the discharge chamber. In this case, the emission resulting from the analyte atoms relaxing back to the ground state, is detected in a straight-on configuration with the hollow cathode.

Theoretical Signal Considerations

The efficiency of detection, ε_d, is defined as the probability that a given atom appearing in the probed volume produces a signal that is detected above the intrinsic and extrinsic noise level. The intrinsic noise level only occurs when the detection sensitivity approaches the single atom detection, SAD, limit and involves the statistics of atomic, photon, and photoelectron events [23-26]. The extrinsic noise case involves all noises associated with the source, the atom (ion) reservoir, the detector, and the electronic measurement system. The efficiency of measurement, ε_m, is defined as the probability that an atom in the sample is detected above the noise level and is essentially the number of detector events per atom in the sample. The relationship between ε_d and ε_m is given by [27,28]:

$$\varepsilon_m = \varepsilon_I \varepsilon_v \varepsilon_{a,i} \varepsilon_T \varepsilon_S \varepsilon_t \varepsilon_d \qquad (3\text{-}4)$$

where ε_I is the sample introduction efficiency, which is less than unity for continuous sample introduction systems, such as nebulization of a sample solution into a spray chamber; ε_v, is the sample matrix vaporization efficiency, which accounts for vaporization of desolvated particles in nebulization systems and vaporization of solids in systems using discrete samples, such as furnaces; $\varepsilon_{a,i}$ is the efficiency (also called free atom or free ion fraction) of atomization or ionization depending upon the measurement method; ε_T is the transport efficiency of the analyte atoms to the atom reservoirs; ε_S is the spatial probing efficiency accounting for the fraction of analyte signal being spatially measured; and ε_t is the temporal probing efficiency accounting for the fraction of analyte species within the detection region during the measurement time, t_m. All efficiencies are dimensionless. The first three efficiencies, $\varepsilon_I\varepsilon_v\varepsilon_T$, can be sample and analyte matrix dependent. The fourth and fifth terms, $\varepsilon_S\varepsilon_t$, depend primarily upon how well the observation system views the process spatially and temporally; for example, in a pulsed laser fluorescence or ionization experiment, it is possible that only one in every 100 analyte species is detected with a low repetition rate, pulsed laser, yielding an ε_t of 0.01.

The efficiency of detection, ε_d, and the efficiency of measurement, ε_m, of atomic spectroscopic methods are means of comparing the potential detection power of individual methods and of determining whether any given atomic method has achieved its maximum capability. The boundary conditions and the derivation of ε_d and ε_m have been given previous publications [23,24]. The general expression for ε_d is given by:

$$\varepsilon_d = 1 - e^{-\phi_s \Delta t_i} \tag{3-5}$$

where ϕ_S is the mean flux of detected events (events/s • atom) and Δt_i is the interaction time (s), which is the time the atom remains within the observation region or the time period over which excitation occurs such as in a pulsed laser fluorescence experiment.

The number of detected events, N_e, occurring during the interaction time of a given atom is:

$$N_e = \varepsilon_m N_A = \varepsilon_I \varepsilon_v \varepsilon_{a,i} \varepsilon_T \varepsilon_S \varepsilon_t (1 - e^{-\phi_S \Delta t_i}) N_A \tag{3-6}$$

For atomic emission methods and for all laser atomic methods, Equation 3-6 can be rewritten as:

$$N_e = \varepsilon_I \varepsilon_v \varepsilon_{a,i} \varepsilon_T \varepsilon_S \varepsilon_t \phi_S \Delta t_i N_A = Y N_A \tag{3-7}$$

where Y is the sensitivity of measurement, counts/atom ($\varepsilon_m \rightarrow Y$ if $\varepsilon_d \leq 0.05$), and N_A is the total number of analyte atoms being analyzed within the time interval, Δt_i. The detection limit, N_L, in number of atoms is determined by the noise level usually expressed as a standard derivation, s_n, and so is given by [27,29]:

$$N_L = \frac{3s_n}{Y} \tag{3-8}$$

If background shot noise is dominant, then $s_n = X_b^{1/2}$, where X_b is the number of background detected events during the interaction time which is also the measurement time.

For optical (atomic or ionic) emission spectrometry, as in chapter 4, ε_d is given by [23]:

$$\varepsilon_d = 1 - e^{-\phi_E \Delta t_i} = \eta_{ex} A_{ul} \Delta t_i \eta_o \eta_{el} \eta_d \tag{3-9}$$

where;

ϕ_E = atomic (ionic) emission rate of analyte detected (photoelectrons/s)

η_{ex} = $[g_u/Z(T)]e^{-E_u/kT}$ = efficiency of thermal excitation of atoms (dimensionless)

g_u = statistical weight of upper state in transition (dimensionless)

Z(T) = electronic partition function (dimensionless)

k = Boltzmann constant (1.38×10^{-23} J/K)

T = plasma temperature (K)

A_{ul} = Einstein coefficient of spontaneous emission for transition from u to lower level l (s^{-1})

η_o $= \dfrac{A_a\Omega_E T_o}{4\pi A_e}$ = collection efficiency of optical system (dimensionless)

A_a = limiting aperture, such as spectrometer slit area (cm^2)

Ω_E = solid angle of emission collected (sr)

A_e = total surface area of emitting plasma (cm^2)

T_o = product of transmittances of optics in collection system (dimensionless)

η_{el} = efficiency of electronics (counts/photoelectron)

η_d = efficiency of detector (photoelectrons/photon)

The efficiency of detection for a pulsed laser fluorescence method assuming optical saturation of the excitation transition is given by [23]:

$$\varepsilon_d = 1 - e^{-\phi_F^S \Delta t_i} = 1 - \exp(-gA_{ul}t_i\eta_F\eta_{el}\eta_d) \qquad (3\text{-}10)$$

where;

ϕ_F^S = fluorescence flux for laser excitation assuming optical saturation (photons/s)

g $= \dfrac{g_u}{g_u + g_l}$; statistical weight of the corresponding level

A_{ul} = Einstein coefficient of spontaneous emission for the fluorescence transition (s^{-1})

t_i = interaction time (s) which is the pulse width of the source Δt_l. If the source has an inverse pulse repetition rate greater than the atom residence time on the atom reservoir, then t_i is $p\Delta t_l$, where p is the number of laser pulses per atom (or ion) per residence time (s)

η_F $= \dfrac{A_a\Omega_F T_o}{4\pi A_F}$; collection efficiency (dimensionless) which is identical to η_o except A_F is the total fluorescence surface area

However, the laser system used for this research does not have the spectral irradiance necessary to saturate the energy transitions for any of the studies performed in chapters 5, 6, and 7. Therefore, the efficiency of detection for this pulsed laser fluorescence system where optical saturation is not achieved is given by [23,24]:

$$\varepsilon_d = 1 - e^{-\phi_F^{ns}\Delta t_i} = 1 - \exp\left(\frac{-E_\lambda Q A_{ul} \lambda_{lu}^5 g_u \Delta t_i \eta_F \eta_{el} \eta_d 10^7}{8\pi h c^2 g_l}\right) \tag{3-11}$$

where the 2 level case is assumed for simplicity and;

g_u, g_l = statistical weights of upper and lower states (dimensionless)

Q = quantum efficiency of fluorescence (dimensionless)

λ_{lu} = wavelength of excitation/fluorescence process (cm)

h = Planck constant (J s)

c = speed of light (cm s^{-1})

E_λ = continuum source of irradiance (J s^{-1} $cm^{-2}nm^{-1}$)

The efficiency of measurement, ε_m, for laser atomic fluorescence spectrometry is given by Equation 3-4, and the number of detected events, N_e, is given by Equation 3-7. It should be stressed that with pulsed laser excitation the spatial (ε_s) and temporal (ε_t) efficiencies can be considerably smaller than unity. The temporal efficiency is given by:

$$\varepsilon_t = \frac{\Delta t_i}{t_r} = \frac{\Delta t_S}{t_r} \leq 1 \tag{3-12}$$

where Δt_S is the source pulse width (FWHM) and t_r is the atom residence time. The temporal efficiency can not exceed unity. If an atom is excited p times during the atom residence time, then t_i in Equation 3-11 is replaced by $p\Delta t_S$.

In chapter 7, Equation 3-11 is developed for the strict purpose of theoretical determination of the analyte signal using laser excited atomic fluorescence in a graphite furnace. With good correlation between theoretical and experimental results, there is the possibility of achieving standardless analysis using the LEAFS-GF technique.

Recent Studies Utilizing Glow Discharge Atomic Fluorescence Spectrometry

Glow discharges (GD) are primarily used to sputter solid, conducting samples. The sputtering rates for DC glow discharges, microsecond pulsed glow discharges, and Rf glow discharges are ~4 μg/s at 4 W, ~0.4 μg/s at 20 W, and ~2 μg/s at 1 W, respectively. Although glow discharges are most commonly used for atomic emission spectrometry and mass spectrometry, they have also been used as atom reservoirs for atomic fluorescence spectrometry (AFS).

Walden, *et al.* have evaluated a cw xenon arc source-GD-AFS system and a xenon flashlamp-GD-AFS system [30]. Both approaches were inherently simultaneous multielement in nature. The simultaneous pulsed glow discharge system with synchronized firing of the flashlamp with boxcar detection resulted in a considerable increase in the fluorescence signal-to-background ratio as compared to the cw xenon arc source case. The pulsed fluorescence spectra of copper and aluminum samples were considerably simpler and of higher signal-to-noise ratios than the comparable emission spectra. The atomic population remained for more than 20 ms after GD termination indicating a long residence time of sputtered atoms. The authors noted an anomalous intensity ratio of the 324.7 and 327.4 nm copper lines at early times following GD termination but noted an approach to the correct intensity ratio at long delay times (up to 25 ms). At about 20 ms, the ratio reached 1.8, which was expected based on the transition probabilities of the lines (at shorter delay times, the ratio was <1).

The analytical usefulness of pulsed xenon flashlamp excited GD-AFS was demonstrated by Walden, *et al.*, by multielement detection of Al, Mg, Cu, Cr, and Mn in an aluminum sample (NIST SRM #601-604) [31]. The excellent multielement capability for ppm concentrations is evident with the fluorescence spectrum. Detection limits in the low ppm range for analytes in conducting solids were obtained. Spectral interferences depended upon the spectral resolution of the spectrometer just as in atomic emission, except the background in GD-AES was considerably greater than in GD-AFS. Although xenon flashlamp GD-AFS does not have the detection power of laser-GD-AFS, it is much simpler, less expensive, and inherently multielement.

Glow discharge (GD) laser excited atomic fluorescence spectrometry (LEAFS) has been used for the analysis of nanoliter solution samples [32-35] and for the analysis of trace elements in solids [36-38]. Davis, *et al.* deposited and dried nanoliter aqueous samples on a Ni cathode and atomized them upon ignition of a miniature GD [32,35]. The atom populations of Y, Eu, Tm, and Pb were measured with excitation by a copper vapor laser pumped dye laser. The temporal profiles consisted of short, approximately 2 ms, transient spikes followed by long tails which lasted more than 60 s as a result of analyte redeposition on the cathode surface. Detection limits of 9 fg, 100 fg, 30 ag and 2 fg for Eu, Y, Tm, and Pb were obtained using the peak areas over a 6 s duration. Peak height detection limits were considerably poorer. The glow discharge chamber was miniaturized compared to the one previously used by Winefordner's group [33,34]. Despite the excellent detection limits, it is doubtful that GD-LEAFS will in the near future compete favorably with the common commercial options for aqueous samples, such as ETA-AAS and ETV-ICP-MS.

The application of GD-LEAFS to the analysis of ultratrace elements in pure solid materials is certainly more attractive than the analysis of elements in aqueous solution because of the possibility of analyses impossible by commercially available analytical methods. Dashin, *et al.* investigated a specially designed hollow cathode atomizer for LEAFS and applied it to the determination of lead contents in copper reference materials [37]. Both cw and pulsed GDs were studied. The formation of the sputtered atom flux for the particular geometry of the atomizer was theoretically calculated. A detection limit of 40 ng/g was obtained for Pb in copper. Dashin, *et al.* also designed a planar magnetron for direct atomization of solid materials by ion sputtering for LEAFS [38]. This design gave a much higher atomic flux than the previous hollow cathode type. The potential of the atomizer was examined through the analysis of silicon in high purity In and Ga. The detection limits were 0.4 ng/g for In and 1 ng/g for Ga. The planar magnetron was also used for Pb in copper and a detection limit of 3 ng/g was obtained.

The background corrected analytical signal in GD-LEAFS is given by [32,37,38]:

$$A_F = n_0 FfCVt_m \frac{\Omega_F}{4\pi} T_0 \varepsilon K \tag{3-2}$$

where n_0 = instantaneous concentration (cm^{-3}) of analyte atoms in the analytical zone of volume V (cm^3), Ω_F = measured fluorescence solid angle (sr), ε = quantum efficiency of photocathode of detector (dimensionless), T_0 = overall transmittance of spectrometric system (dimensionless), K = the analog to digital output corresponding to mean charge of a one electron pulse, f = laser repetition rate (s^{-1}), t_m = measurement time (s), F =coefficient accounting for particular spectroscopic characteristics of the analyte atom and the parameters of the laser pulse that can be calculated by solving the rate equations for the free analyte atom in a pulsed resonance field of the particular laser radiation (dimensionless), and t_m = measurement time (s). The instantaneous concentration of analyte atoms in the analytical zone of volume V, n_0, is given by [37,38]:

$$n_0 = \frac{C_a I Y_S}{8eSb} \int_S \frac{\cos\theta \cos\psi}{R^2} dS \qquad (3\text{-}3)$$

where C_a = atomic fraction of analyte in sample matrix (dimensionless), Y_S = sputtering yield of matrix (dimensionless), S = area of sputtered surface (cm^2), R = distance from element of volume V to sputtered surface (cm), θ and ψ = angles that the velocity vector of the emitted atom makes with the normal to the volume element V and the normal to the surface of the lower boundary of the analytical zone, b = coefficient defined by the sublimation energy, E_{sub} where $b = \sqrt{2E_{sub} / m}$, where m = mass of ejected atom (g) and I = sputtering current (C/s). The geometry of the system is shown on Figure 3-4. The integral in Equation 3-3 can is dependent upon the sputtering geometry. The constant F must be solved for the specific atom and laser characteristics. Using the above approach, Dashin, *et al.* obtained theoretical signal expressions for continuous and pulsed sputtering in a hollow cathode discharge and ion sputtering in a planar magnetron [37,38]. The theoretical signal expressions gave signal levels within a factor of 5 in all samples studied by the hollow cathode device and within a factor of 3 in all samples studied by the planar magnetron approach. Similarly, Davis, *et al.* obtained theoretical signal values within an order of magnitude of the experimental values [32]. It is extremely gratifying to obtain such excellent correlation of theoretical with experimental signal values.

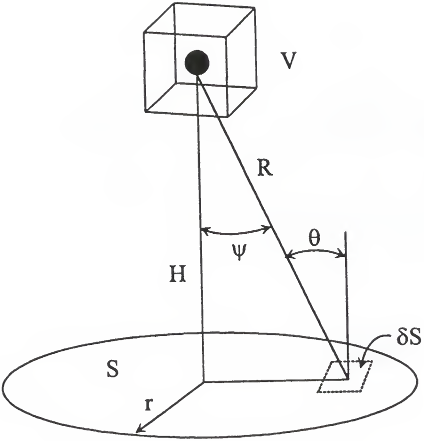

Figure 3-4. Sputtering geometry of a planar electrode. R is the distance between the element on the sample surface, δS is the center of the analytical zone, θ and ψ are the angles between the velocity vector of a sputtered atom and the normals to the sample surface and the lower surface of the analytical zone (of volume V), respectively, H is the distance between the center of the analytical zone and the sample surface, r is the radius of the analytical zone, and S is the analytical surface area.

At this point in time, it is apparent that standardless analysis of trace elements in solids and solutions is possible within a factor of 10 or better by GD-LEAFS. With more careful evaluation of the sputtering geometry and better evaluation of experimental parameters, it should be possible to obtain standardless analyses within a factor of 2 or better. Because of the difficulties of preparing or obtaining solid standards for GD-LEAFS, the standardless approach has great potential for the future analysis of trace elements in high purity materials.

Recent Studies Utilizing Glow Discharge Atomic Emission Spectrometry

Certainly glow discharge-atomic emission spectrometry (GD-AES) is the most used glow discharge atomic spectrometric method, being commercially available for bulk solids analysis and quantitative depth profiling of solid conducting materials. Glow discharge-mass spectrometry (GD-MS) [15,39] is also a fairly well-studied analytical method which is commercially available for quantitation (mainly ppm level) of elements in conducting solids (DC-GD). In both systems, the GD is operated primarily in the DC mode although work by Marcus [40] and Harrison [15] have shown the GD operated in the RF mode can be used for nonconducting solids. The lower sputtering rates, the greater complexity of the RF-GD device, and the relatively poor precision and detection limits greatly limits the application of the RF-GD to AES or MS. In fact, in most cases, it would be far better to either dissolve the nonconductor and analyze the solution by ICP-MS, ICP-AES or ETA-AAS or to make a conducting briquette of the sample and analyze by GD-AES or GD-MS. However, some recent studies by Giglio and Caruso [41] have shown RF-GD-MS is of potential use for non-metals in a He plasma and Heintz, *et al.*

[42] have shown that the RF-GD may be of use as an ion source for time-of-flight mass spectrometry.

Glow discharges have been powered by DC, RF, and pulsed sources. The DC-GD has been by far the most commonly used method. The RF-GD has found increasing popularity for the analysis of nonconductors. Pulsed GDs have been of limited interest, except in the area of boosted hollow cathode lamps. Chakrabarti, *et al.* [43] used pulsed cathodic sputtering in the millisecond region for atomic absorption spectroscopy and Mixon, *et al.* [44] combined a pulsed discharge with a DC discharge for atomic emission spectrometry. Marcus [45] has reviewed the use of RF-glow discharges in atomic emission and mass spectrometry. Perhaps the most significant work so far in the area of glow discharges for atomic emission and mass spectrometry has been the use of a microsecond pulsed glow discharge mass spectrometric system by Hang, *et al.* [46] and an AES system by Walden, *et al.* [31]. The latter group used a microsecond glow discharge (1-300 μs, 5-5000 Hz) pulsed at an average power of 25 mW (2 kV at up to 100 mA). The pulsed GD had an average power (25 mW), 100 x lower than the average power for a commonly used DC-GD. The sputtered atoms remained within the discharge region for milliseconds, whereas the atomic emission remained for only the microsecond duration of the pulse, indicating the possibility of emission free background atomic absorption and atomic fluorescence. Certainly, GD-mass spectrometry would also benefit from the use of a micropulsed GD. It is clear that the MP-GD resulted in a more intense, lower background spectrum (larger S/B, S/N) than with the DC-GD. Several diagnostical studies indicated that the emission lasted only 10-20 μs, whereas the neutral atom concentration lasted for milliseconds.

Magnetically enhanced glow discharges have generated considerable interest in the past few years because of the enhanced sputtering and/or excitation characteristics for optical emission spectrometry. Sacks and coworkers have evaluated the application of magnetic fields to glow discharges and have shown the increase in atomic populations of the sputtered atoms and the excited atoms [47-50]. The magnetic field results in trapping of electrons near the cathode surface. For a discharge at low pressure, the reduced collisional losses of electrons and positive ions result in increased sputtering rates. Magnetron glow discharge sources, in which permanent magnets are placed behind the cathode, have found wide applications in the thin film industry. McCaig, *et al.* have explored the analytical potential of planar magnetron sources for atomic spectroscopy and mass spectrometry for the direct analysis of solid samples [48-50]. Heintz, *et al.* have applied a magnetic field to a Grimm glow discharge lamp and showed an increase of at least 2-fold in the sputtering rate in the presence of the magnetic field [42]. However, the benefit is only moderate for resonance lines as a result of self-absorption and self-reversal. Heintz, *et al.* compared an RF glow discharge with and without the presence of a magnetic field and obtained about an order of magnitude greater signal for Cu in the presence of the magnetic field; detection limits in the 10-100 ppm range were obtained for trace elements in monel alloys [51]. Heintz and Hieftje also evaluated a planar magnetron RF glow discharge and obtained highest sputtering rates at 0.05 Torr and detection limits in the range of 1-50 ppm for elements in a conducting matrix [52]. Heintz and Hieftje studied the effect of driving frequency on the operation of an RF glow discharge for elements in conducting and non-conducting samples [53]. The greatest signals were obtained for non-conductors at 6-13 MHz because insufficient power was available at 20

MHz, whereas for conductors, 20 MHz was best. Detection limits of 0.1-20 ppm for trace elements in the conducting solids and 30-110 ppm for trace elements in the non-conductors were obtained.

Raghani, *et al.* designed and evaluated a miniature planar magnetron glow discharge for the analysis of sub-microliter amounts of aqueous solutions by atomic emission spectrometry [54]. They obtained detection limits, which were 3 to 40 times lower in the presence than in the absence of the magnetic field for Mg, Ag, B, Eu, and Cu. The improved detection limit for the magnetically-enhanced glow discharge-AES system were a result of the increased current density (and sputtering rate) of the discharge in the presence of the magnetic field which formed a plasma ring localized at the cathode surface.

Weiss has shown that it is possible to use a multi-element calibration for high-speed tool steels analyzed by GD-AES, since GD-AES is nearly matrix independent [55,56]. In this approach, sputtering rates estimated from the calibration curves for matrix emission line combinations were used. Only the ratios of sputtering rates, rather than the absolute values, were important. Consequently, multielement calibration was performed without knowing the sputtering rates of any reference samples. It was therefore possible to perform the calibration at any arbitrarily chosen discharge operating conditions and to avoid voltage and current corrections which are normally necessary for quantitation. The model for matrix-independent emission yields for depth profile analysis needs further study. Nevertheless, the capability of a matrix independent emission calibration with minimal use of standards is indeed exciting.

Cserfalvi and Mezei have described a new GD-AES source for the direct determination of metals in aqueous solutions by applying an atmospheric glow discharge in the air gap (2-6 mm) between an electrolyte solution cathode and a W-rod anode [57]. Cathodic sputtering of the solution surface and subsequent excitation occurred when the pH of the solution was below 2.5. The emission spectrum mainly consisted of resonance lines from 213.9 nm (Zn) to 769.9 nm (K) with ion lines of Mg and Ca and strong OH, NH, and N_2 bands. To avoid overheating, the cathode should be water-cooled. The electron temperature was found to be approximately 5000 K. Pulse modulation combined with time resolved signal processing increased the signal-to-background ratio. Despite the uniqueness, simplicity, and capability for direct analysis of solutions, calibration curves were only linear from 1 to 50 ppm and detection limits were between 0.06 ppm for Na and Cu to 0.8 ppm for Mn, Pb, and Ca. It is doubtful that this approach will ever be used on a routine basis.

Saprykin, *et al.* described an atomic emission method using the excitation of atoms by electron impact (AES-EAEI) [58]. The atomic vapor, produced by an electrothermal atomizer, was excited by the electron flux emitted from the cathode of the atomizer. With He as the plasma gas with an ionization potential of 24.6 eV, an electron energy sufficient for excitation of the analyzed elements (most elements have excitation potentials of 2-10 eV) is available. Under these conditions, a self-sustaining plasma discharge is not formed, thereby minimizing the continuum background and maximizing the signal-to-noise ratio. The absolute detection limits (picograms) of this method, AES-EAEI, are comparable to ETA-AAS. The Saprykin, *et al.* approach is similar to furnace atomic non-thermal excitation spectrometry, (FANES) except for the reduction of the continuum background, present in FANES, which results from the recombination of electrons with positive ions.

Schroeder and Horlick have described an unique hollow cathode discharge capable of continuous operation with solution sample introduction [59]. Discharge current densities of up to 0.64 A/cm^2 were maintained in the helium plasma. Detection limits for several elements ranged from 0.03 ng/mL for Li to 200 ng/mL for Zn. The energetic gas discharge was capable of atomizing and exciting a wide variety of nebulized solution samples. A desolvation system was used to reduce the water loading. Based on the emission intensities of elements ranging from Li with a resonance line at 670.8 nm to Zn with a resonance line at 213.9 nm, the innovative hollow cathode discharge source behaved more like a N_2O-C_2H_2 flame than a non-thermal glow discharge.

Williams, *et al.* [60] and Morgan, *et al.* [61] have evaluated the characteristics of hollow cathode design for GD-AES. Both groups have found the cavity must be nearly spherical in shape either by construction or by aging of the hollow cathode through operation.

Barshick, *et al.* [62] have described an innovative GD-optogalvanic spectrometric method for evaluation of uranium isotope ratios. The experimental system consisted of a 150 mW diode laser at 832 nm which was chopped, the laser wavelength was scanned across the ^{235}U and ^{238}U excitation lines, and the optogalvanic signal was measured. The ^{235}U was found to agree within 3.7% of the value obtained with thermal ionization mass spectrometry.

CHAPTER 4
IMPROVEMENTS TO THE EXPERIMENTAL DESIGN AND EVALUATION OF A MAGNETICALLY-BOOSTED CATHODE AND A MICROSECOND PLUSED GLOW DISCHARGE

Introduction

Development of laser excited atomic fluorescence in a glow discharge has been pursued for several years as an analytical technique with the copper vapor laser pumped dye laser system in the Winefordner lab. In order to improve upon previous efforts and detection limits achieved with this instrumentation [63,64], it was necessary to analyze the system in use and make significant changes in an effort to achieve better sensitivity and lower detection limits. The following experiments and results reported here were attempts to improve upon the current GD-LEAFS system. The four areas addressed in these studies were; 1) assessment and improvements of the laser system, 2) glow discharge chamber design, 3) evaluation of a magnetically coupled cathode, and 4) evaluation of a microsecond pulsed discharge system.

Improvements to the Experimental Design

The existing laser system consisted of a copper vapor laser (Model CU15-A, Oxford Lasers, Acton, MA) pumped dye laser (model DLII, Molectron) with a repetition frequency typically around 10 kHz. The dye laser output was frequency doubled in a KDP "B" crystal to achieve the excitation wavelength and the fundamental wavelength was filtered by a UG-11 filter. The frequency doubled laser power at 291 nm was typically 600 nJ in a pulse duration of 2.5 ns (FWHM). [63] The spectral irradiance necessary to saturate most atomic transition lines in the range of 267 nm to 296 nm, could not be achieved with this laser system (see chapter 7). The beam was directed by a 90° quartz prism and a mirror and then gently focused into the glow discharge chamber by a 25.4 cm focal length fused silica lens. The emitted fluorescence was collected at 90° from the excitation beam path and imaged onto the monochromator (Minimate Model, 1200 groves/mm grating, Spex, Edison, NJ) entrance slit (250 µm wide) by a 2 in diameter biconvex fused silica lens [63]. The signal was detected with a R647 PMT (Hamamatau Corp., Bridgewater, NJ) conditioned with a laboratory built transimpedence amplifier and processed with a boxcar integrator (SR250, Stanford Research, Sunnyvale, CA) interfaced to a personal computer (Figure 4-1). The dye laser was designed for a low repetition rate nitrogen laser as the pump source and used one dye circulation system for both the amplifier and oscillator cells that flowed at approximately 900 ml/min. Consequently, it was believe that this system was inadequate to replenish the laser dye in the cells completely between laser shots. This would lead to photobleaching, heating, and premature degradation of the laser dye resulting in poor and unstable laser power and a shortened lifetime of the laser dye. To observe the pulse to pulse laser power, a photodiode was positioned in the laser beam path after the copper laser, the dye laser, and the frequency doubling crystal. Neutral density filters were used in front of the photodiode to maintain linearity in the signal response. The results of this study are shown in Figure 4-2. The shot to shot RSD was within the manufactures specifications

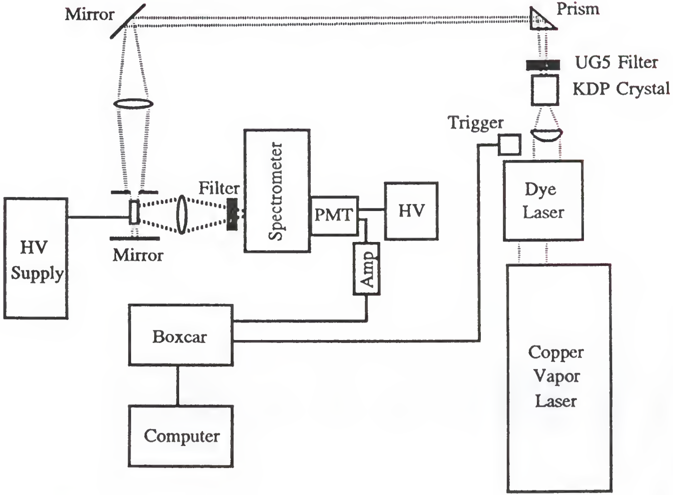

Figure 4-1. Experimental design used by Davis [63].

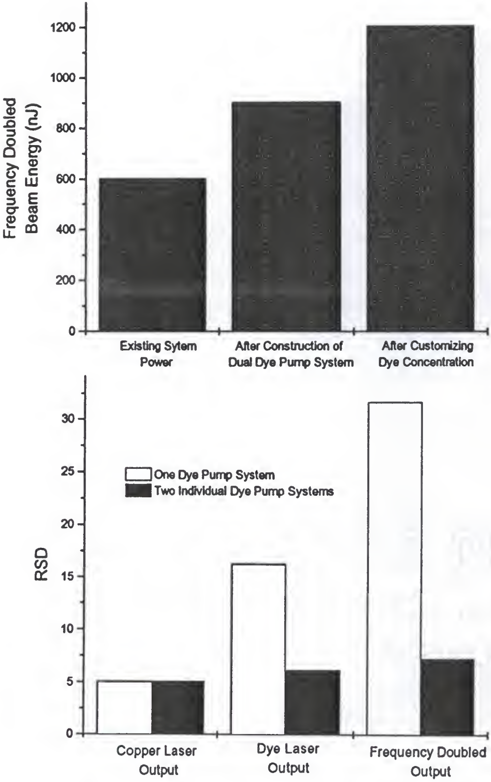

Figure 4-2. Improvements to the laser beam energy and RSD as a result of implementation of the dual dye circulation system.

for the copper laser. However, the RSD increased drastically after the dye laser and this poor shot to shot stability was propagated through the frequency doubling crystal resulting in a final shot to shot RSD of over 31%. To improve this situation, another pump was rebuilt and connected to the amplifier cell to provide a separate circulation system for each dye cell. The flow rate was increased to 2 L/min for the amplifier and 1.85 L/min for the oscillator cell. This resulted in a reduction of the frequency doubled pulse to pulse RSD to 7.2% and a 50% increase in the average laser power. Further, with the two separate circulation systems, the dye concentrations were customized for each dye cell which resulted in another 50% increase in the laser power (Figure 4-2). The setup was also moved to a larger laboratory. By eliminating the prism and mirror used to direct the laser beam in the cramped area, the beam divergence was decreased and better focus into the discharge chamber was achieved without the losses of the prism and the mirror.

The monochromator and PMT were also evaluated and compared to other equipment for possible improvements. A cathode was made by pressing silver powder with 250 ppm TmO to produce a constant fluorescence signal at 391.64 nm. The existing Minimate monochromator and R647 PMT setup was compared with a 340E monochromator (holographic grating, Spex, Edison, NJ) and a R928 PMT (Hamamatau Corp., Bridgewater , NJ). The signal to noise was ratio improved by 15% when the 340E monochromator was used in conjunction with the R928 PMT.

Glow Discharge Chamber Design

The glow discharge chamber previously designed and used by Davis [32] consisted of a 1.5 ml chamber volume with a ground glass joint for the fitting between the removable cathode and the chamber (Figure 4-3). The purpose of the removable cathode

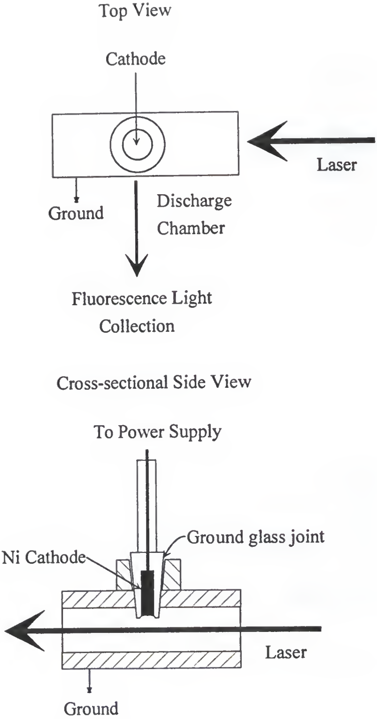

Figure 4-3. Miniature glow discharge chamber design used by Davis [63].

was to simplify the process of depositing an aqueous sample on the cathode tip, drying it, and then replacing the cathode back into the chamber. The small chamber could be evacuated and flushed with the Ar fill gas quickly allowing faster analysis times. It was also believed that the small chamber design produced a more dense atom cloud resulting in a larger fluorescence signal intensity [34,63]. The excellent detection limits obtained by Davis [32] with the miniature glow discharge chamber directed the immediate attention to improvements to the discharge chamber in hopes of further increasing the detection sensitivity. These improvements, shown in Figure 4-4 consisted of; 1) placing the windows for the laser entrance and exit and an angle to reduce laser scatter, 2) replacing the ground glass joint, which used vacuum grease for the seal, with a Cajon fitting and a ¼ in. Macor cathode sleeve as the insulator and joint seal, and 3) placing solenoid flow valves at the fill gas inlet and exit to allow the possibility of stop flow analysis. It has been theorized that there is a rapid loss of analyte atoms under flowing Ar conditions and the poor vacuum seal made by the ground glass joint did not allow the possibility of this type of stop flow study.

In this research, fill gas stop flow conditions resulted in a four fold fluorescence signal intensity increase for a 2 μg Tm aqueous sample dried onto the cathode tip compared with flowing conditions (Figure 4-5). However, with the increase in signal, there was also an increase in the background emission intensity. Typically, the background intensity was 4 times the analyte intensity regardless of the fill gas flow setting. Although this DC signal offset can be eliminated with the boxcar filter, the background noise can not be eliminated. This problem led to investigation of a new design of magnetically coupled cathode and incorporation of a microsecond pulsed

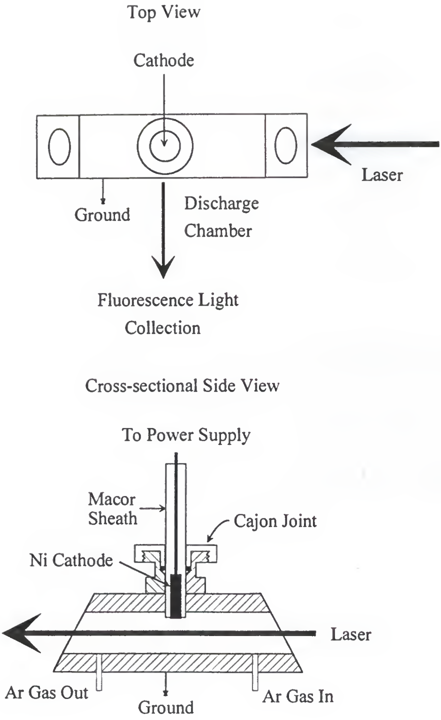

Figure 4-4. New design of the miniature glow discharge chamber used in these experiments [63].

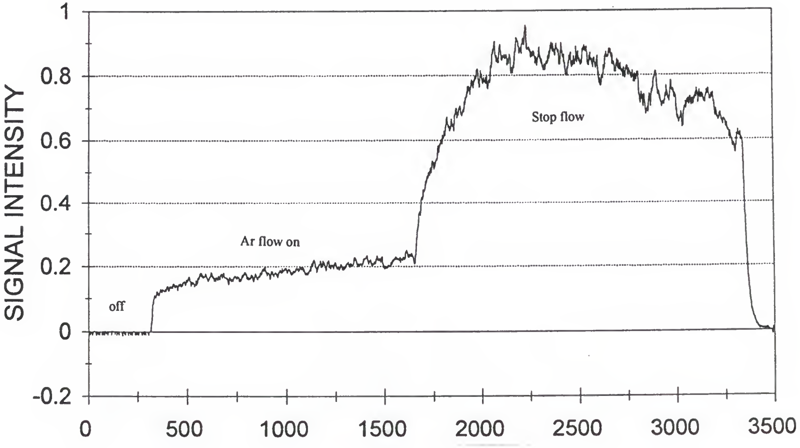

Figure 4-5. Comparison of fluorescence signal intensity for stop flow and flowing Ar fill gas conditions for a solution containing 2 µg of Tm.

discharge that would allow analysis of the analyte without the huge background emission intensity. There was also problems with the Macor sleeve cathode design. To eliminate any arcing of the cathode to the grounded discharge chamber, the Ni cathode needed to be pressed tightly into the Macor insulating sleeve. When the discharge was on, the Ni cathode would heat up significantly and expand. Since the coefficient of expansion of the Macor material was much less than the Ni, the Macor sleeve would crack and begin to arc after approximately 10 runs. Various insulating glues were used between the cathode and sleeve to avoid this problem. However, the glues did not withstand the erosion from the impacting ions at the cathode-glue interface. Consequently, the glue would break down and arcing would occur. This overheating and rapid degradation of the cathode was also typical of the previous ground glass cathode design. The benefits of the new design were excellent vacuum integrity without the contamination of vacuum grease and simple and exact placement of the cathode into the discharge chamber. A microsecond pulsed discharge power supply was investigated for the possibility of eliminating the overheating problems.

Evaluation of a Magnetically Boosted Cathode

To increase the signal intensity of the analyte, a magnetically coupled cathode, similar to the design used by Raghani [65] for emission studies, was evaluated. A theoretical discussion for the interaction of a magnetic field upon a glow discharge system has been described by others [42,51,66-77] and a simple explanation of the interaction is described here.

The purpose of using a magnetic field in a sputtering system is to make more efficient use of the electrons, and cause them to produce more ionization of the fill gas.

For the magnetic fields used in sputtering, typically 100 G, only the electrons are affected; the ions are too massive. When an electron is subjected to a magnetic field, B, it will drift along the field lines with a speed, $v_{||}$, an orbit of radius, R, and at a cyclotron angular frequency, ω.

$$R = \frac{m_e v_{//} \sin \theta}{Be} \tag{4-1}$$

$$\omega = \frac{e \vec{B}}{m_e} = 1.76x10^{11} \vec{B} \tag{4-2}$$

The charge on an electron is, e, and m_e is the mass of an electron. When a perpendicular field, $E_\perp$, is applied in relation to B, the electron has a drift speed, v, that is perpendicular to both $E_\perp$ and B.

$$v = \frac{\vec{E_\perp}}{\vec{B}} \text{ cm/s} \tag{4-3}$$

In a magnetron, the electric field is strongest next to the cathode and diminishes quickly away from the cathode and the magnetic field is parallel with the cathode surface. When the electrons are emitted from the cathode surface, they follow a radial path back to the cathode surface due to the diminishing electric field, while maintaining the orbit and frequency about the magnetic field lines,. When the perpendicular electric field initiated, the velocity of the orbit of the particles is increased resulting in an increase of the number of collisions with the discharge fill gas as well as an increase in the number of ionizing collisions. The increase in collision rate also results in an increased sputtering rate of the analyte on the cathode and a greater density of analyte atoms in the analytical volume. The magnetically coupled cathode used for these experiments is shown in Figure 4-6. The cathode surface was approximately 40 mm in diameter. One of the magnets was ring shaped and the other, of opposite polarity, was cylindrical in shape and fit inside of the ring magnet. This arrangement set up a circular magnetic field line on the surface of the cathode. A cylindrical Macor shield was placed at the center of the cathode surface to block excessive background emission from entering the monochromator. The cathode was positioned so that the laser spot and the imaged monochromator slit, which define the analytical volume, was just below the cathode surface. The cathode sample spot was directly below the magnetic field line where the collision density, and thus, the sputtered analyte density, should be at a maximum. A 2 µL 10 ppm solution of Tm was dried on the depression of the cathode surface by gently blowing N_2 across the surface. The Tm was excited at 291.48 nm and fluorescence was measured at 391.64 nm. Using peak area, the signal intensity was approximately four times greater than without the magnet under the same pressure and current parameters (Figure 4-7). The magnitude of this signal enhancement was similar to the enhancement Raghani reported for emission [65]. However, there was also an increase in the background emission due to the increased ion density and collisionally excited species associated with the magnetic field. The cathode would also heat up rapidly due the increased sputtering rate and the large surface area of the cathode. The cathode would take several minutes to cool before another sample could be dried on it. Also, the large discharge chamber took several minutes to evacuate and flush with Ar. The time to run each sample was increased greatly due to these problems. The overheating of the cathode also made it difficult to obtain consistent results for a specific sample concentration.

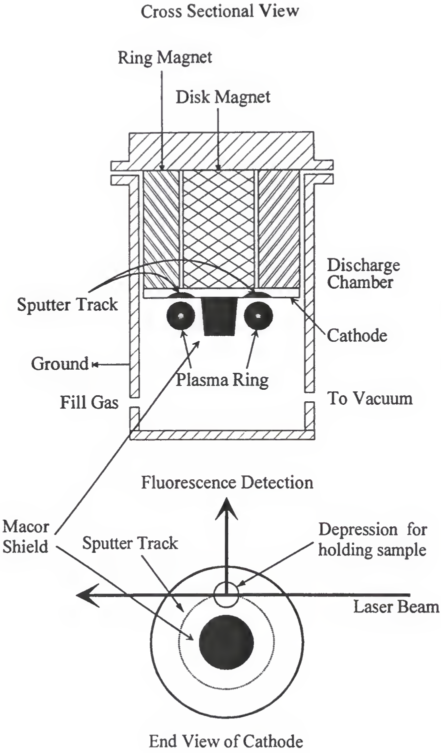

Figure 4-6. Schematic diagram of the magnetically coupled cathode.

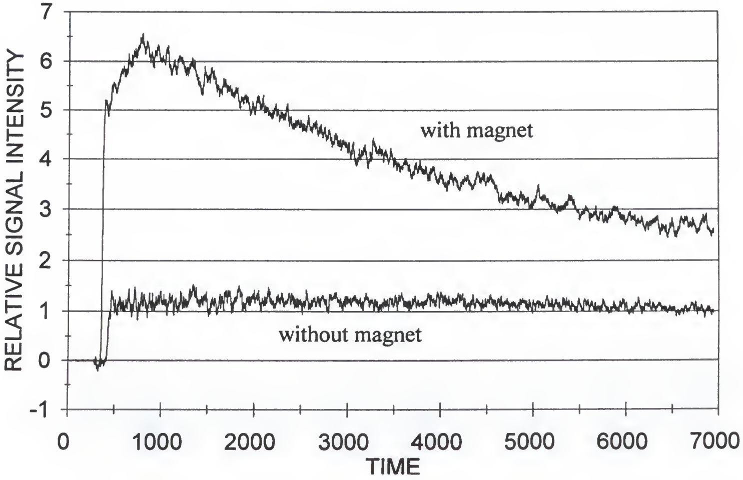

Figure 4-7. Comparison of the fluorescence signal obtained with and without the magnet in place behind the cathode. The peak area was approximately 4 times greater with the magnet

Evaluation of a Microsecond Pulsed Discharge System

Using a microsecond pulse power supply with a glow discharge opens the possibility of eliminating many of the overheating and background emission problems associated with a DC glow discharge. By using a pulsed power supply, the glow discharge is off the majority of the time which allows the cathode to cool. Since shorter duty cycles allow higher driving voltages without overheating, the sputtering rate and emission intensity are increased over a short period of time [78,79].

The characteristics of a millisecond pulsed glow discharge has been studied for many years. Originally, it was studied for its ability to produce higher ion currents for glow discharge mass spectrometry [80,81]. The millisecond pulsed discharge was also used for atomic emission studies [32]. This pulsed power supply had rise times of approximately 1 ms and a width of several ms. A rise in the emission and ion signal and density, termed the afterpeak, occured after the plasma was terminated. An increase in detection was observed by probing the afterpeak emission time region. More recently, Walden, *et al.* have used a microsecond pulsed power supply to observe an enhanced emission signal compared to a DC glow discharge [82]. The reduction in pulse rise time and width of the microsecond pulsed system allowed even greater driving voltages and emission signal intensity compared to previous millisecond pulsed systems. The pulsed glow discharge has also been casually investigated for its use with atomic fluorescence in the Winefordner lab [83,84]. After the plasma is extinguished, the emission decays rapidly while the atomic population diffuses at a slower rate. This creates a dark period in which the atomic fluorescence can be observed without the overwhelming background emission.

In these experiments, a microsecond pulse power supply, (Model 350,Velonex, Santa Clara, CA) was connected to the microcavity glow discharge discussed above. A waveform generator, (Wavetek, San Diego, CA) that was synchronized to the copper laser pulse, via a photodiode, supplied the necessary trigger signal for the power supply (Figure 4-8). A HV probe was used in conjunction with 1 GHz oscilloscope to observe the μs pulse. The oscilloscope was also connected to the output of the waveform generator, the boxcar gate, and the raw signal out from the PMT. The oscilloscope permitted the observation of the timing sequence of the HV pulse, emission signal, fluorescence signal, and the triggering gates. The separation in time of the large emission signal and the relatively small fluorescence signal can be seen in Figure 4-9. The emission signal, which rises quickly after the initiation of the HV pulse tails off quickly and was minimal at the time in which the fluorescence signal was observed. Although the HV pulse was approximately 10 μs in duration at 1500V, Figure 4-9 shows the slow decrease in the voltage due to the capacitance of the discharge chamber. The noise on the background emission, during the signal collection gate, was approximately an order of magnitude less compared to the background noise on a DC glow discharge at 391.64 nm (Figure 4-10). The time integrated signal for a 2 μL, 10 ppm solution of Tm was also recorded. The signal intensity for the pulsed glow discharge was approximately half that of the DC glow discharge. However, the signal to noise ratio for the pulsed system was over six times greater than the DC system. Judging by past work in this area, the fluorescence signal enhancement should have been greater. It is possible that the time interval between the end of the HV pulse and the adequately diminished background

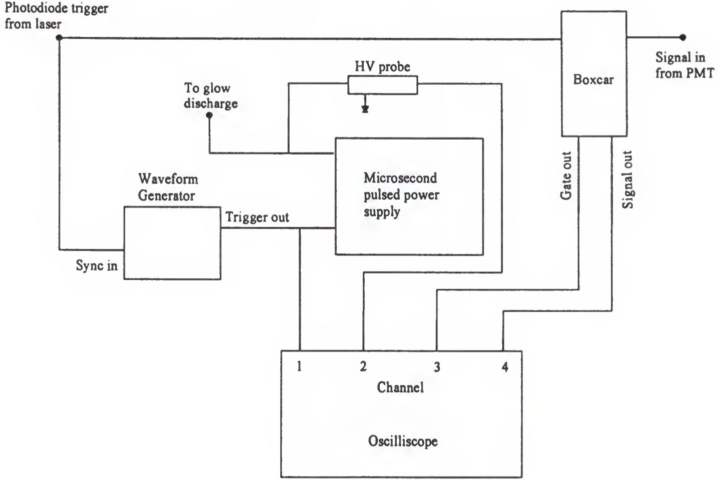

Figure 4-8. Schematic diagram of the setup used for the microsecond pulsed glow discharge experiments.

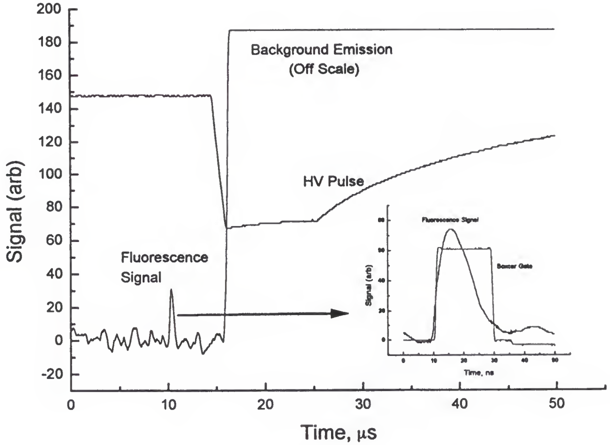

Figure 4-9. Timing sequence of the HV pulse, emission signal, fluorescence signal, and boxcar gate. The separation in time of the large emission signal and the relatively small fluorescence signal can be observed.

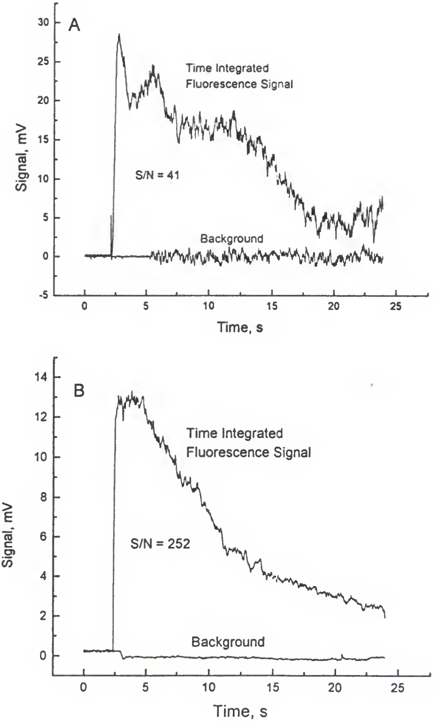

Figure 4-10. Time integrated fluorescence signal and background emission noise obtained for a 2 μL, 10 ppm solution of Tm using a DC power supply (A) and the microsecond power supply (B).

emission was excessively long and the atom density population decreased substantially over this time period. This time period could be greatly reduced if the HV power could be immediately pulled to ground at the end of each pulse allowing both the HV and emission intensity to decay more rapidly. Even though the improvement in signal was not quite as much as anticipated, the pulsed system allowed the cathode to operate at a much lower average temperature. None of the overheating and degradation problem associated with the DC system were observed with the pulsed discharge system when operated at a pulse width of 10 μs and 1500 V. Above this voltage, the cathode would arc due to the poor interface between the insulating Macor sleeve and the Ni cathode.

Conclusions

The improvements made to the laser system were beneficial. Since this system does not produce enough power to saturate most atomic transitions, any increase in laser power proportionally increased the fluorescence signal intensity. The design changes to the miniature glow discharge chamber were also advantageous. The laser scatter was much less with the slanted window design. The better vacuum integrity achieved with the new cathode design allowed the possibility of stop flow analysis which resulted in a great increase in fluorescence signal intensity. However, the problem of insulating the cathode with a material and design that will not crack or degrade easily still needs to be addressed. The present design was, at best, adequate for a pulsed discharge system. The effect of the size of the discharge chamber upon the atom density is still, in this author's opinion, unknown. The magnetically coupled cathode showed an increase fluorescence signal intensity for Tm, but, the large surface area of the cathode, necessary for the magnets, heated rapidly. If the magnets were smaller to decrease the cathode surface area, the magnetic force would be severely decreased and little, if any, effect would be observed on the discharge plasma. Finally, the microsecond pulsed glow discharged system proved to be the avenue where future research efforts should be directed. Good enhancement of the Tm fluorescence signal to noise ratio, without the overheating effects of the cathode, was observed.

CHAPTER 5

DETERMINATION OF SILICATE BY HOLLOW CATHODE GLOW DISCHARGE-ATOMIC EMISSION SPECTROMETRY WITH HYDRIDE GENERATION TECHNIQUE

Introduction

The hollow cathode glow discharge source has been widely used for elemental analysis with solid samples [85,86]. In general, it has proven to be a difficult task to develop alternative sample introduction techniques for this emission source. One approach has been to introduce discrete aqueous samples on the cathode, dry them, insert the cathode into the discharge chamber, and observe the transient emission signal which is produced. This approach has been successfully carried out with hollow cathodes of various geometries and operating conditions [61,87-90]. However, it is cumbersome to remove the cathode for each measurement and there has been a continuing interest in developing techniques for continuous sample introduction. Continuous sample introduction has been done in several ways. Hollow cathode discharges have been interfaced as gas chromatography detectors, especially for non-metals [91,92]. Perhaps the most successful approach for continuous solution sample introduction so far has been that of Schroeder and Horlick [59] where the nebulized sample was desolvated and injected into a hollow cathode discharge operating at 295 mA with 20 Torr of helium as the fill gas. With their system, eleven elements were studied and detection limits ranging from 0.03 to 200 ng/mL were obtained [59]. Hieftje and co-workers [93,94] have used an approach which they call a gas sampling glow discharge, whereby the sample is introduced as a discrete volume of molecular gas or from volatilized organic compounds. This device has also been used to detect arsenic which was generated from solution as arsine in a continuous flow apparatus and transported into the discharge [95]. A limit of detection of 20 ng/mL was obtained.

The method of gaseous introduction described here was an approach to discrete hydride introduction using silicon as the evaluation element. It is based upon the *in situ* solid-phase generation of silane with subsequent trapping in a liquid N_2 cooled tube. The technique was similar to that used by Fujiwara *et al.* [96,97] for hydride sample introduction in the inductively coupled plasma. A hole (about 0.1 cm in diameter) was drilled through the center of the hollow cathode, and the sample gas was introduced into the hollow cathode directly from the hydride generator.

In this work, the conversion technique of silicate to silane [96,97] was combined with hollow cathode glow discharge atomic emission. The silane (b.p.: -111.9 C) generated from silicate was introduced into the glow discharge chamber through the pinhole of the cathode, and the atomic emission of silicon was observed.

Instrumentation

Figure 5-1 shows schematically, the complete experimental system. A glow discharge chamber was constructed from a four-way vacuum cross (Huntington Lab, Inc.) and was similar in design to the device used by Raghani, *et al.* [65]. The discharge was operated at a constant current of 150 mA (at about 500 V) between the cathode and anode (chamber). The hollow cathode, machined from high purity copper, was

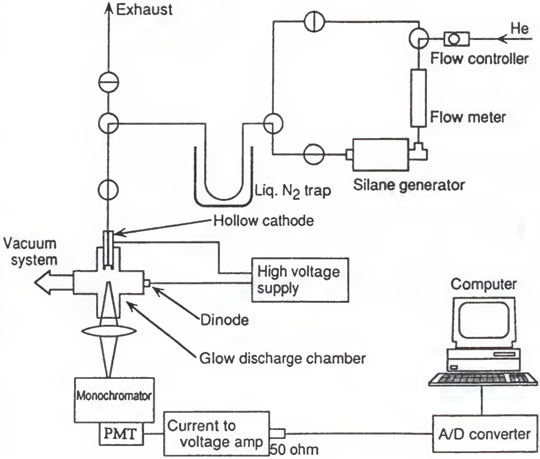

Figure 5-1. Schematic of the experimental setup.

0.6 cm in interior diameter and 1.3 cm deep. The sample introduction hole in the base of the hollow cathode was 1 mm in diameter (Figure 5-2). A monochromator was used to isolate the atomic emission (SPEX type 340 E, f/5.8) with slit widths of 400 μm and 100 μm for the analytical lines of 251.6 and 288.1 nm, respectively. The output of the photomultiplier was fed into a current to voltage amplifier (10^4 V/A) which was connected to analog processor (Stanford, type SR-235 analog processor) *via* a 50Ω resistor. After the signal was converted from an analog to digital (Stanford, type SR-245 A/D converter), the data obtained were processed by a computer.

Procedure

A 1 g of $Na_2SiO_3 \bullet 9H_2O$ was dissolved in 100 mL of purified water (Millipore, Marlborough, MA). The stock solution was then diluted to the necessary concentrations for measurement. A sample solution volume of up to 500 μL was transferred to a molybdenum boat (Nilaco Co., Japan, type SF-210), and dried in an oven at 150 °C for about 1 hour. Powdered $LiAlH_4$ was then added to the dried sample in the boat and the boat was immediately inserted into the silane generator made of a quartz tube. The boat was heated at 200 °C for 10 min by a cylindrical heater which was controlled by a voltage transformer and was monitored by a digital thermocouple. The details of silane generation from silicate are given in more detail by Fujiwara, *et al.* [96]. The helium carrier gas, had a flow rate of about 700 mL/min. The generated silane was collected in a U-tube packed with glass wool, which was cooled with liquid nitrogen. During the silane generation step, helium flowed through the silane generator and the liquid nitrogen U-tube trap to the exhaust hood. A vacuum was maintained in the glow discharge chamber during this step. After the silane gas was generated for 10 min and collected in the U-tube trap, the He

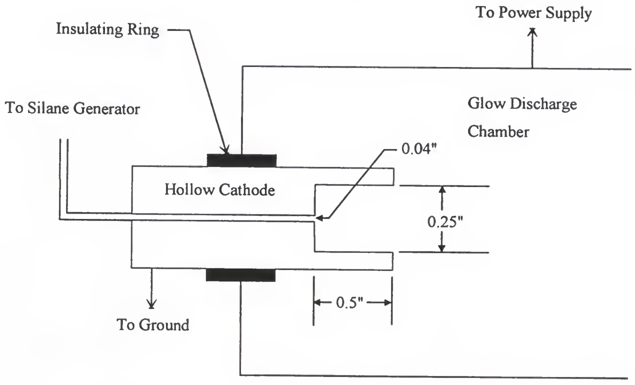

Figure 5-2. Design for the hollow cathode with a capillary for introduction of silane.

flow was routed around the silane generator and into the glow discharge chamber through the hollow cathode. Changing the flow route of helium was necessary to minimize contamination of the glow discharge chamber by the gases evolved in the silane generator. When the pressure inside the glow discharge chamber reached about 0.5 Torr, the U-tube silane trap was warmed to room temperature by soaking the trap in a bottle containing tap water. The signal was approximately 4 s (FWHM) in duration.

Results and Discussion

Three atomic lines, 288.1 nm, 252.9 nm, and 251.6 nm, were evaluated. In ICP atomic emission spectrometry, the 251.6 nm line is the most sensitive line, whereas the 288.1 nm line was the most sensitive in the present glow discharge, and the 252.9 nm line was not detectable. Figure 5-3 shows the temporal emission profile obtained at 288.1 nm during the evolution of silane. Two peaks appeared in this case. However, only the first peak corresponded to the amount of silicate. Since the blank ($LiAlH_4$) did not give any peaks, it is possible that the second peak might be a result of one or more silicon compounds. Therefore, the first peak height was used for quantitation. Generally, only a single peak appeared when observing 251.6 nm (Figure 5-4). The second peak would only appear at this wavelength when the amount of silicate exceeded more than 20 mg. It is probable that silane polymers (Si_nH_{2n+2}) were generated in the case of higher amounts of silicate. Calibration curves were constructed for the 288.1 and 251.6 nm emission lines, for which the detection limits were 6 μg and 30 μg (3σ of the blank signals), respectively. Figure 5-5 shows the calibration curve constructed for the 288.1 nm emission line and Figure 5-6 shows the calibration curve for the 251.6 nm emission line. For both atomic emission lines, the calibration curves are linear up to 1 mg Si. The sensitivity at 288.1 nm

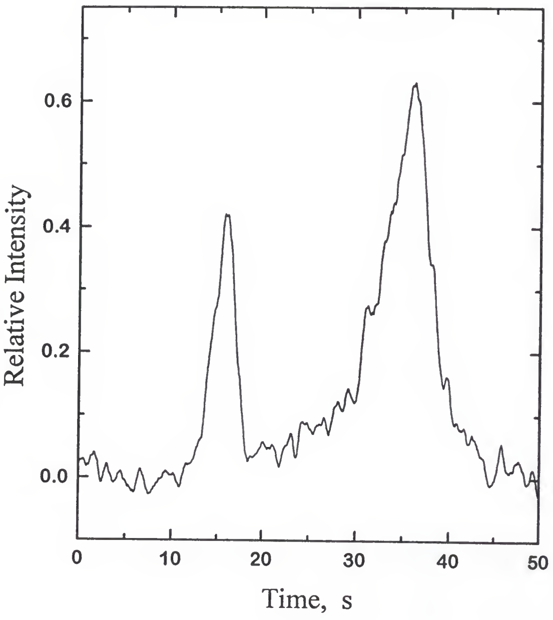

Figure 5-3. Transient signal pattern observed at 288.1 nm atomic emission line for 77 µg of silicon. The second peak is unidentified.

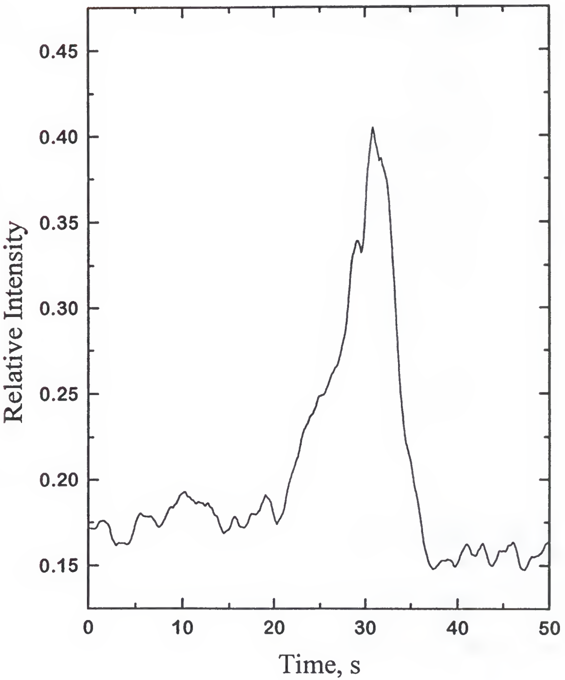

Figure 5-4. Transient signal pattern observed at 251.6 nm atomic emission line for 89 μg of silicon. Note the absence of the second peak.

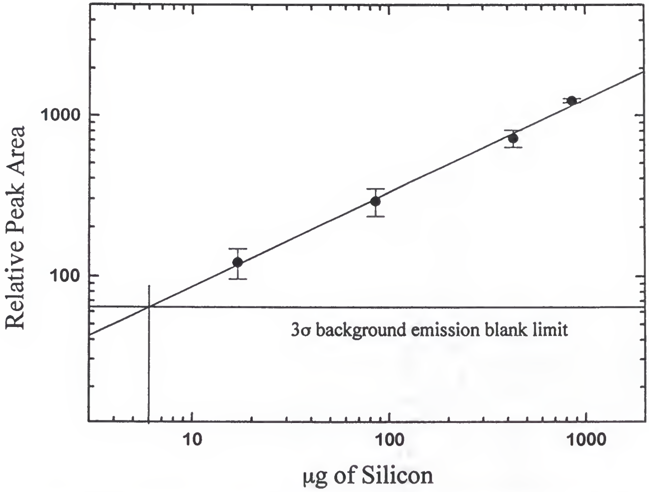

Figure 5-5. Calibration curve for silicon at 288.1 nm. The detection limit using this emission line was 6 µg.

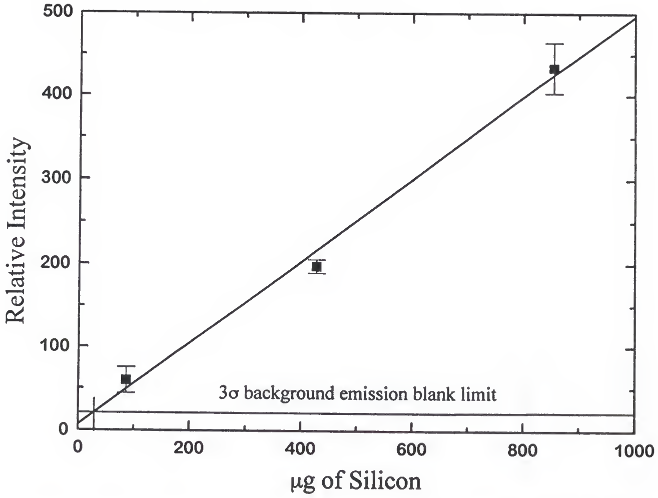

Figure 5-6. Calibration curve for silicon at 251.6 nm. The detection limit using this emission line was 32 μg.

is about 3 times better than that at 251.6 nm (which is commonly used in ICP-AES). Although the detection limit is not better than ICP-AES or chemiluminescence in the present glow discharge atomic emission spectrometry, the system itself is rather simple and the present result proved that the hydride generation technique is suitable for this type hollow cathode glow discharge atomic emission spectrometry. It is believed that with further research of this analytical technique, the detection limit for silicon will improve and the technique could be applied to other hydrides, such as AsH_3 and SbH_3.

CHAPTER 6

THREE-DIMENSIONAL DENSITY PROFILES OF SPUTTERED ATOMS AND IONS IN A DIRECT CURRENT GLOW DISCHARGE: EXPERIMENTAL STUDY AND COMPARISON WITH CALCULATIONS

Introduction

During the last few decades, glow discharges have been finding increased application as atomization, excitation, and ionization sources in analytical chemistry [98-100]. To improve the analytical results a better insight into glow discharge processes is desirable. This can be obtained by mathematical modeling and by experimental plasma diagnostics. In analytical glow discharges, special interest exists for the behavior of the sputtered atoms. Therefore, attention was given to these species in this research. A mathematical model for the description of the sputtered atoms and corresponding ions was developed by Bogaerts and Gijbels in one dimension [101] and in three dimensions [102]. This model fits into a more complex network of models describing the most important species in the glow discharge (electrons, argon atoms and ions, argon metastable atoms, and sputtered atoms and ions) [103-109]. However, to test the validity of the models, the theoretical results must be compared with experimental data. Sputtered atom density profiles in a glow discharge have been measured by many authors. In references 110-112, relative number density profiles were obtained by atomic absorption and in reference 113, by atomic fluorescence. Also, absolute number density profiles have been presented in literature, resulting from atomic absorption measurements[114-116] and from the COMAS (Concentration-Modulated Absorption Spectroscopy) technique [117,118]. These density profiles are, however, mostly one-dimensional, i.e. as a function of axial position from the cathode. To our knowledge, measurements of the sputtered species ion densities have not been reported in literature.

In this research, complete three-dimensional absolute density profiles of the sputtered atoms and corresponding ions, obtained by laser fluorescence measurements is presented. Moreover, the absolute sputtered atom density was also measured by atomic absorption to verify the fluorescence results. Tantalum was chosen as the sputtered species, since it has atom and ion spectral lines lying close enough together to be excited with the same type and concentration of dye in the dye laser.

Theoretical Background of Fluorescence Measurements

Fluorescence measurements yield a three-dimensional fluorescence intensity profile. From this fluorescence intensity, it is possible to calculate the absolute number density. A part of the energy level scheme of the Ta atoms and ions is illustrated in Figures 6-1A and 6-1B respectively together with the relevant wavelengths and corresponding transition probability values of the laser excitation and of the fluorescence pathways. These transition probability values were obtained from Corliss and Bozman [119]. However, since these values are known to be not very accurate, they were only used as branching ratios (i.e. relative values). The absolute values were obtained by measuring the lifetime of the upper energy level, level 3, by fluorescence. It was ascertained that there was no collisional quenching in the glow discharge so that the lifetime of level 3 is only determined by the spontaneous emission coefficients given in

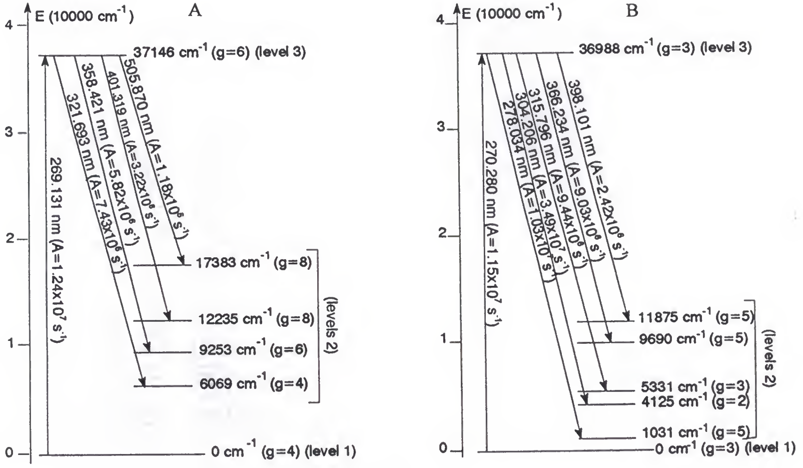
A
E (10000 cm^{-1})
4
3
2
1
0
37146 cm^{-1} (g=6) (level 3)
505.870 nm (A=1.18x10^6 s^{-1})
401.319 nm (A=3.22x10^6 s^{-1})
358.421 nm (A=5.82x10^6 s^{-1})
321.693 nm (A=7.43x10^6 s^{-1})
269.131 nm (A=1.24x10^7 s^{-1})
17383 cm^{-1} (g=8)
12235 cm^{-1} (g=8)
9253 cm^{-1} (g=6)
6069 cm^{-1} (g=4)
(levels 2)
0 cm^{-1} (g=4) (level 1)
B
E (10000 cm^{-1})
4
3
2
1
0
36988 cm^{-1} (g=3) (level 3)
398.101 nm (A=2.42x10^6 s^{-1})
366.234 nm (A=9.03x10^6 s^{-1})
315.796 nm (A=9.44x10^6 s^{-1})
304.206 nm (A=3.49x10^7 s^{-1})
278.034 nm (A=1.03x10^7 s^{-1})
270.280 nm (A=1.15x10^7 s^{-1})
11875 cm^{-1} (g=5)
9690 cm^{-1} (g=5)
5331 cm^{-1} (g=3)
4125 cm^{-1} (g=2)
1031 cm^{-1} (g=5)
(levels 2)
0 cm^{-1} (g=3) (level 1)

Figure 6-1. Part of the energy level scheme and relevant excitation and fluorescence lines for the Ta atom (A) and Ta ion (B). g is the level degeneracy, A is the spontaneous emission coefficent.

Figures 6-1A and 6-1B. The lifetime of the excited Ta atoms was measured to be 33.3 ns; the lifetime of the excited Ta ions was 12.9 ns. No literature values were found for the lifetime of the excited Ta atoms. But, the lifetime obtained for the excited Ta ions is in excellent agreement with reference [120] where a lifetime value of 12.2 ns was reported.

The laser excites the species from the ground state level 1 to level 3, which can relax by fluorescence to level 2. In these experiments, the 358.42 nm wavelength for the Ta atoms and the 304.2 nm wavelength were selected for the Ta ions since both fluorescence lines have a high transition probability. From the fluorescence intensity the absolute number density of level 3 can be derived, and from the number density of this level the total number density of Ta atoms and ions can be calculated. Since the experiments were performed with a pulsed laser, the level populations do not reach a steady state value. Therefore, the measured fluorescence intensity yields the number density of level 3 integrated over time [121]:

$$\mathrm{B_F} = h\upsilon_{32}\left(\frac{l}{4\pi}\right)A_{32}\int n_3 dt \tag{6-1}$$

where B_F is the fluorescence intensity resulting from a single laser pulse (in J/cm^{2}sr), h is Planck's constant (Js), ν_{32} is the frequency of the fluorescence line (in s^{-1}), l is the path length in which fluorescence takes place defined by the laser beam diameter of 0.050 cm, A_{32} is the Einstein transition probability of the fluorescence transition 5.82x10^6 s^{-1}, and n_3 is the number density (cm^{-3}) of level 3, which was integrated over time from one laser pulse to the next.

In order to relate n_3 to the total number density of Ta atoms and ions, a software program based on a density matrix model known as Densmat [122,123] was used. This program calculates the relative level populations as a function of time when the laser irradiance, the laser bandwidth, the laser pulse temporal profile, the rate constants of different relaxation pathways, and the level of degeneracies are given. Figures 6-2A and 6-2B show the results of the Densmat calculations for the Ta atoms and ions respectively. The laser pulse had a duration of about 2.5 ns, and the laser repetition rate was 9 kHz. As a result of the laser pulse, the population of level 1 initially showed a sharp drop, and the population of level 3 increased. After a few nanoseconds, the population of level 3 decreased again as a result of relaxation to the second level. Consequently, the population of the second level begins to rise, but it then decreased again as the second level relaxed to the ground state. The level 1 population returned again to its initial value of 1 after a period of time. For comparison, the experimentally obtained temporal profiles of level 3 for the Ta atoms and ions, derived from the fluorescence temporal profiles are also presented with their intensities scaled to the calculated profiles.

The temporal profiles of the level populations calculated by Densmat are on a relative scale where the total number density of Ta atoms and ions was equal to one. By dividing the time integrated absolute population density calculated from the fluorescence intensity (see above) by the relative temporal profile of level 3 calculated from Densmat, the absolute number densities of the Ta atoms and ions can finally be obtained.

Theoretical Background of Absorption Measurements

To test the reliability of the above fluorescence density measurements, absorption measurements were also performed. The fluorescence measurements served now only to yield the relative number density profile, and the absorption measurements were carried out to put an absolute number on this profile. The absorption measurements yielded an

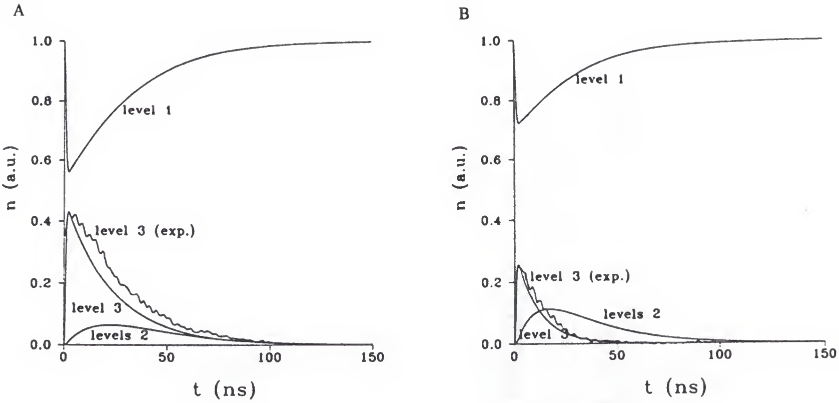

Figure 6-2. Relative population time profiles of levels 1, 2, and 3, calculated with the DensMat program and comparison with the experimental time profile of level 3 obtained with fluorescence for the Ta atoms (A) and the Ta ions (B).

integrated absorbance signal at a certain axial position, also known as side-on measurements, and can be converted to an integrated number density (see below), which is the sum of the fluorescence intensities for all radial positions at that axial position. This integrated number density is related to the sum of the fluorescence intensities for all radial positions at that axial position, which provided the absolute number densities at all the different radial positions.

It was not possible to use the laser for the absorption measurements, since the laser bandwidth (ca. 20 pm) was much larger than the absorption profile (ca. 0.35 pm). Therefore, a Ta hollow cathode lamp (HCL) with Ne fill gas was used. The absorption measurements were only performed for the Ta atoms, since the Ta ion lines emitted by the HCL were either too weak or could not sufficiently be distinguished from other lines to permit reliable measurements. For the Ta atom measurements, the 271.467 nm line was selected.

The absorbance curve for this line was first calculated for a range of densities. Since the emission line width of the excitation source (HCL) and the absorption line width of Ta atoms in glow discharge are of comparable magnitude, the approximations usually made for a line source or a continuum source [124] cannot be carried out, and the complete formula has to be used [125,126]:

$$A = \log\frac{I_i}{I_t} \tag{6-2}$$

$$I_i = \int I_o f(\nu) d\nu \tag{6-3}$$

$$I_t = \int I_o \exp[-k_o g(\nu) l] f(\nu) d\nu \tag{6-4}$$

where A is the absorbance, I_i is the total incident line intensity, I_t is the total transmitted line intensity, I_o is the incident line intensity at the maximum of its profile, f(ν) is the line profile of the HCL, k_o is the absorption coefficient, g(ν) is the absorption line profile and *l* is the absorption path length. The line profile of the source line, or the emission line of the HCL, is almost entirely determined by Doppler broadening [127].

$$f(\nu) = \exp\left[-\left(\frac{2(\nu - \nu_0)\sqrt{\ln 2}}{\Delta\nu_D}\right)^2\right] \tag{6-5}$$

where:

$$\Delta\nu_D = \frac{2\sqrt{\ln 2}}{\mathrm{c}}\nu_0\sqrt{\frac{2\mathrm{RT}}{\mathrm{M}}} \tag{6-6}$$

Since a HCL and a conventional glow discharge emit lines with comparable profiles, the absorption line profile, g(ν), can be taken to be equal to f(ν). This yields the absorbance formula shown below.

$$\mathrm{A} = \log\frac{\mathrm{I_i}}{\mathrm{I_t}} = \log\left(\frac{\int \mathrm{I_0 f}(\nu)\mathrm{d}\nu}{\int \mathrm{I_0 f}(\nu)\exp(-\mathrm{k_0 f}(\nu)l)\mathrm{d}\nu}\right) \tag{6-7}$$

The absorption coefficient, k_o, correlates to the number density, n [124-127].

$$k_0 = \frac{2\lambda^2}{\Delta\lambda}\sqrt{\frac{\ln 2}{\pi}}\frac{\pi e^2}{mc}nf \tag{6-8}$$

where e and m are the electronic charge and mass, c is the speed of light, λ_o is the wavelength at the center of the profile, $\Delta\lambda_D$ correlates to $\Delta\nu_D$ (see above), and f is the oscillator strength of the absorption transition. Hence, these formulas are used to calculate the absorbance for a range of densities resulting in an absorbance curve (Figure 6-3). By comparing the measured absorbances with the calculated absorbance curve, the absolute or integrated number densities can be obtained. Combining this with the fluorescence data, the individual number densities at each position can be derived.

Experimental Setup

For the fluorescence measurements, a copper vapor laser (Model CU15-A, Oxford Lasers, Acton, MA) was used to pump a dye laser (model DLII, Molectron) at a repetition frequency of 9 kHz. The dye laser (Rhodamine 560, Exciton Corp., Dayton, OH) output was frequency doubled in a KDP "R6G" crystal and the fundamental frequency filtered to obtain the 269.131 nm Ta atom excitation line and the 270.28nm Ta ion excitation line which were typically 1μJ in a pulse duration of 2.5 ns (FWHM). The spectral irradiance necessary to saturate these transition lines was not reached (see Chapter 7). The beam was gently focused into the glow discharge chamber by a 25.4 cm focal length fused silica lens. The emitted fluorescence was collected at 90 degrees from the excitation beam path and imaged onto the monochromator (Minimate Model, 1200 grooves/mm grating, Spex, Edison, NJ) entrance slit by a 2 in diameter biconvex fused silica aperatured to 0.8 in. The slit width was 250 μm, and the height was masked to 1 mm to match the laser beam geometry and to provide good spatial resolution. The signal was detected with a PMT (R955, Hamamatau Corp., Bridgewater, NJ) conditioned with a transimpedence amplifier (Model A1, Thorn EMI Gencom, Inc., New York) and processed with a boxcar integrator (SR250, Stanford Research, Sunnyvale, CA) interfaced to a personal computer.

For the absorption measurements, a Ta (Fisher Scientific, Pittsburgh, PA) hollow cathode lamp operating at 20 mA was used. The transmitted light was imaged on the entrance slit of another monochromator (GCA McPherson Instruments) with better spectral resolution to clearly resolve the Ta 271.467 nm line.

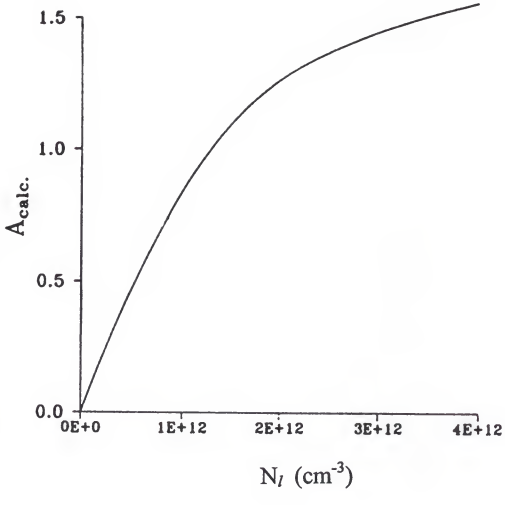

Figure 6-3. Calculated absorbance curve for the Ta atoms. l is the optical path length in cm and N is the atom density in cm^{-3}.

The glow discharge chamber was a stainless steel six way cross with 4 cm diameter ports. Four ports lying in the same plane were provided with quartz windows and were used for the absorption and fluorescence measurements. The fifth port went to the vacuum pump, and the sixth port had a fitting which permitted the insertion of the cathode probe. The glow discharge chamber was mounted on a table which could be moved in the x, y, and z directions in order to carry out three-dimensional spatially resolved measurements. Measuring points were taken at 1 mm intervals from the cathode until 8 mm from the cathode, and then measurements were taken at each 2 mm further away from the cathode. It was tested that different x-y combinations which corresponded to the same radial distance from the cell axis yielded the same fluorescence signal. This demonstrated the approximate cylindrical symmetry of the discharge cell and showed that the incoming laser light and outgoing fluorescence light were not further absorbed in the glow discharge plasma, e.g. that optically thin conditions prevailed.

The entire glow discharge chamber was grounded and acted as anode, and the cathode was connected to high voltage. Tantalum disks of about 1 mm thick were obtained by cutting from a tantalum rod (99.99% pure, 4.5 mm in diameter; Aesar Ward Hill, MA.) and were used as the cathode surface. The disks were glued onto the cathode insertion probe using silver impregnated conductive paint. A Teflon shield was placed around the tip of the probe and the edge of the sample disk so that only the Ta sample was exposed to the discharge. A schematic overview of the experimental setup and of the glow discharge in detail are given in Figures 6-4 and 6-5, respectively.

The output signal from the fluorescence measurements at the computer is given in volts. To calculate the level population, the fluorescence intensity must be expressed in

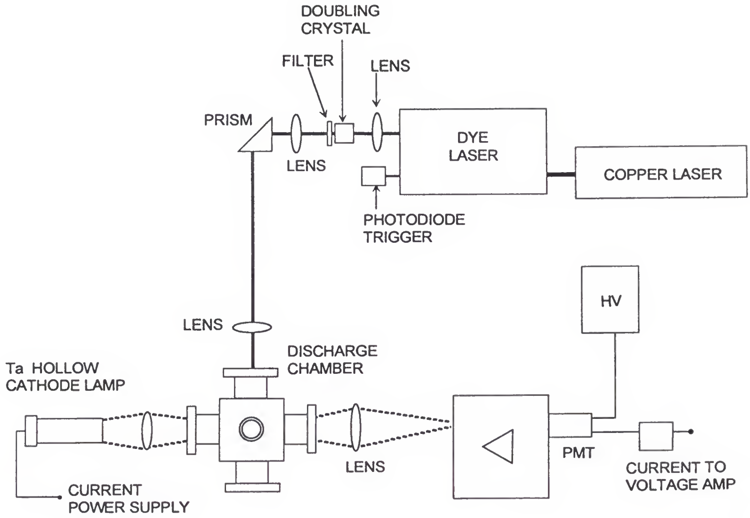

Figure 6-4. Schematic overview of the experimental setup.

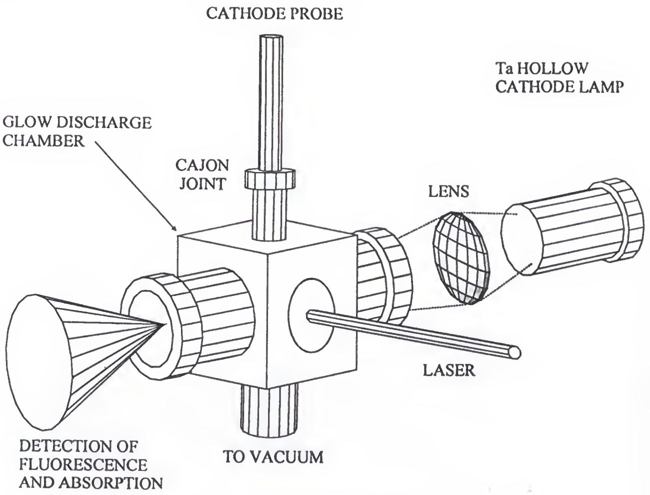

Figure 6-5. Perspective view of the glow discharge chamber.

J/cm^{2}sr. The conversion of this fluorescence intensity was accomplished in the following manner. B_F(J/cm2sr) was the output signal divided by (i) the gain of the electronics (preamplifier and boxcar, k_1 in V/As), (ii) the response of the monochromator and PMT (k_2 in A/W), (iii) the slit area of the monochromator (250 mm x 1mm = 0.0025 cm^2), (iv) the solid angle of the system, calculated to be 0.00784 sr, and (v) the transmission of the windows, measured to be 0.865, and lenses, 0.92 when assuming 4% surface losses at each side. To achieve accurate values of k_1 and k_2, the electronics, the monochromator, and the PMT had to be calibrated. The gain of the electronics was obtained by measuring the fluorescence peak directly with an oscilloscope (in A's) and correlating it with the fluorescence signal after passage through the preamplifier and boxcar (in V). This yielded a k_1 value equal to 1.11 x 10^{11} V/As. The monochromator and PMT were calibrated with a He-Cd laser (Liconix, Santa Clara, CA) of 0.94 mW at 325 nm, imaged with the same optics as used for the fluorescence measurements. The power exiting the entrance slit of the monochromator was measured with a calibrated photodiode (United Detector Technologies, PIN-10DP). The photocurrent reaching the PMT corresponding to this amount of radiation was measured at the different PMT voltages used for the experiments. Dividing the measured photocurrent by the measured power exiting the entrance slit yielded a response of the monochromator and PMT at 325 nm. The response at the fluorescence wavelengths 358.42 nm and 304.206 nm was obtained by using a 1000 W quartz-halogen tungsten coiled-coil filament lamp which served as a Standard of Spectral Irradiance (Model FEL-C). The resultant k_2 for a PMT voltage of 1000 V at 358 nm and 304 nm was found to be 76300 and 56560 A/W, respectively.

Mathematical Model

A mathematical model for the sputtered atoms and ions was developed earlier in one dimension [101] and later for the three-dimensional geometry of the standard cell for analyzing flat samples in the VG9000 glow discharge mass spectrometer [102]. The atoms sputtered from the cathode lose their initial energies of a few eV almost immediately by collisions with gas particles (thermalization process). When they are thermalized, further transport is diffusion dominated. The sputtered atoms can be ionized by Penning ionization, asymmetric charge transfer and electron impact ionization. Penning ionization is when a metastable atom, in this case Ar, collides with a neutral, Ta, and the neutral becomes ionized. This can only occur if the ionization energy is less than the excitation energy of the excited metastable atom. Electron impact ionization is an inelastic collision in which the primary electron removes an electron from the target atom, producing a positive ion and two electrons. The two electrons can be accelerated by the electric field until they can produce ionization. This multiplication process maintains the glow discharge. Asymmetric charge transfer is a collision that results in the exchange of charge between two different atomic species. The transport of the ions created in this way is controlled by diffusion and migration. In order to compare the experimental and modeling results, the complete three-dimensional model network [102,108] was modified and applied to the experimental cell geometry. The experimental cell geometry, or six-way cross, was approximated by a cylinder of 4 cm diameter, and 2 cm length, and a Ta cathode of 4.5 mm diameter. The secondary electron emission coefficient of Ta was taken as 0.11 [128]. A sticking coefficient of 0.5 for Ta and 1.0 for Ta+ was assumed.

Results and Discussion

Figures 6-6 through 6-12 show the three-dimensional Ta atom density profiles at various pressure, current, and voltages, obtained by the fluorescence measurements. Because of the cylindrical geometry of the discharge plasma, the three-dimensional profile can be presented in two dimensions. The position of the cathode is indicated with the black line at the z and r equal to zero. The number density was low close to the cathode, and it increased until it reached a maximum at about 3 mm from the cathode. Thereafter, it decreased gradually toward the cell walls. The cathode (0-0 point) was located at the center of the cell. Since the cell windows were only 20 mm in radius, fluorescence intensity could only be detected within 20 mm from the 0-0 point. The dip in the sputtered atom number density in front of the cathode was also reported in other papers [110,112,115]. It was explained by assuming that not all the cathode material is sputtered as neutral atoms, but that a certain amount was possibly released as clusters or excited state species which were not detected by atomic absorption or fluorescence. This is a reasonable explanation. A similar profile also resulted from the modeling calculations without taking into account sputtering in the form of clusters. Indeed, the sputtered atoms leave the cathode with energies of several eV. They lose these initial energies very rapidly by collisions with argon gas atoms until they are thermalized. This gives rise to a thermalization profile, which is the number of sputtered atoms thermalized as a function of position from the cathode, that showed a maximum at about 1 mm from the cathode [102,104]. Since thermalization is much faster process than diffusion, it is already finished when diffusion starts and the thermalization profile serves as a starting distribution for the diffusion away from the cathode and back to the cathode. This explains why the sputtered

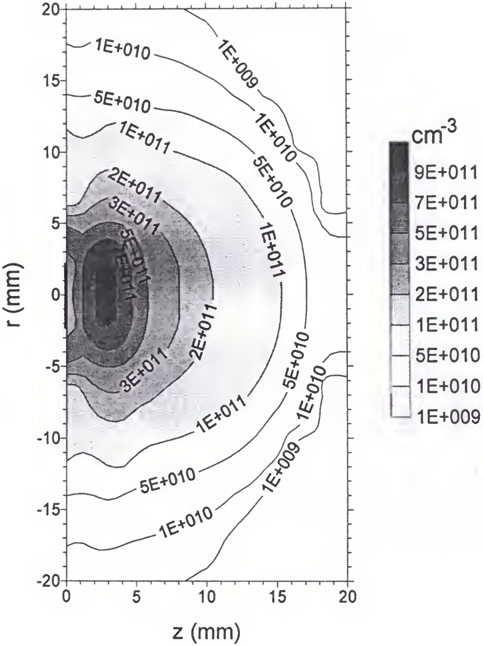

Figure 6-6. Experimental Ta atom density profile at 700V, 1 torr and 1.25 mA, obtained by fluorescence measurements.

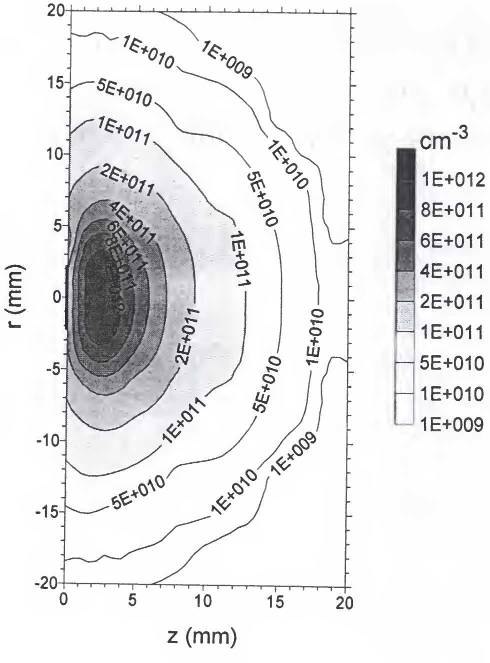

Figure 6-7. Experimental Ta atom density profile at 850V, 1 torr and 1.7 mA, obtained by fluorescence measurements.

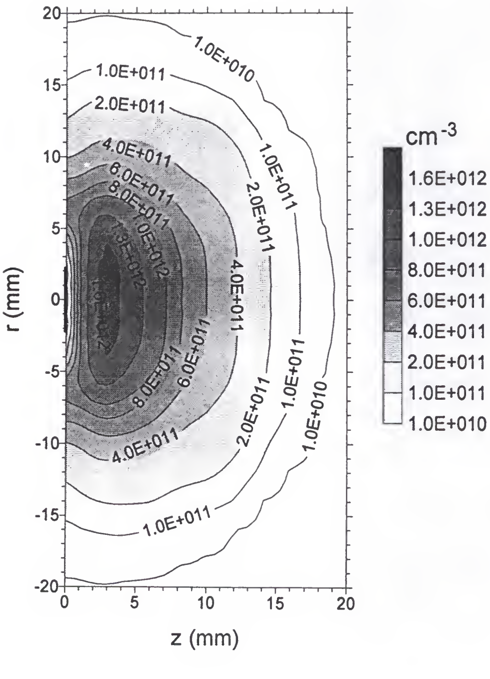

Figure 6-8. Experimental Ta atom density profile at 1000V, 1 torr and 2.1 mA, obtained by fluorescence measurements.

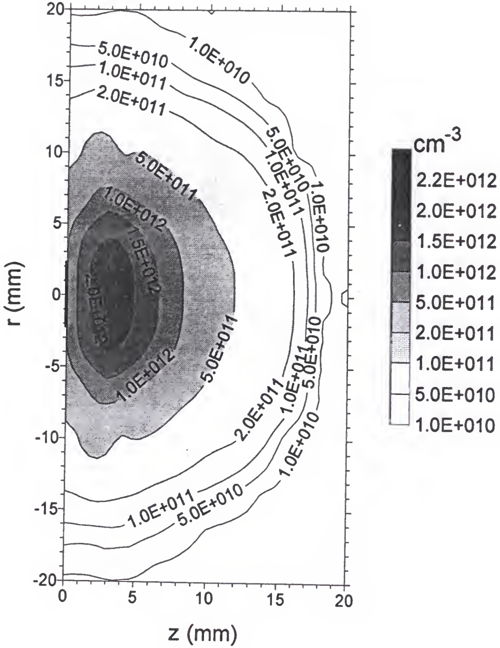

Figure 6-9. Experimental Ta atom density profile at 1200V, 1 torr and 2.45 mA, obtained by fluorescence measurements.

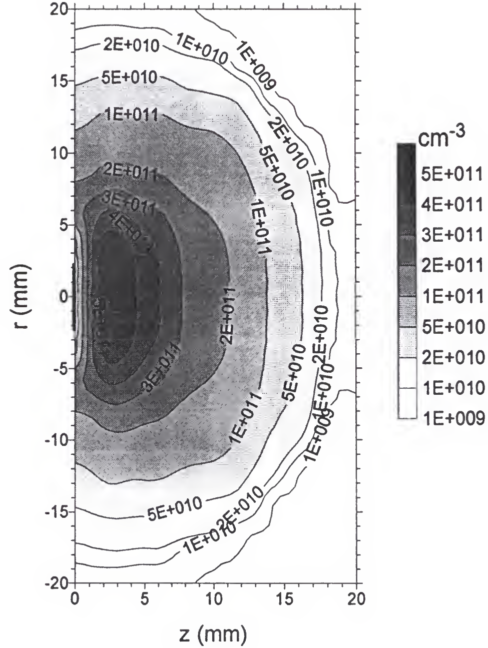

Figure 6-10. Experimental Ta atom density profile at 1000V, 0.7 torr and 1.2 mA, obtained by fluorescence measurements.

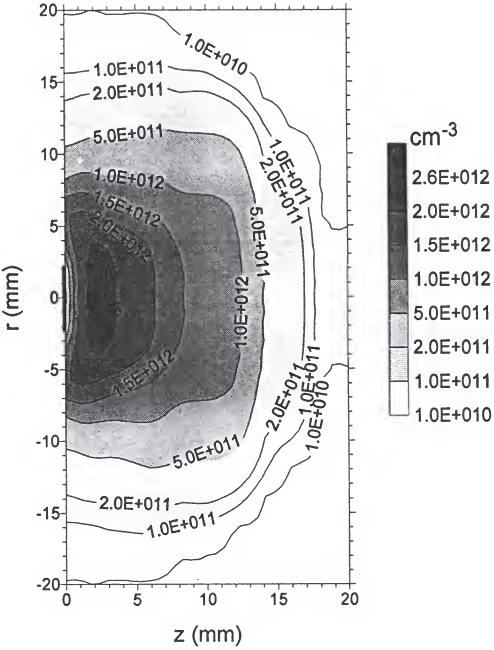

Figure 6-11. Experimental Ta atom density profile at 1000V, 1.6 torr and 3.9 mA, obtained by fluorescence measurements.

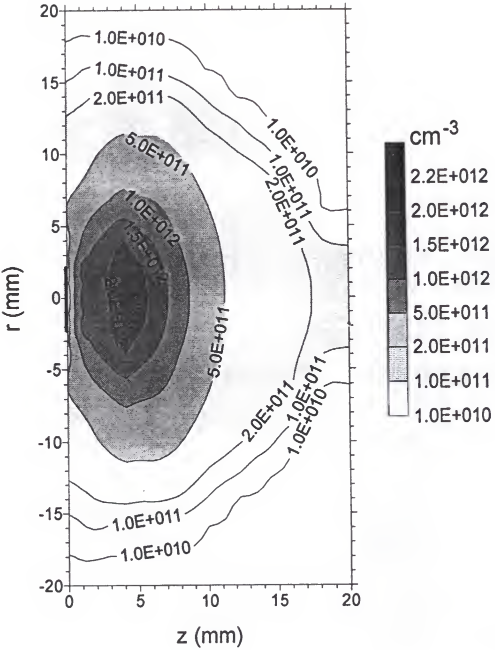

Figure 6-12. Experimental Ta atom density profile at 1000V, 1.3 torr and 3.0 mA, obtained by fluorescence measurements.

atom population is at a maximum a few mm away from the cathode. Indeed, a model where such an initial thermalization step is not included [115] cannot predict the dip in front of the cathode. Figures 6-13 through 6-19 show the three- dimensional Ta atom number density profiles at various pressures, currents, and voltages, obtained by the absorption measurements at approximately the same discharge conditions obtained by atomic fluorescence. The relative profile is the same since it results from the same fluorescence measurements. The absolute value of the atom number densities is a factor of 3 lower than those in the fluorescence experiment. This illustrates the magnitude of the relative errors encountered in these experiments.

In Figure 6-20, the Ta atom density profile resulting from the modeling calculations at 1000 V, 1 torr, and 2 mA is presented. Comparison of Figures 6-8, 6-15, and 6-20 show that the relative profiles of experimental and theoretical results are very similar. A maximum atom number density was also reached at a few mm from the cathode. The modeling results are slightly different only at the point $z = 0$. This is explained by the fact that, for simplicity sake, a cell wall was assumed at $z = 0$ in the model. However, in reality an insertion probe is used as the cathode and the glow discharge chamber also extended to negative z-values for $r > 2.25$ mm. The absolute value at the maximum of the calculated number density profile was a factor of 2 higher than the fluorescence results and a factor of 6 higher than the absorption results. However, at distances further into the discharge, the calculated result was in between the fluorescence and the absorption result. Indeed, the atom number density from the modeling seemed to drop somewhat more rapidly from the maximum than the experimental results. Taking into account the experimental errors and the approximations

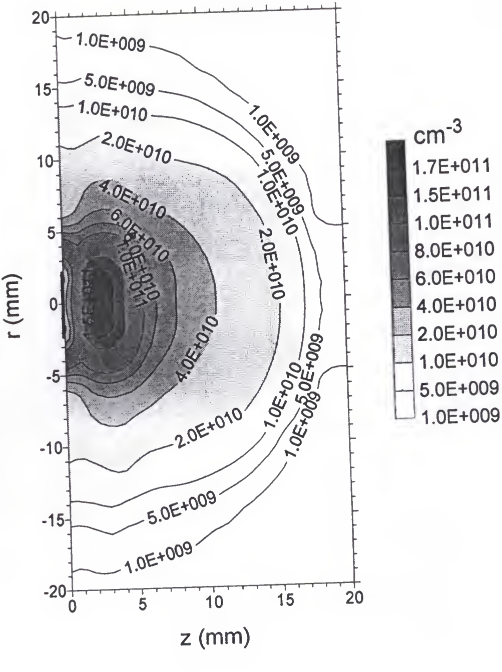

Figure 6-13. Experimental Ta atom density profile at 700V, 1 torr and 1.1 mA, obtained by absorption measurements.

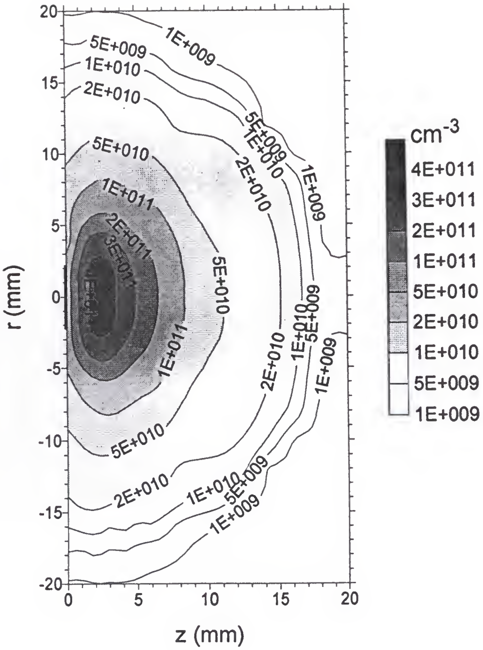

Figure 6-14. Experimental Ta atom density profile at 850V, 1 torr and 1.7 mA, obtained by absorption measurements.

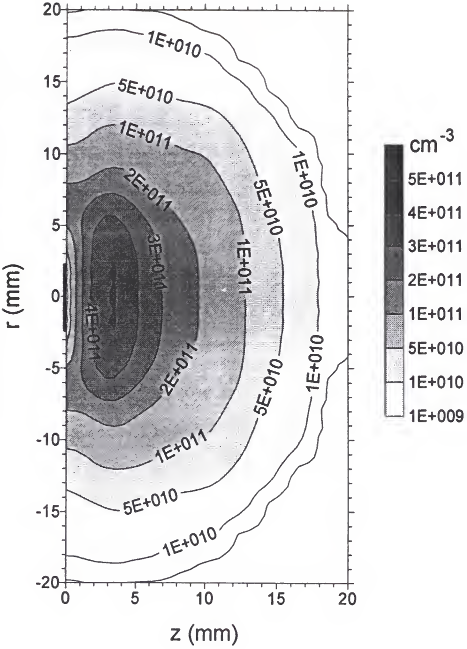

Figure 6-15. Experimental Ta atom density profile at 1000V, 1 torr and 2.0 mA, obtained by absorption measurements.

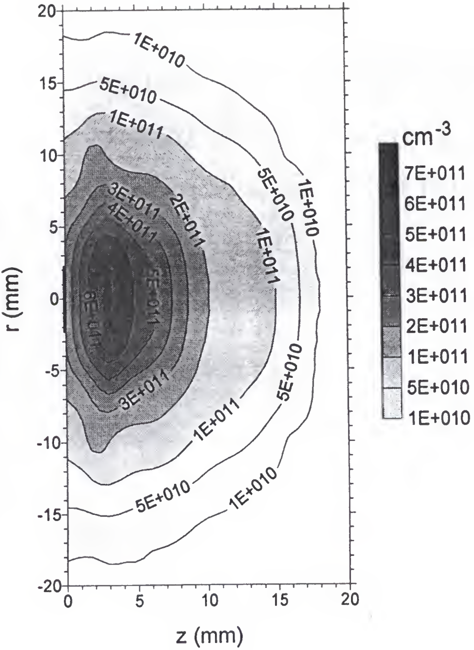

Figure 6-16. Experimental Ta atom density profile at 1200V, 1 torr and 2.5 mA, obtained by absorption measurements.

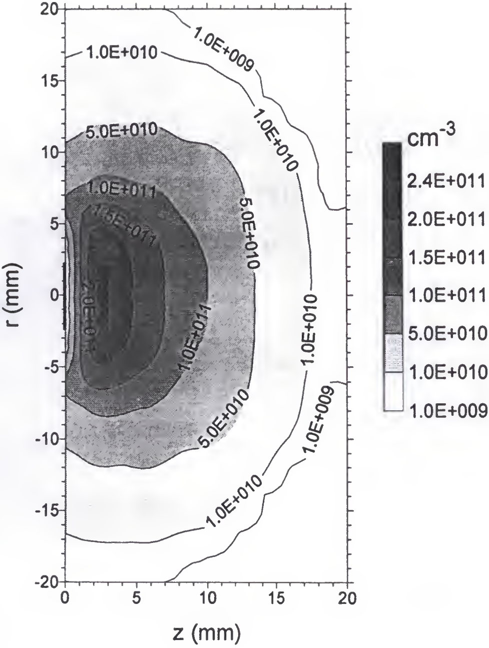

Figure 6-17. Experimental Ta atom density profile at 1000V, 0.7 torr and 1.0 mA, obtained by absorption measurements.

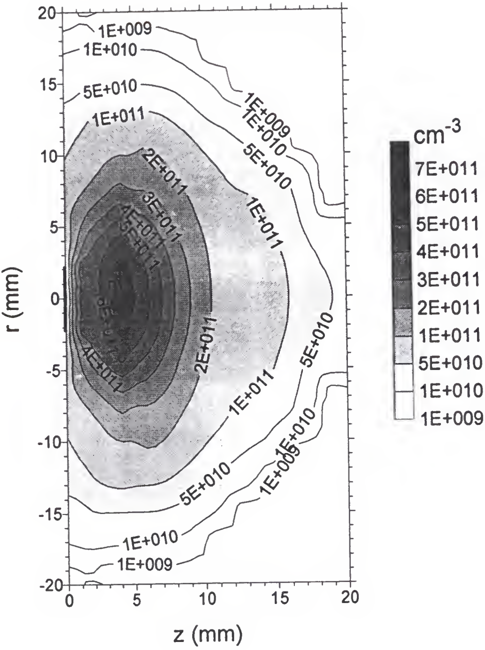

Figure 6-18. Experimental Ta atom density profile at 1000V, 1.3 torr and 3.0 mA, obtained by absorption measurements.

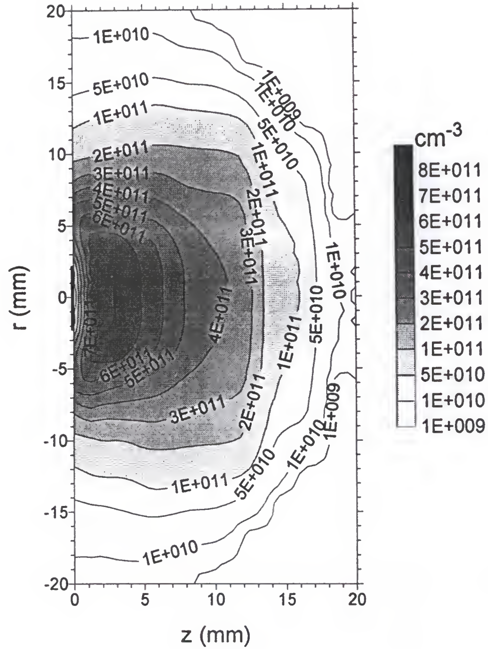

Figure 6-19. Experimental Ta atom density profile at 1000V, 1.6 torr and 3.8 mA, obtained by absorption measurements.

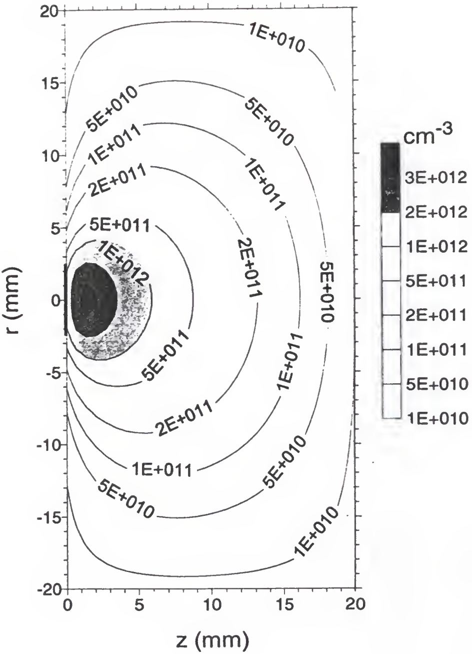

Figure 6-20. Ta atom density profile obtained by the modeling calculations at 1000 V, 1 torr, and 2 mA.

of the model, it can be concluded that an excellent agreement was reached between experiment and theory.

The number densities reported in the literature are generally higher than the values obtained in this work, about 1-5x10^{13} cm^{-3} for both a hollow cathode lamp [114,116] and a Grimm-type glow discharge [115]. However, both the hollow cathode lamp and the Grimm-type glow discharge operate at much higher currents so that higher sputtered atom number densities are expected. The results obtained with the COMAS technique [117,118], however, were lower than these results, about 10^{11} cm^{-3} for a hollow cathode lamp and about 10^{9}-10^{10} cm^{-3} for a plane parallel glow discharge.

To investigate the influenced of voltage, pressure, and current on the density profiles, the experiments were performed for a range of discharge conditions. Figures 6-21A and 6-21B show the one-dimensional density profiles at the cell axis at constant pressure for four different voltage and current values obtained by fluorescence and absorption. Also, Figures 6-22A and 6-22B present the one dimensional density profiles for four different pressures and currents at constant voltage by fluorescence and absorption. The shapes of the profiles do not appear to be influenced by the discharge conditions. However, the absolute values of the densities clearly increase with increasing voltage pressure and current. Indeed, at higher pressures and currents, there is a higher flux of plasma species bombarding the cathode leading to more sputtering and hence a higher sputtered atom population. At higher voltages, the energy of the bombarding plasma species is higher and also results in more sputtering.

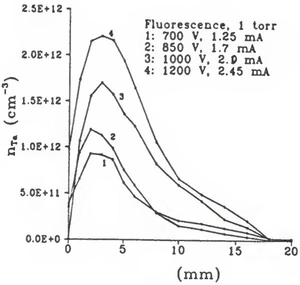

A

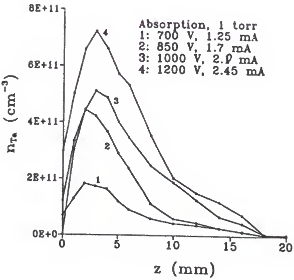

B

Figures 6-21. One-dimensional density profiles of the Ta atom along the cell axis at 1 torr for four different voltage and current values obtained by (A) fluorescence and (B) absorption.

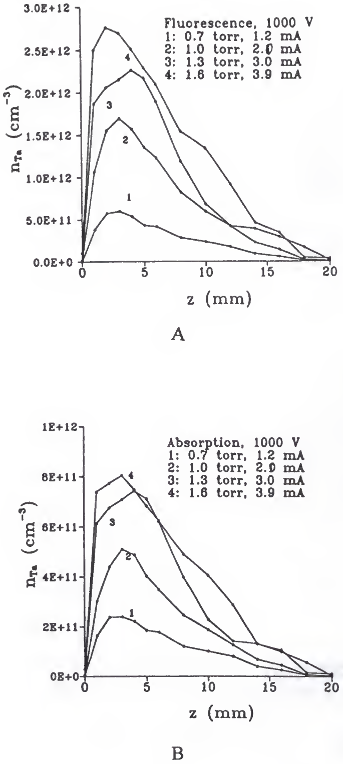

Figures 6-22. One-dimensional density profiles of the Ta atom along the cell axis at 1000 V for four different pressure and current values obtained by (A) fluorescence and (B) absorption.

Figure 6-23 through 6-29 show the three-dimensional density profile of the Ta ions at various pressures, currents, and voltages, obtained by fluorescence measurements. The Ta ion number density was low and rather constant in the cathode dark space, increased to a maximum at about 6 mm from the cathode, and decreased also toward the cell walls. The maximum number density profile shows excellent qualitative agreement with the result of the modeling calculations for the same discharge conditions presented in Figure 6-30. Indeed, the number density was low in the cathode dark space, and it reached a maximum at about 5-6 mm from the cathode. The fact that it was slightly different near the cathode was again due to the geometric approximations of the model. However, the absolute value at the maximum in the modeling result was almost a factor of 10 lower than the experimental result. In the model, the Ta ion number density was calculated from the Ta atom density taking into account three ionization processes; 1) electron impact ionization, 2) Penning ionization, and 3) asymmetric charge transfer. Since the Ta atom number density was in good agreement with the experiment, it seemed that the amount of ionization in the calculations was too low. Either one of the above mentioned ionization mechanisms was underestimated, or there were still other ionization pathways which were not incorporated in the model. The amount of electron impact ionization was determined by the electron flux and the cross section of electron impact ionization. Since the calculated electron flux was directly related to the calculated electrical current, and the latter one was in perfect agreement with the experimental 2 mA, it was believed that the electron flux was correct. The cross section of electron impact ionization was derived from a formula in reference 129, and this value was rather well known in the literature for different elements. Therefore, the amount of electron impact ionization was assumed to

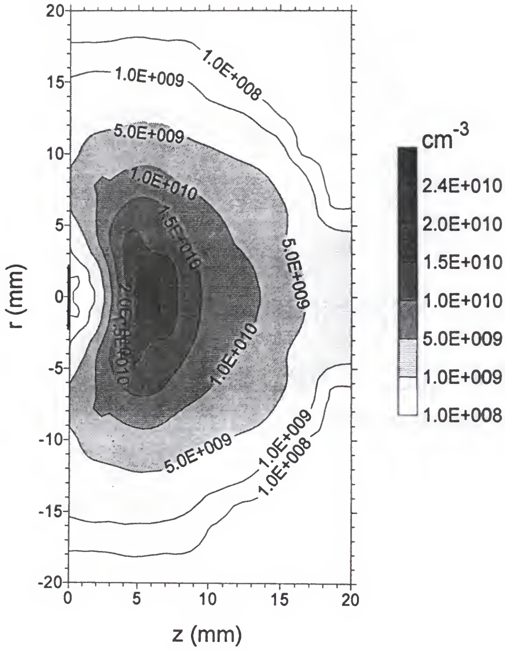

Figure 6-23. Experimental Ta ion density profile at 700V, 1 torr and 1.25 mA, obtained by fluorescence measurements.

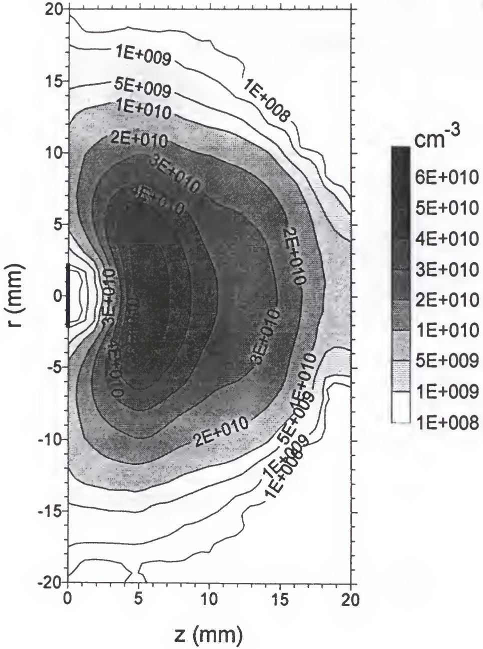

Figure 6-24. Experimental Ta ion density profile at 850V, 1 torr and 1.7 mA, obtained by fluorescence measurements.

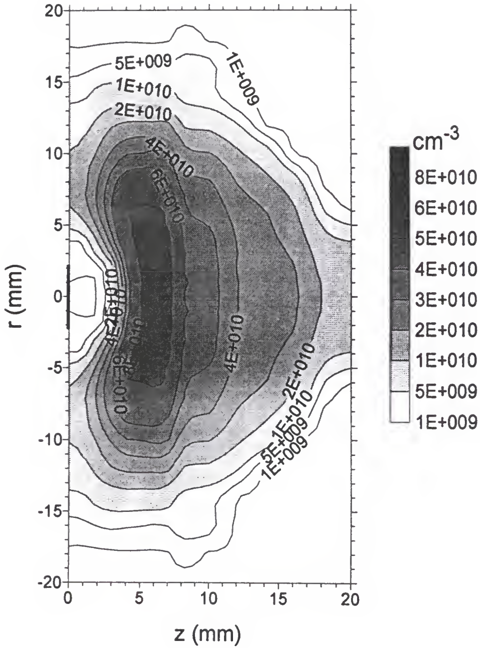

Figure 6-25. Experimental Ta ion density profile at 1000V, 1 torr and 2.1 mA, obtained by fluorescence measurements.

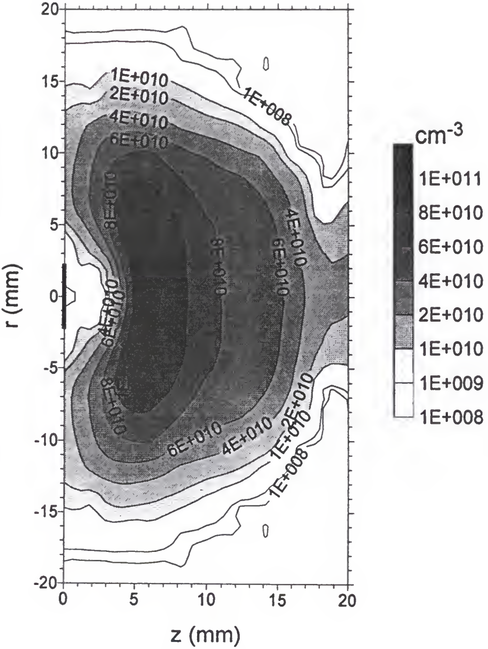

Figure 6-26. Experimental Ta ion density profile at 1200V, 1 torr and 2.45 mA, obtained by fluorescence measurements.

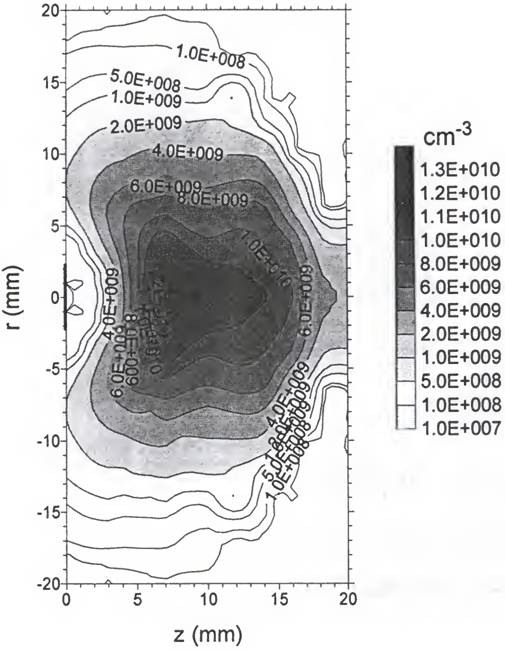

Figure 6-27. Experimental Ta ion density profile at 1000V, 0.7 torr and 1.2 mA, obtained by fluorescence measurements

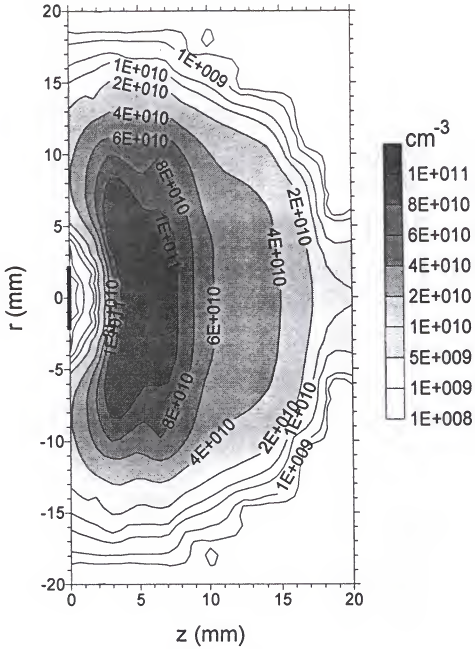

Figure 6-28. Experimental Ta ion density profile at 1000V, 1.3 torr and 3.0 mA, obtained by fluorescence measurements.

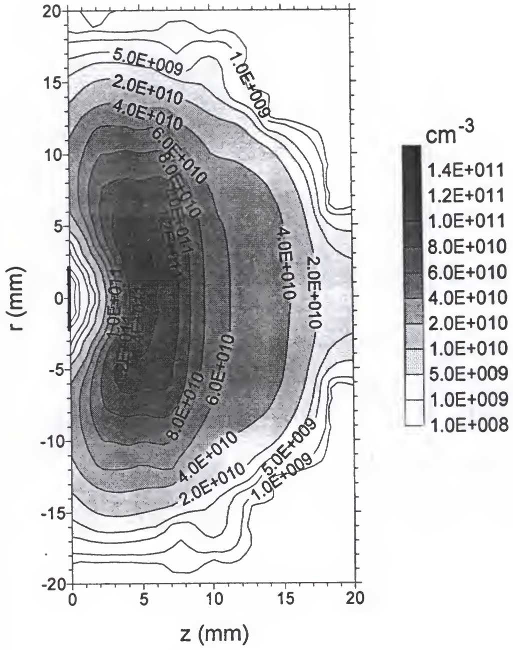

Figure 6-29. Experimental Ta ion density profile at 1000V, 1.6 torr and 3.9 mA, obtained by fluorescence measurements.

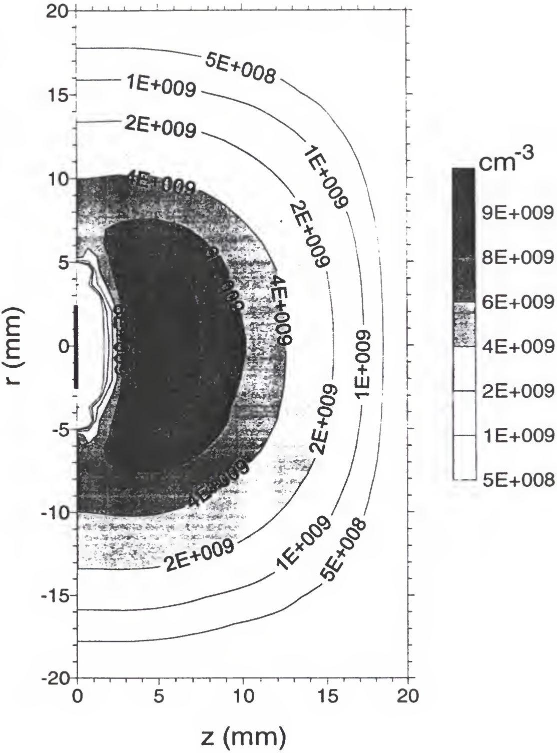

Figure 6-30. Ta ion density profile obtained from the modeling calculations at 1000 V, 1 torr, and 2 mA.

be calculated correctly. The amount of Penning ionization was given by the argon metastable atom density and the rate constant of Penning ionization. The calculated argon metastable atom density has been compared with experimental [130], and the absolute values showed satisfactory agreement. Close to the cathode, the modeling results were even too high compared with the experimental. Therefore, it is not very likely that the calculated argon metastable atom density was underestimated. The rate constant of Penning ionization was calculated from a formula in reference 131 to be 2.76×10^{-10} cm^3/s. A value on the order of 10^{-10} cm^3s^{-1} has been generally cited in the literature for Penning ionization of different elements. Hence, the amount of Penning ionization was also expected to be calculated correctly. The extent of asymmetric charge transfer depends on the argon ion density and the rate constant of this process. The argon ion density was also related to the total electrical current, and its value was therefore assumed to be also correct. The rate constant of asymmetric charge transfer between Ar ions and Ta atoms could not be found in the literature. In previous work [106], this rate constant was taken to be equal to the Penning ionization rate constant if the element possessed ionic energy levels suitable for asymmetric charge transfer, or lying close to the argon ion energy levels. An extensive study about the availability of such levels for most elements of the periodic table was made in reference 132. Ta was not included in this study since the Ta ion energy level scheme in the literature, the energy levels lying in the region of interest, were not recorded in reference 133. However, based on the periodic table, Ta belongs to the group of elements which possess many levels for asymmetric charge transfer. Therefore it was assumed that the rate constant of asymmetric charge transfer between Ar ions and Ta atoms was equal to the Penning ionization rate constant. Based on this assumption, it was calculated that the relative contributions of electron ionization, Penning ionization and asymmetric charge transfer at 1000 V, 1 torr, and 2 mA amount to about 1%, 8%, and 91% respectively. Hence, asymmetric charge transfer was calculated to be clearly dominant. Although in earlier reviews of GDMS, it has often been stated that Penning ionization was the dominant process and that asymmetric charge transfer only plays a secondary role. Some other papers demonstrate that this process was very important in a glow discharge for certain ion-atom combinations [134-142]. Due to the uncertainties in the rate constant, we have to be cautious about the role of asymmetric charge transfer. However, the fact that the calculated Ta ion density was too low compared to the experimental could indicate that this process was indeed important and may still be underestimated. In reference 116, a rate constant of 10^{-9} cm^3s^{-1} was used between Ne ions and Cu atoms. Using such a high rate constant would indeed give good agreement between the calculated and experimental Ta ion density. An alternative explanation for the discrepancy between experimental and theoretical would be that other ionization pathways were important which were currently neglected in the model. These include photoionization, ion or atom impact ionization, and dissociative ionization involving clusters of Ta. The latter assumption was not excessively unreasonable since Ta has a high affinity for oxygen. It may be possible that TaO molecules were dissociated and ionized into Ta^+ upon impact by electrons or other plasma species. However, since the necessary data to prove this, such as the TaO number density in the plasma and cross sections of possible alternative ionization processes were not available, this explanation remains only speculative. On the other hand, it was also possible that the difference between experiment and theory was due to the fact that the experimental results were too high. It is difficult to estimate the experimental uncertainties. From the experimentally constructed and calculated atom number density profiles, it was deduced that the error could be at least a factor of 3. It is very reasonable to believe that the discrepancy between theory and experiment was a combination of some limitation in the model and some experimental errors. After all, a factor of 10 difference between experiment and theory is not bad when it is considered that neither such experiments nor such modeling calculations have ever been performed.

The influence of voltage pressure, and current on the one-dimensional Ta ion density profile is illustrated in Figures 6-31A and 6-31B. In analogy to the Ta atom density, the absolute value of the Ta ion number density clearly increased with voltage, pressure, and current, but the shape of the profile remains rather unaffected.

Finally, from the ratio of the Ta ion number density to the Ta atom number density, the ionization degree of Ta can be deduced. Experimentally, a value of about 5% was obtained, whereas the modeling calculations predict a value of 1.7%. Hence, although the absolute values of the number densities were not in complete agreement between experiment and theory, the ratio of atom and ion number densities was in satisfactory agreement. These values were higher than general statements of 1% or less in the GDMS literature [98,99]. However, it would be dangerous to generalize the value of the ionization degree since it depends on specific atom-ion combinations, particularly asymmetric charge transfer, on the discharge conditions and on the cell geometry. In the cell of the VG9000 mass spectrometer, the same mathematical model yielded values of 0.1% and less for Cu [102].

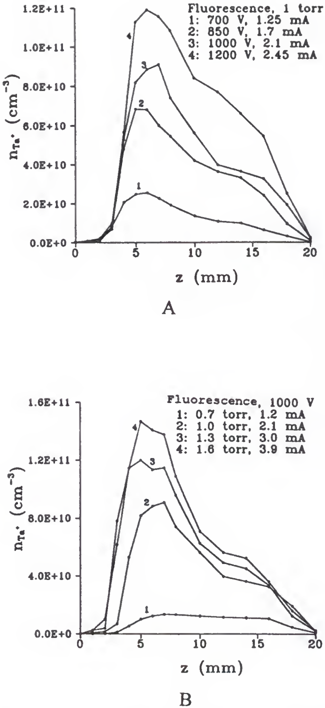

Figure 6-31. (A) The influence of voltage and current on the one-dimensional Ta ion density profile at 1 torr. (B) The influence of pressure and current on the one-dimensional Ta ion density profile at 1000 V.

Conclusions

Three-dimensional number density profiles of sputtered Ta atoms and Ta ions have been measured in a glow discharge by atomic fluorescence and absorption. The Ta atom number density reached a maximum at about 3 mm from the cathode and decreased gradually toward the cell walls. The results of the fluorescence and absorption measurements differ by a factor of 3 which illustrates the magnitude of the errors that can be expected for the present results. The Ta ion number density was low and rather constant in the cathode dark space and reached a maximum in the center of the negative glow at about 5-6 mm from the cathode. The influence of voltage, pressure, and current on the densities was investigated, and it was found that both the atom and ion number densities increased with voltage, pressure, and current. The experimental number density profiles have been compared with results of modeling calculations, and reasonable agreement was reached. The combination of both experiments and the mathematical modeling has never been performed before. Therefore, although perfect agreement has not been obtained, the results certainly give a better understanding of the glow discharge.

CHAPTER 7

ULTRATRACE DETERMINATION OF LEAD IN WHOLE BLOOD AND AQUEOUS SOLUTIONS USING ELECTROTHERMAL ATOMIZATION LASER EXCITED ATOMIC FLUORESCENCE SPECTROMETRY

Introduction

The detection of trace levels of lead in blood has been a challenging analytical problem of long standing interest [143]. Over the years the level of concern for lead in blood, as set by the CDC and EPA, has been lowered considerably. Presently the level is set at 100 ppb which is the level in which effects on the human body are first observed [144]. Most likely this level of concern will be lowered again. While these levels of blood lead levels are within the range of analytical techniques used today, the accuracy and precision of many routine techniques below this level become questionable. There is also a recognized need for measurements of substantially lower blood lead levels to establish the threshold of subclinical lead toxicity in humans. To date physiological relationships between lead doses and toxic responses have been primarily based upon individuals suffering from elevated exposure to lead [153]. It would be advantageous to develop an analytical method that can measure lead levels in blood as well as in the environment at concentrations well below the established levels of concern. In doing so, the option of monitoring and preventing lead concentrations before they reach a critical level of concern, is possible [154].

The most widely used methods include electrochemical techniques, such as anodic stripping voltametry [145], coulometric stripping potentiometry [146] and atomic absorption spectrometry [147]. Graphite furnace atomic absorption spectrometry is perhaps the most accepted technique and is widely used in clinical blood lead measurements [148-150]. The methodology, involving matrix modification with ammonium phosphate, nitric acid, and a surfactant is well developed and reliable at concentrations in whole blood above about 50 ng/ml. When lower detection limits are required, isotope dilution inductively coupled plasma mass spectrometry (ICP-IDMS) has been used [151]. When coupled with electrothermal sample introduction, this method has achieved a limit of detection of 16 fg [152]. However the difficulty of using and maintaining trace metal-clean techniques for any analytical method that requires matrix modification places it at a disadvantage for detection at these low lead levels.

Undoubtedly the most successful atom reservoir for laser excited atomic fluorescence spectrometry (LEAFS) has been the graphite furnace. Commercial furnace technology has been highly developed for use in atomic absorption spectrometry, is widely available and especially practical from the standpoint of sample introduction. Moreover, its adaptation for atomic fluorescence measurements is straightforward. Spatial interaction of the laser excitation with the atomic population is highly efficient in the furnace and practical optical detection of the fluorescence can be made with a pierced mirror in a 90° geometry. Absolute limits of detection in the low fg range have been obtained by several workers for a variety of elements. Lead is especially amenable to detection by ETA-LEAFS, having an easily accessible excitation wavelength at 283.30 nm and a strong direct line fluorescence which is well separated spectrally, at 405.7 nm. As early as 1974, Neumann and Kriese [155] obtained a limit of detection of 200 fg for lead in a furnace and since that time numerous studies have resulted in improvements which have made limits of detection of 1 fg for lead in aqueous solutions routine [156-159]. Up to the present, ETA-LEAFS has only been applied to the detection of lead in aqueous matrices. The purpose of the present study was to evaluate the performance of ETA-LEAFS in a carefully optimized experiment for the detection of lead in whole blood. The goal was to develop an approach involving a minimum of sample handling or treatment with the lowest possible limit of detection in this very complex matrix. Aqueous standards were used first to evaluate the experimental design and optimize all parameters. Theoretical calculations of the aqueous lead solutions were also developed to determine the future possibility of achieving absolute analysis with this technique and to lend credibility to the empirical results.

Experimental Design

This type of laser excited atomic fluorescence spectrometer has been described in several previous publications [156,160,161]. For these experiments, a copper vapor laser (Model CU15-A, Oxford Lasers, Acton, MA) was used to pump a dye laser (Model DLII, Molectron) at a repetition frequency of 9 kHz. Although this laser possesses the capability of operating at frequency repetition rates up to 12 kHz, the optimum pulse power has been found to be at approximately 9 kHz. The dye laser (Rhodamine 590, Exciton Corp., Dayton, OH) output was frequency doubled in a KDP crystal and the fundamental frequency filtered to obtain the 283.3 nm excitation line that was typically 1.2 μJ in a pulse duration of 4 ns (FWHM). The spectral irradiance necessary to saturate the 283.3 nm transition line can be estimated by the following equation [162]:

$$E_{theoretical} = \frac{6\times10^4}{Y}(W/cm^2nm) \qquad ; \qquad Y = \frac{A_{3,2}}{A_{3,2}+A_{3,1}} \qquad (1)$$

where Y is the quantum efficiency of the 405.8 nm transition line A_{ul} are the radiative transition probabilities for the $3 \rightarrow 2$ and $3 \rightarrow 1$ transitions. The experimental laser spectral irradiance can be calculated by the following equation:

$$E_{\exp erimental} = \frac{P}{\Delta t S \Delta\lambda}(W/cm^2nm) \qquad (2)$$

Where P is the laser pulse power, in J, S is the laser beam cross-sectional area, in cm^2, $\Delta\lambda$ is the spectral FWHM band width of the laser, in nm, and Δt is the FWHM pulse length, in s. From these calculations, it was found that

$$E_{\exp erimental} \approx E_{theoretical} = 1\times10^5(W/cm^2nm) \qquad (3)$$

These calculations also compared favorably to those obtained using the Densmat atom density matrix simulation program [123,124]. The following parameters were used to simulate the lead fluorescence scheme described previously.

Laser Profile	Scan Profile
Rectangular Pulse	End Time = 4 ns
3 ns in Duration	Resolution = 1 x 10^{-3}
7.476 x 10^{10} Hz band width	Oversampling = 12
10 Irradiance Scans from 1 to 1 x 10^{10} W·cm^{-2}	

Energy Level Profiles

Coupled Levels	Wavelength	Spontaneous Emission
1→3	283.3 nm	5.8×10^7
3→2	405.8 nm	9.0×10^7

However, the uneven energy distribution within the laser beam as well as any collisional deactivation not incorporated into this simple model, does not permit saturation over the entire beam area. Therefore, the necessary pulse energy to saturate the 283.3 nm transition line was not obtained over the entire analytical volume. Smith et. al. [163] have also empirically determined the validity of these calculations. The beam was focused through a 4 mm diameter hole in a plane mirror and into the graphite furnace (Perkin Elmer, Model HGA-400, Norwalk, CT) by a 25.4 cm focal length fused silica lens (Figure 7-1). The furnace was modified by replacing the conventional windows with 1 mm thick fused silica windows mounted at 45° to minimize laser scatter into the monochromator. Pyrolytic graphite furnace tubes with L'vov platforms were used for atomization. In the furnace, the laser beam was rectangular in shape, due to frequency doubling, with dimensions approximately 4 mm wide and 0.5 mm in height. The pierced plane mirror was positioned at 45 ° from the laser and approximately 9 cm in front of the furnace. The emitted fluorescence was imaged onto the monochromator (Model 340E, 340 mm focal length, F/n = 5.9, 1200gr/mm holographic grating, Spex, Edison, NJ) entrance slit by a matched pair of 8 in focal length biconvex fused silica lenses. The monochromator was positioned on its side so that the slit geometry would match that of the laser beam which appeared as a horizontal rectangle. The slit width was 0.5 mm and the height was masked

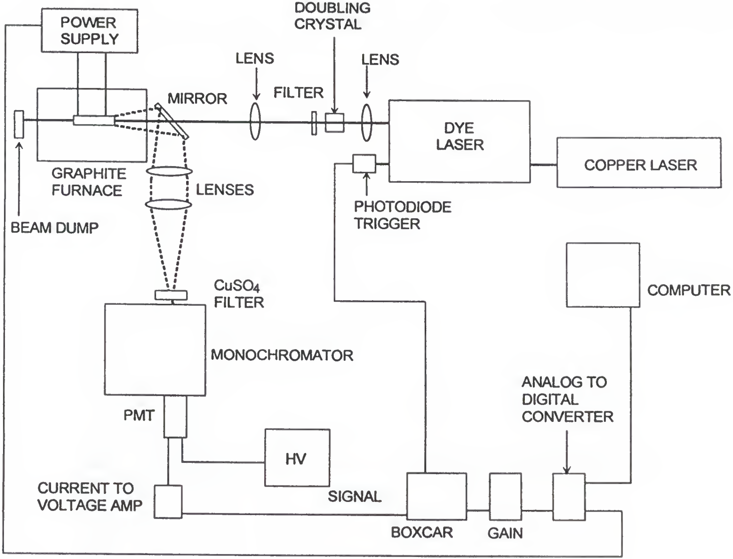

Figure 7-1. Experimental design for ETA-LEAFS.

to 4 mm to match the laser beam geometry as well as to minimize the detection of blackbody emission from the furnace. A 1 cm path length solution filter (100 g/L $CuSO_4$ in water) was placed in front of the entrance slit to eliminate laser scatter, and neutral density filters were used as necessary to maintain detector linearity. The signal was detected with a PMT (R928, Hamamatsu Corp., Bridgewater, NJ) and the current pulse from the PMT was converted to a voltage pulse using a simple laboratory constructed transimpediance amplifier which consisted of an OP-37 operational amplifier (Precision Monolithics, Inc., Santa Clara, CA) with a 10^4 kΩ feedback resistor in parallel with a 15 pF capacitor. This circuit was powered by two 9V batteries. The signal was then processed with a boxcar integrator (SR245, Stanford Research, Sunnyvale, CA) and interfaced to a personal computer. Blood reference materials were obtained from the Center for Disease Control and Prevention Blood Lead Laboratory Reference System (CDC-BLLRS) and from the National Institute of Standards and Technology (NIST).

Experimental Results and Discussion

Initial studies were performed with aqueous lead solutions to determine the capabilities of the instrumentation. Figure 7-2 shows the excellent linearity achieved over several orders of magnitude. This is typical for laser induced fluorescence. The extrapolated instrumental limit of detection is 6 ag. The blank limit was several orders of magnitude above this but could easily be improved with clean room conditions. On this smaller linear calibration curve (Figure 7-3) excellent correlation and precision of the instrumentation was observed. To utilize the great detection sensitivity in blood samples the whole blood samples must be analyzed without any matrix modifier. Conventional blood sample preparation techniques used for graphite furnace atomic absorption involve

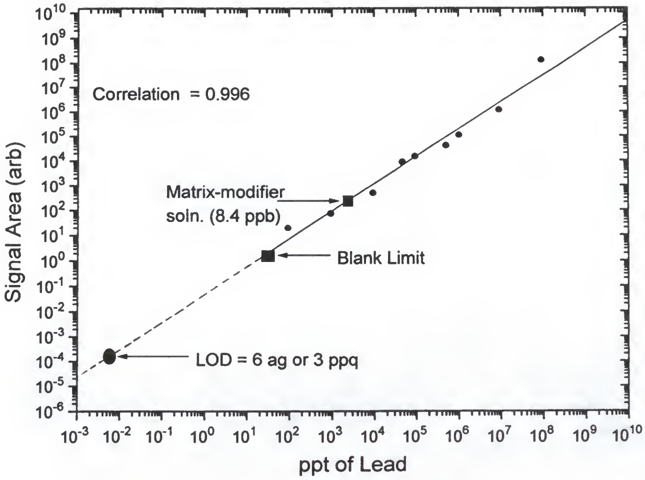

Figure 7-2. Logarithmic calibration curve for aqueous lead. The measured linearity spans seven orders of magnitude.

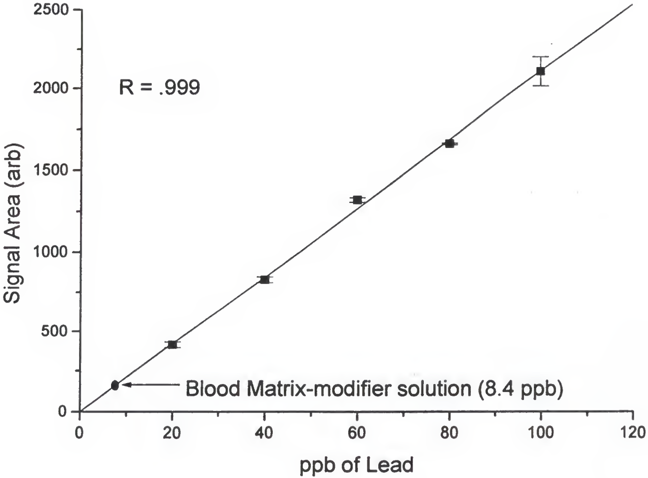

Figure 7-3. Linear calibration curve for aqueous lead for one orders of magnitude.

a 1:10 dilution of the whole blood with a matrix modifier solution containing 0.2 % w/v $NH_4H_2PO_4$, 0.5 % v/v Triton X-100, and 0.2 % HNO_3 in ultrapure water [147-149]. However, in order to make full use of the extremely high sensitivity of the ETA-LEAFS technique, the use of a matrix modifier needed to be eliminated due to its relatively high level of lead contamination of approximately 8 ppb. Instead, the CDC blood lead standards were not modified in any way for the initial studies. The furnace program used in the initial studies involved two drying steps, an ash or pyrolysis step, atomization , and a cleaning step as shown in Table 7-1A. The fluorescence peak profiles obtained for a 2 μl injection of whole blood lacked precision as well as intensity as shown in Figure 7-4A. Further evaluation of these peak profiles revealed that a fluorescence signal was present during the ashing step. This observation led to the elimination of the ashing step and the second drying step was extended in duration (Table 7-1B). The new furnace program resulted in fluorescence peak profiles that were 1.5 s FWHM with a reproducible shape and good intensity (Figure 7-4B). However, the poor precision for the 2 μL whole blood injections was not acceptable. A large part of this poor precision was due to the difficulty encountered when attempting to pipette the very viscous whole blood into the furnace. The imprecision may also be due to the strong lead-organic complexes formed in blood and the viscosity of the whole blood, which may not allow complete atomization of the lead. Instead, to make the blood easier to pipette, the whole blood was diluted 1:21 with purified water to reduce the viscosity (Millipore, Marlborough, MA) and was run 5 times for each blood sample. This sample preparation method resulted in an average within run precision of 3.7 % for the certified lead in blood standards.

Table 7-1. Parameters for the PE HGA-400 Graphite Furnace.

A. Setup for Initial Studies with 2 µL Injection of Whole Blood.

	Dry	Dry	Ash	Atomization	Clean
Temperature °C	180	260	850	1900	2600
Ramp (s)	5	5	5	0	1
Hold (s)	10	10	20	8	4
Ar flow (30 ml/min)	ON	ON	ON	OFF	ON

B. Final Program for 10 µL Injections of Whole Blood Diluted 1:21 with Millipore Water.

	Dry	Dry	Atomization	Clean	Cool	Clean
Temperature °C	180	260	1900	2500	20	2600
Ramp (s)	5	5	0	1	5	1
Hold (s)	10	35	8	4	10	4
Ar flow (30 ml/min)	ON	ON	OFF	ON	ON	ON

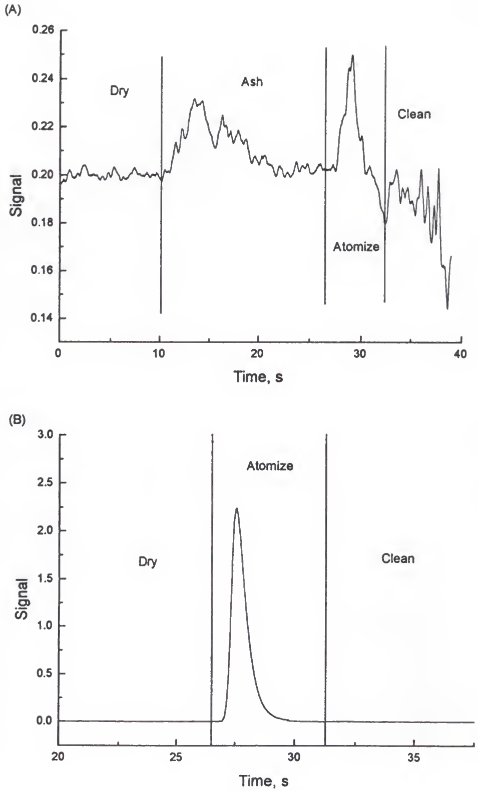

Figure 7-4. (A) Typical fluorescence signal for lead in blood before the elimination of the ash step in the furnace program. Note that a fluorescence signal was present during the ashing step. (B) Typical fluorescence peak shape for a 10 μL injection of 50 ppb lead blood sample after elimination of the ash step in the furnace program.

The CDC blood standards were compared to a calibration curve constructed with aqueous lead standards (Figure 7-5). The fluorescence signal intensity for a blood sample was approximately 20% lower than for an aqueous standard with the same lead concentration. The reduced signal with blood samples was assumed to be caused by the smoke generated from the sample as it was heated to the atomization temperature. As the smoke filled the analytical volume, it would attenuate the laser beam as well as the fluorescence. To test this hypothesis, a photodiode was positioned after the furnace in the path of the laser. The laser intensity was then monitored throughout a typical run for aqueous solutions and whole blood solutions that were diluted to various ratios using ultrapure water. 10 μL of each of these solutions was injected into the furnace. Figure 7-6 shows the obvious decrease in laser intensity for the blood samples during the atomization step. This fluctuation coincided with the evolution of the smoke and with the appearance of the fluorescence peak (Figure 7-7). The slight increase in laser intensity prior to the atomization step coincided with the stopped argon flow before this step. The decrease in laser intensity for the blood samples was directly proportional to the absolute amount of blood contained in the sample and the amount of smoke generated by the sample. From these observations and experiments, it was concluded that the decreased signal of the blood samples as compared to the aqueous standards could be corrected by using the photodiode, which measured the laser intensity, as a scaling factor. This was achieved by incorporating a two channel signal processor system in which the fluorescence signal in channel one was divided by the laser intensity fluctuation measured in channel two. This signal correction process was used on the blood samples, which were diluted 1:21 with ultrapure water, as well as the aqueous solutions to account for any laser

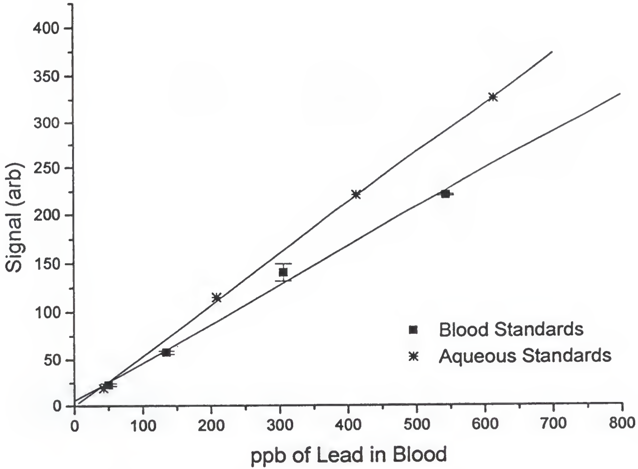

Figure 7-5. Correlation of aqueous standards with blood standards diluted 1:21 with Millipore before laser absorption correction.

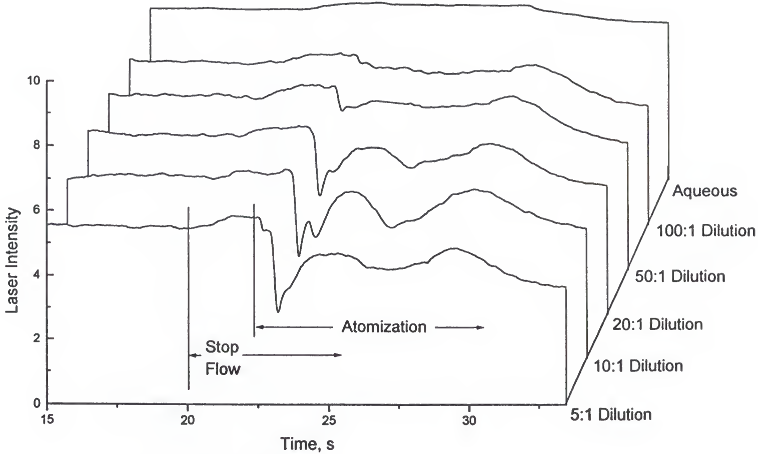

Figure 7-6. Comparison of laser intensity after exiting the furnace during a typical run for 10μL injections of aqueous samples and whole blood diluted to various ratios.

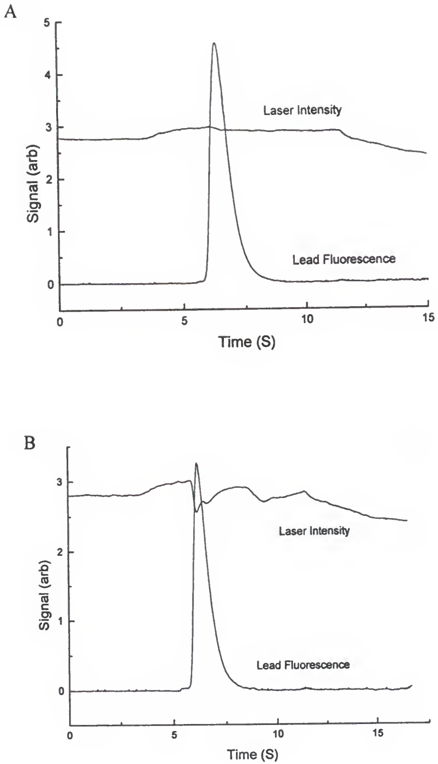

Figure 7-7. The coincidence of the laser fluctuation with the appearance of the fluorescence peak for (A) a 30 ppb aqueous lead solution and (B) a 25 ppb blood sample.

intensity variance. The results of this process, Figure 7-8, proved that the signal attenuation of the blood samples was due to the evolution of smoke in the graphite furnace. The two channel measurement technique provided a good correlation between aqueous and blood matrices for the measurement of lead.

A blood matrix calibration curve was constructed using the CDC lead in blood standards and the NIST lead in blood standards (SRM 955a, 1-4) were treated as unknowns (Figure 7-9). The lead concentrations obtained were compared to the certified values. The NIST standards were also evaluated by the standard addition method. Each NIST sample was measured after the 1:21 dilution with Millipore water and then after each of three subsequent spikings with an aqueous lead standard. The linear regression curve fit correlation was better than 0.999 for the four NIST standards (Figure 7-10). The lead values obtained for this method are reported in Table 7-2 and correlate well with the certified values and the values obtained by the calibration curve method. Finally, the 3σ LOD for lead in blood was calculated to be 10 fg/ml, or 100 ag absolute. This is 7 orders of magnitude lower than the current level of concern for lead in blood and 2 orders of magnitude lower than the current technique of ICP-IDMS, used by the CDC and NIST, which involves a complicated chemical treatment.

Theoretical Calculation of the Aqueous Lead Signal

To lend some credibility to the sensitivity and detection power of this instrumentation, a first approximation equations has been developed and these theoretical values are compared with the experimental values. This type of approach has also been used by others in past publications [32,38,163]. The approach involves three parts or separate calculations and is based on peak height, not area as in the actual experiments.

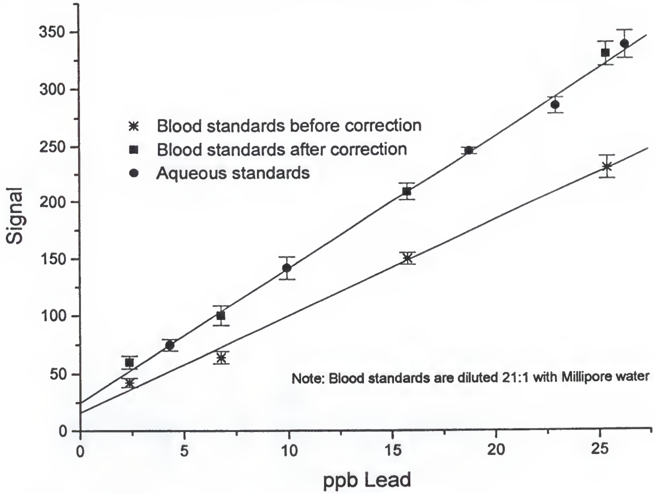

Figure 7-8. Correlation of aqueous standards with blood standards diluted 1:21 with Millipore water before (*) and after (■) correction of laser intensity.

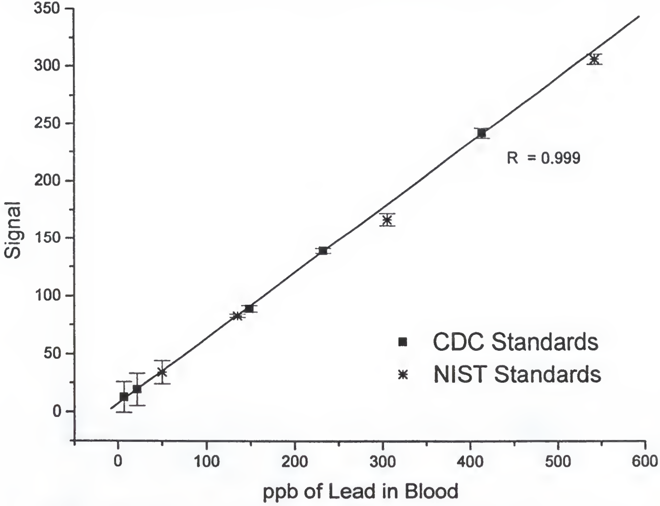

Figure 7-9. Calibration curve constructed using CDC certified standards. The NIST certified standard values were plotted to compare the accuracy of the ETA- LEAFS technique.

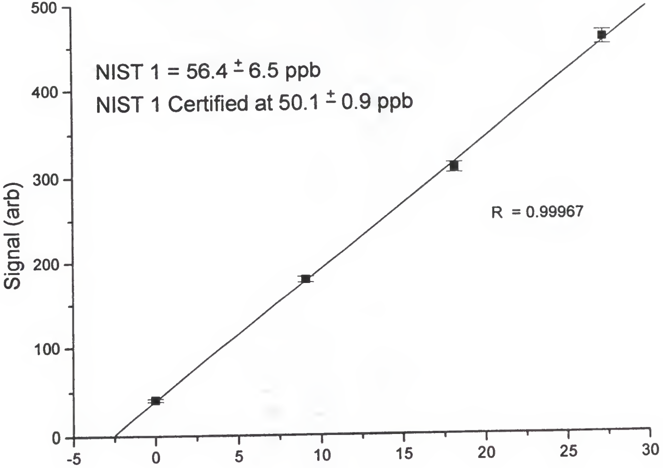

Figure 7-10. Typical standard addition calibration curve for NIST 1 blood standards.

Table 7-2. Comparison of Lead in Blood NIST Standards with Values Obtained In These Studies (ppb) .

Nist Sample #	NIST Certified	Calibration Curve	Standard Addition
455a-1	50.1 ± 0.9	48.1 ± 2.45	56.6 ± 2.6
455a-2	135.3 ± 1.3	134.4 ± 0.94	125.7 ± 7.1
455a-3	306.3 ± 3.2	283.0 ± 7.5	287.1 ± 12.7
455a-4	544.3 ± 3.8	530.3 ± 12.2	530.7 ± 23.7

These calculations are; 1) the maximum atom density in the furnace, 2) the optics throughput efficiency and signal processing, and 3) the calculation of the number of photons produced per atom per pulse of the laser beam. The result should be within a factor of 5 of the experimental value, due to uncertainty in the values used for the calculation.

Atom Density Calculation

The main assumption that must be made was that the atom density was uniform in the graphite furnace. The atom density in the furnace was then calculated according to the sample size and concentration. A 2 μL, 20 ppb aqueous lead sample was used for these calculations. Using the ratio of the furnace volume (2.08 cm^3) to the analytical volume (0.007 cm^3), defined by the focused laser spot size and the slit height and width, it was determined that there are 1.16×10^{11} atoms in the furnace and 3.9×10^{8} atoms in the probe volume.

Signal Processing Calculation

Next the throughput of the optics and the voltage gain of the signal processing, SP, must be determined by the equation shown below.

$$SP = \frac{\Omega}{4\pi} n_T n_{PMT} Ge \frac{R}{\Delta t} \tag{7-1}$$

The solid angle of collection of the fluorescence is $\Omega/4\pi$, n_T is the transmission efficiency of the optics and the monochromator, n_{PMT} is the quantum efficiency of the PMT, G is the gain of the PMT, e is the charge on an electron, and R is the gain of the transimpediance amplifier.

Determination of the Number of Photons

The final calculation is the number of photons produced per atom per laser pulse. The expression is shown below [163]:

$$N = \left[1 - e^{-(n_s A_{32} t_l)}\right] \tag{7-2}$$

where t_l is the laser pulse length, A_{32} is the spontaneous transition coefficient, and n_s is the saturation parameter which is expressed by the equation below:

$$\left(\frac{g_3}{g_3 + g_1}\right)\left(\frac{I_\lambda}{I_\lambda + I_\lambda^S}\right) \tag{7-3}$$

where g_3 and g_1 is the degeneracy of the respective energy levels, and I_λ is the laser energy, and I_λ^S is the energy necessary to saturate the lead energy level at 35287 cm^{-1} from the ground state (283.3 nm). In the argon atmosphere, the collisional deactivation from this level has been experimentally determined by measuring the fluorescence lifetime and comparing it to the theoretical lifetime. The difference between these two values was found to be insignificant, thus, the collisional deactivation is negligible. The losses from the energy level are predominately due to spontaneous emission. Therefore, in order to saturate the energy level, the radiative rate of the laser must be larger that the spontaneous emission coefficients in order to saturate the energy level.

Theoretical Results Compared to Experiment

Multiplying these three parts of the equation together a signal, based on peak height, of 12 V for a 2 μL 20 ppb aqueous lead sample has been determined Experimentally, the peak height for this concentration of lead was found to be 18 V. The calculations, although simplistic, lends credibility to the experimental values and the great

---

sensitivity and limit of detection achieved with this instrumentation.

Conclusions

The good precision and accuracy of the values for lead in blood obtained by ETA-LEAFS in these studies is within the same range as furnace atomic absorption spectrometry [147-150] and is comparable to ETV-ICPMS [152,164]. The small volume needed for analysis combined with the extremely low detection limits make it a good alternative to ETV-ICPMS when the sample size is limited. Furthermore, the ability to detect the analyte of interest in a complex matrix without complicated sample preparation reduces the possibility of contamination and is an important advantage over ETA-AAS and ETV-ICPMS. The cost of this type of setup is competitive ($100K-$150K) when compared to ICP systems ($170K-$500K). This may still seem a little expensive since ETV-LEAFS is a single element analysis method. However, ETA-LEAFS is able to detect ultratrace levels of lead in blood and does not require blood reference standards for calibration. This is not possible with any other analytical method available. Also, it is no more complicated to use than AAS or ICP instruments and every part of the ETV-LEAFS setup is commercially available. In fact, with respect to sample preparation, it is a much simpler method. The ability of the two channel system to correct for the blood matrix and laser variations and correlate the blood standards to the aqueous standards simplifies the calibration curve process and eliminates the need for blood standards for this technique. The good correlation achieved between blood and aqueous solutions by using the two-channel background correction approach proves that the signal attenuation was due to the evolution of smoke which resulted in fluorescence signal attenuation and was not due to fluorescence quenching by the smoke or other interferences. Also any variations that may occur due to differences in blood matrices can also be corrected by using this method. The advantages of this system as compared to ETA-AAS or ETV-ICPMS makes it a viable option for detection of lead in blood, especially at extremely low levels. Finally, the ability of the theoretical calculations to be within a factor of 5 of the experimental value, gives this technique the possibility of absolute analysis; the capability of providing quantitative results without the use of standard reference materials or a calibration curve.

CHAPTER 8
FUTURE CONSIDERATIONS

Much of the research in this dissertation still has many areas that should be explored. The construction of a DMD spectrometer was certainly novel. The future development of this project hinges on Texas Instrument's, Inc. interest. Without constructing a DMD chip that is designed specifically for this application, there will be no development of this instrument. There are important advantages that this spectrometer possesses over other spectrometers. The cost of the instrument would be very low, the resolution could be on the sub-nm scale, it has the possibility of scanning a complete UV-visible spectrum in a few milliseconds, and it can scan a specific range of wavelengths without collecting the entire spectrum. The DMD spectrometer has the capability of random pixel access, just like a CCD, but without the expense, since the DMD spectrometer uses a PMT for detection. The DMD spectrometer can be made to be rugged and portable and does not require cooling since it uses a PMT for detection. A possible competitor to the DMD spectrometer has been developed by Ocean Optics, which also has the advantages of low cost, and portability. However, the Ocean Optics spectrometer suffers from poor optical throughput and is only capable of 1 nm resolution. The advantages that the DMD spectrometer has over the Ocean Optics spectrometer, it's closest competitor, are important, and still makes the DMD spectrometer worth further investigation and development.

The detection of silicon using a continuous introduction method into the discharge chamber has practical merit. In the semiconductor production industry, in is important to analyze both air and water samples for levels of silicon. Mass spectrometry can certainly provide the precision, accuracy, and detection sensitivity necessary for the semiconductor industry. However, the cost of such a system is rather high. The emission spectroscopy method developed and used in this research does not exceed the capabilities of mass spectrometry in any way except for cost. For the emission spectroscopy method to become practical, the detection sensitivity needs to be improved. Also, a continuous sample introduction method must be developed which can essentially dry the aqueous Si sample before entering the discharge chamber. Some work has already been accomplished in this area by Horlick *et al.*[59] Until these two problematic areas are addressed, this technique holds little practical significance regardless of it's cost advantage.

The results of the number density profiles of Ta and Ta^+ were excellent and fit well with the current knowledge base about atom density profiles in a glow discharge as well as with the simulated density profiles conducted by Bogaerts *et al.* Future fundamental studies on glow discharge should focus on determining the reasons for the maximum number density lying a few mm away from the cathode surface instead of adjacent to it. Two possible hypotheses are; 1) the sputtered atoms for the cathode are coming off as clusters and do not completely atomize until they reach the high collision area of the negative glow region, and 2) the atoms are sputtered off of the cathode as an excited species and must return to the ground state before fluorescence can occur. It would also be interesting to repeat the experiment in this dissertation with discharge chambers of varying size and geometry to elucidate the influence of the chamber geometry upon the discharge and the atom and ion number densities. One final experiment of interest would be the measurement of the spatial and temporal sputtered atom and ion densities with the microsecond pulsed discharge system described in this dissertation. This could be accomplished by absorption measurements or by fluorescence with the use of a continuous laser system.

The ETA-LEAFS analytical technique is a very promising for the use in ultratrace elemental analysis. The ability to measure trace Pb levels in blood, one of the most complex matrixes, lends credibility to the possibility of conducting elemental analysis for other complex matrices such as sea water, soil samples, oils, and other body fluids. There are some restrictions when choosing an element of study. The element must have a ground state transition that is within the range of the laser used for the excitation energy. For the copper vapor laser pumped dye laser system used in these experiments the best range of wavelengths is between 267 nm and 295 nm. This is the range in which the energy of the frequency doubled output from the dye laser sufficiently populates the upper energy level so that fluorescence may be observed. Of course, there must be good transition probability coefficients for the two connected levels. It may be possible to excite atoms at wavelengths outside of this range if the copper vapor laser power is improved. Presently, the copper vapor laser is capable of 6.5 W at a 9kHz repetition rate but is rated to 12.5 W. The detected fluorescence of the element should be below 450 nm. Above this wavelength, the blackbody radiation of the furnace is too intense and results in saturating the detection electronics. Blackbody radiation intensity is related to the temperature by the following equation.

$$T = (BB_r)^4 \qquad (8\text{-}1)$$

Therefore, it is extremely important to use the lowest temperature possible that still sufficiently atomizes the element of interest. If an element has an atomization below 1800 °C, it may be possible to detect fluorescence above 400 nm without saturating the detection electronics. However, it is recommended that an element to be studied should be excited between 267 nm - 295 nm and have a fluorescence transition below 400 nm. This seems to limit the number of elements that could be detected by ETA-LEAFS. However, in actuality, there are still many elements to study that fit into these rather strict parameters. Some of the possibilities are, Tl, Pt, Pd, Ge, Hf, Y, Eu, Tm, Ru, Rh, Re, Ta, and Ga. This is certainly not a complete list but gives the reader an idea of possible avenues of research using this method. Pt is probably the one element in this list that should be investigated. It is used in automotive catalytic converters, and has been found at elevated toxic levels in roadside soil and water. It is important that research is conducted to investigate the use of matrix modifiers to aid in the atomization of elements. Some investigation into the possibility of ETA-LEAFS analysis above the furnace has been conducted. By probing the effluent of the fill gas just above the dosing hole on the outside of the graphite tube, the blackbody background can be virtually eliminated. This allows this ability to detect fluorescence at any wavelength within the range of the detector. However, the furnace would need to be enclosed by a argon atmosphere. Otherwise, the exposed area of the graphite tube oxidizes and degrades quickly. The analyte exiting the furnace with the argon fill gas also oxidizes quickly. Poor result have

---

been obtained using this method without surrounding the furnace in an argon atmosphere. However, Gornushkin *et al.* have obtained excellent results for silver, with an experimental setup very similar to this one, when an argon atmosphere was used [165]. There is also the possibility of studying U and Pu. This would be an excellent area to investigate since ETA-LEAFS may be developed into an absolute analysis technique eliminating the need for standards which, in the case of U and Pu, can be expensive as well as hazardous. Also, if a dye laser with a narrow bandwidth is used, isotopic ratio analysis of these two elements may be possible. By tuning back and forth between the two different excitation wavelengths of the specific isotopes, the isotopic ratio can be determined by the ratio of the fluorescence peak areas.

APPENDIX A
ACRONYMS USED IN TEXT

AAS - Atomic Absorption Spectroscopy

AES - Atomic Emission Spectroscopy

AFS - Atomic Fluorescence Spectroscopy

CDC - Centers for Disease Control and Prevention

COMAS - Concentration Modulated Absorption Spectroscopy

DC - Direct Current

DMD - Digital Micromirror Device

EAEI - Excitation of Atoms by Electron Impact

ETA - Electro-Thermal Atomization

FANES - Furnace Atomic Non-thermal Excitation Spectrometry

FWHM - Full Width Half Maximum

GD - Glow Discharge

GF - Graphite Furnace

ICP - Inductively Coupled Plasma

LEAFS - Laser Excited Atomic Fluorescence Spectroscopy

LIF - Laser Induced Fluorescence

MP - Microsecond Pulse

MS - Mass Spectrometry

NIST - National Institute of Standards and Technology

PMT - Photo-Multiplier Tube

RF - Radio Frequency

APPENDIX B
LIST OF PERSONAL PUBLICATIONS AND MANUSCRIPTS

Presentations

Ultratrace Determination of Lead in Whole Blood Using Electrothermal Atomization Laser Excited Atomic Fluorescence Spectroscopy, March 4, 1996, Pittsburgh Conference, Chicago, IL.

Publications and Manuscripts

Three-Dimensional Density Profiles of Sputtered Atoms and Ions in a Direct Current Glow Discharge: Experimental Study and Comparison with Calculations. Bogaerts, A.; Wagner II, E. P.; Smith, B. W.; Winefordner, J. D.; Pollmann, D.; Harison, W. W.; Gijbels, R. Submitted, *Spectrochimca Acta B.*

Ultratrace Determination of Lead in Whole Blood Using Electrothermal Atomization Laser Excited Atomic Fluorescence Spectroscopy. Wagner II, E. P.; Smith, B. W.; Winefordner, J. D. Accepted, *Analytical Chemistry.*

The Status of and Perspectives on Microwave and Glow Discharges for Spectrochemical Analysis. Winefordner, J. D.; Wagner II, E. P.; Smith, B. W. in press, *Journal of Analytical Atomic Spectroscopy,* **1996**.

Determination of Silicate by Hollow Cathode Glow Discharge - Atomic Emission Spectroscopy with Hydride Generation Technique. Fujiwara, K; Wagner II, E. P.; Smith, B. W.; Winefordner, J. D. in press, *Analytical Letters,* **1996**.

Construction and Evaluation of a Visible Spectrometer Using Digital Micromirror Spatial Light Modulation. Wagner II, E. P.; Smith, B. W.; Madden, S.; Winefordner, J. D.; Mignardi, M. *Applied Spectroscopy,* **1995**, 49, 1715.

REFERENCES

1. Schulz, W. *Chem. & Eng. News.* **1995**, 73, 6.
2. Breslow, R. C. *Chem. & Eng. News.* **1995**, 73, 29.
3. Jacobs, M. *Chem. & Eng. News.* **1994**, 72, 4.
4. Kaiser, J. *Science.* **1995**, 270, 133.
5. Florence, J. M. *Opt. Lett.* **1989**, 14, 341.
6. Collins, D. R.; Sampsell, J. B.; Hornbeck, L. J.; Florence, J. M.; Penz, P. A.; Gately, M. T. *Appl. Opt.* **1989**, 28, 4900.
7. Cohn, R. W.; Sampsell, J. B. *Appl. Opt.* **1988**, 27, 937.
8. Mannion, P. *Electronic Prod.* **1994**, 36, 21.
9. Hornbeck, L. J. *Proc. of SPIE.* **1989**, 1150.
10. Laporta, P.; Zaraga, F. *Appl. Optics.* **1981**, 20, 2946.
11. Cobine, J. D. *Gaseous Conductors.* Dover, New York, **1958**.
12. Fang, D.; Marcus, R. K. *Fundamental Plasma Processes, in Glow Discharge Spectroscopies.* Plenum Press, New York, **1966**.
13. Liewellyn-Jones, F. *The Glow Discharge.* Wiley, New York, **1993**.
14. Penning, F. M. *Electrical Discharges in Gases.* Katwijk and Zee, Netherlands, **1957**.
15. Harrison, W. W.; Bentz, B. L. *Prog. Anal. Spectrosc.* **1988**, 11, 53.
16. Boumans, J. M. *Anal. Chem.* **1972**, 44, 1219.

17. Stuart, R. V.; Wehner, G. K. *J. Appl. Phys.* **1962**, 33, 2345.

18. Chapman, B. *Glow Discharge Processes.* Wiley & Sons, Inc., New York, **1980**.

19. Caroli, S. *Improved Hollow Cathode Lamps for Atomic Spectroscopy.* Wiley & Sons, Inc., New York, **1985**.

20. Siegmund, P. *Phys. Rev.* **1969**, 187, 768.

21. Hess, K. R.; Marcus, K. R. *Spectrosc.* **1987**, 2, 24.

22. Dashin, S. A.; Karpov, Y. A.; Kushlyansky, O. A.; Mayorov, I. A. *Spectrochim. Acta.* **1991**, 46B, 467.

23. Winefordner, J.D.; Petrucci, G.A.; Stevenson, C.L.; Smith B.W. *J. Anal. At. Spectrom.* **1994**, 9, 131.

24. Winefordner, J.D.; Stevenson, C. *Spectrochim. Acta.* **1993**, 48B, 757.

25. Alkemade, C. *Appl. Spectrosc.* **1981**, 35, 1.

26. Stevenson, C.L.; Winefordner, J.D. *Chemtracts--Anal. Phys. Inorg. Chem.* **1990**, 2, 217.

27. Fang, D.; Marcus, R.K. *Spectrochim. Acta,* **1990**, 45B, 1053.

28. Falk, H.; Hoffman, E.; L dke, Ch. *Spectrochim. Acta.* **1984**, 39B, 283.

29. Marcus, R.K. *J. Anal. At. Spectrom.* **1993**, **8**, 935.

30. Hang, W.; Walden, W.O.; Harrison, W.W. *Anal. Chem.* **1996**, 68, 1148.

31. Walden, W.O.; Hang, W.; Smith, B.W.; Winefordner, J.D.; Harrison, W.W. *Fres. J. Anal. Chem.* in press.

32. Davis, C.L.; Smith, B.W.; Bolshov, M.A.; Winefordner, J.D. *Appl. Spectrosc.* **1995**, 49, 907.

33. Womack, J.B.; Gessler, E.M.; Winefordner, J.D. *Spectrochim. Acta.* **1991**, 46B, 301.

34. Deavor, J.P.; Becerra, E.; Smith, B.W.; Winefordner, J.D. *Can. J. Appl. Spectrosc.* **1993**, 33, 7.

35. Davis, C.L.; Smith, B.W.; Winefordner, J.D. *Microchem. J.* in press.

36. Grazhulene, S.; Khovostrikov, V.; Sorkin, M. *Spectrochim. Acta.* **1991**, 46B, 459.

37. Dashin, S.A.; Mayorov, I.A.; Bolshov, M.A. *Spectrochim. Acta.* **1991**, 46B, 467.

38. Dashin, S.A.; Mayorov, I.A.; Bolshov, M.A. *Spectrochim. Acta.* **1993**, 48B, 531.

39. Harrison, W.W.; *J. Anal. At. Spectrom.* **1992**, 7, 75.

40. Marcus, R.K. *Glow Discharge Spectroscopies.* Plenum Press, New York, **1993**.

41. Giglio, J.; Caruso, J.A. *Appl. Spectrosc.* **1995**, 49, 900.

42. Heintz, M.J.; Mifflin, K.; Broekaert, J.A.C.; Hieftje, G.M. *Appl. Spectrosc* **1995**, 49, 241.

43. Chakrabarti, C.L.; Headrick, K.L.; Hutton, J.C.; Bicheng, Z.; Bertels, P.C.; Back, M.H. *Anal. Chem.* **1990**, 62, 574.

44. Mixon, P.D.; Griffin, S.T.; Williams, T.C. Jr.; Cai, X.J.; Williams, J.C. *J. Anal. At. Spectrom.* **1994**, 9, 697.

45. Marcus, R.K. *J. Anal. At. Spectrom.* **1994**, 9, 1029.

46. Hang, W.; Yang, P.; Wang, W.; Yang, C.; Su, Y.; Huang, B. *Rapid Commun. Mass Spectrom.* **1994**, 8, 590.

47. Trevide, K.; Brewer, S.; McCaig, L.; Sesi, N.; Sacks, R. *Spectrochim. Acta.* **1991**, 46B, 229.

48. McCaig, L.; Sacks, R. *Appl. Spectrosc.* **1992**, 46, 18.

49. McCaig, L.; Sesi, N.; Sacks, R. *Appl. Spectrosc.* **1990**, 44, 1176.

50. McCaig, L.; Shi, E.; Woodrum, T.; Brewer, S.; Sacks, R. *Appl. Spectrosc.* **1992**, 46, 1792.

51. Heintz, M.J.; Galley, P.J.; Hieftje, G.M. *Spectrochim. Acta.* **1994**, 49B, 745.

52. Heintz, M.J.; Hieftje, G.M. *Spectrochim. Acta.* **1995**, 50B, 1109.

53. Heintz, M.J.; Hieftje, G.M. *Spectrochim. Acta.* **1995**, 50B, 1125.

54. Raghani, A.R.; Smith, B.W.; Winefordner, J.D. *Spectrochim. Acta B.* in press.

55. Weiss, Z. *J. Anal. At. Spectrom.* **1994**, 9, 351.

56. Weiss, Z. *J. Anal. At. Spectrom.* **1995**, 10, 891.

57. Cserfalvi, T.; Mezei, P. *J. Anal. At. Spectrom.* **1994**, 9, 345.

58. Saprykin, Y.A.; Colovko, B.M.; and Pazderskiy, Y.A. *Spectrochim. Acta.* **1995**, 50B, 815.

59. Schroeder, S.; Horlick, G. *Spectrochim. Acta.* **1994**, 49B, 1759.

60. Williams, J.C.; Kung, J-Y.; Chen, Y.; Cai, X.; Griffin, S.T. *Appl. Spectrosc.* **1995**, 49, 1705.

61. Morgan, C.; Davis, C.L.; Smith, B.W.; Winefordner, J.D. *Appl. Spectrosc.* **1994**, 48, 261.

62. Barshick, C.M.; Shaw, R.P.; Young, J.P.; Ramsay, J.M. *Anal. Chem.* **1995**, 67, 3814.

63. Davis, C. D. Doctoral Dissertation, Department of Chemistry, University of Florida, Gainesville, FL. **1994**.

64. Womack, J. B. Doctoral Dissertation, Department of Chemistry, University of Florida, Gainesville, FL. **1991**.

65. Raghani, A. R. Doctoral Dissertation, Department of Chemistry, University of Florida, Gainesville, FL. **1995**.

66. Grimm, W. *Abstracts*, XII *Spektrometertagung*, Salzburg. **1978**, 139.

67. Kruger, R. A.; Bombelka, R. M.; Laqua, K. *Spectrochim. Acta.* **1980**, 35B,581

68. Thorton, J. A. *J. Vac. Sci. Technol.* **1978**, 15, 171.

69. Ferreira, N. P.; Kruger, R. A.; Human, H. G. C. *Spectrochim. Acta.* **1981**, 36B, 145.

70. McCaig, L.; Sacks, R.; Lubman, D. *Appl. Spectrosc.* **1989**, 43, 912.

71. McCaig, L.; Sesi, N.; Sacks, R. *Appl. Spectrosc.* **1990**, 44, 1176.

72. Trivedi, K.; Brewer, S.; McCaig, L.; Sesi, N.; Sacks, R. *Spectrochim. Acta.* **1991**, 46B, 229.

73. McCaig, L.; Sacks, R. *Appl. Spectrosc.* **1992,** 46, 18.

74. Dehegan, K.; Shi, Z.; Holbrook Woodrum, T.; Brewer, S.; Sacks, R. *Appl. Spectrosc.* **1994,** 48, 553.

75. Shi, Z.; Holbrook Woodrum, T.; Dehegan, K.; Brewster, S.; Sacks, R. *Appl. Spectrosc.* **1992,** 46, 749.

76. McCaig, L.; Shi, Z.; Holbrook Woodrum, T.; Brewer, S.; Sacks, R. *Appl. Spectrosc.* **1992,** 46, 1762.

77. Brewer, S.; Holbrook, T.; Shi, Z.; Trivedi, K.; Sacks, R. *Appl. Spectrosc.* **1991**, 45, 1327.

78. Mixon, P. D.; Griffin, S. T.; Williams Jr., J. C.; Cai, X. J.; Williams, J. C. *J. Anal. Atom. Spectrosc.* **1994**, 9, 697.

79. Dawson, J. B.; Ellis D. J. *Spectrochim. Acta.* **1967**, 23A, 565.

80. Klinger, J. A.; Savickas, P. J.; Harrison W. W. *J. Am. Soc. Mass Spectrom.* **1990**, 1, 138.

81. Klingler, J.A.; Barshick, C.M.; Harrison, W.W. *Anal. Chem.* **1991**, 63, 2571.

82. Walden, W. O. Doctoral Dissertation, Department of Chemistry, University of Florida, Gainesville, FL. **1995**.

83. Glick, M.; Smith, B. W.; Winefordner, J. D. *Anal. Chem*. **1990**, 62, 157.

84. Walden, W. O.; Harrison W. W.; Smith, B. W.; Winefordner, J. D. *J. Anal. Atom. Spectrosc.* **1994**, 9, 1039.

85. Slevin, P. J.; Harrison, W. W. *Appl. Spectrosc. Rev.* **1975**, 10, 201.

86. Caroli, S. *J. Anal. At. Spectrom.* **1987**, 2, 661.

87. Raghani, A. R.; Bolshov, M. A.; Smith B. W.; Winefordner, J. D. *Talanta*, in press.

88. Ryu, J. Y.; Davis, R. L.; Williams J. C.; Williams, Jr., J. C. *Appl. Spectrosc.*, **1988,** 42, 1379.

89. Chen, F.; Williams, J. C. *Anal. Chem.* **1990**, 62, 489.

90. Becerra, E. B.; Deavor, J.; Winefordner, J. D. *Spectrosc. Lett.* **1992**, 25, 1257.

91. Klemp, M.; Puig, L.; Trivedi K.; Sacks, R. *J. Chromatogr. Sci.* **1992**, 30, 136.

92. Puig L.; Sacks, R. *Appl. Spectrosc.* **1989**, 43, 801.

93. Starn, T. K.; Pereiro R.; Hieftje, G. M. *Appl. Spectrosc.* **1993**, 47, 1555.

94. Pereiro, R.; Starn, T. K.; Hieftje, G. M. *Appl. Spectrosc.* **1995**, 49, 616.

95. Broekaert, J. A. C.; Pereiro, R.; Starn T. K.; Hieftje, G. M. *Spectrochim Acta.* **1993,** 48B, 1207.

96. Fujiwara, K.; Uchida, M.; Chen, M.; Kumamoto Y.; Kumamaru, T. *Anal. Chem.* **1993**, 65, 1814.

97. Kumamaru, T.; Uchida, M.; Fujiwara, K.; Okamoto, Y.; Fujiwara, K.; *Appl. Spectrosc.* **1995**, 49, 76.

98. Harrison, W.W. *Glow Discharge Mass Spectrometry*, in *Inorganic Mass Spectrometry*, Adams F.; Gijbels R.; Van Grieken R. Wiley, New York, **1988**.

99. Hess, K.R.; Marcus R. K. *Spectroscopy*, **1987**, 2.

100. Marcus, R. K. *Glow Discharge Spectroscopies*. Plenum Press, New York, **1993**.

101. Bogaerts, A.; Gijbels R. *J. Appl. Phys.* **1996**, 79, 1279.

102. Bogaerts, A.; Gijbels R. *Anal. Chem.* (submitted).

103. Bogaerts, A.; van Straaten, M.; Gijbels R. *Spectrochim. Acta.* **1995,** 50B, 179.

104. Bogaerts, A.; van Straaten, M.; Gijbels R. *J. Appl. Phys.* **1995,** 77, 1868.

105. Bogaerts, A.; Gijbels R.; Goedheer, W. J. *J. Appl. Phys.* **1995,** 78, 2233.

106. Bogaerts, A.; Gijbels R. *Phys. Rev.* **1995,** 52, 3743.

107. Bogaerts, A.; Gijbels R. *J. Appl. Phys.* **1995,** 78, 6427.

108. Bogaerts, A.; Gijbels, R.; Goedheer, W.J. *Anal. Chem.* in press, **1996**.

109. Bogaerts, A.; Gijbels, R. Fres. *J. Anal. Chem.* in press, **1996**.

110. Stirling, A. J.; Westwood, W.D. *J. Phys. D: Appl. Phys.* **1971**, 4, 246.

111. Absalan, G.; Chakrabarti C.L.; Hutton J.C.; Back M.H.; Lazik C.; Marcus, R.K. *Anal. Atom. Spectrom.* **1994**, 9, 45.

112. Hoppstock, K.; Harrison, W.W. *Anal. Chem.* **1995**, 67, 3167.

113. van Dijck, C.; Smith, B.W.; Winefordner, J.D. *Spectrochim. Acta.* **1982**, 37B, 759.

114. de Hoog, F.J.; McNeil, J.R.; Collins, G.J.; Person, K.B. *J Appl. Phys.* **1977**, 48 3701.

115. Ferreira, N.P.; Human, H.G.C. *Spectrochim. Acta.* **1981**, 36B, 215.

116. van Veldhuizen E. M.; de Hoog, F.J. *J. Phys. D: Appl. Phys.* **1984**, 17, 953.

117. Allott, R.M.; Miller, P.D.; Jones, J.J.; Mason, R.S. *Recent Advances in Plasma Source Mass Spectrometry*. Exeter, **1995**, 102-115.

118. Allott, R. M.; Kubinyl, M.; Grofcsik, A.; Jones, W.J.; Mason, R.S. *J. Chem. Soc., Faraday Trans.* **1995**, 91, 1297.

119. Corliss, C.H.; Bozman, W.R. *Experimental Transition Probabilities for Spectral Lines of Seventy Elements*, NBS Monograph 53, Washington D.C., **1962**.

120. Schade, W.; Helbig, V. *Phys. Lett. A*. **1986**, 115, 39.

121. Omenette, N.; Winefordner, J.D. *Prog. Anal. At. Spectrosc*. **1979**, 2, 1.

122. Ljungberg, P.; Boudreau, D.; Axner, O. *Spectrochim. Acta*. **1994**, 49B, 1491.

123. Boudreau, D.; Ljungberg, P.; Axner, O. *Spectrochim. Acta*. **1996**, 51B, 413.

124. Ingle, J.D.; Crouch, S.R. *Spectrochemical Analysis*. Prentice Hall, New York, **1988**.

125. Rann, C.S. *Spectrochim. Acta.* **1968**, 23B, 245.

126. Rann, C.S. *Spectrochim. Acta.* **1968**, 23B, 827.

127. Bruce, C. F.; Hannaford, P. *Spectrochim. Acta*. **1971**, 26B, 207.

128. Oechsner, H. *Phys. Rev. B*. **1978**, 17, 1052.

129. Vriens, L. *Phys. Lett.* **1964**, 8, 260.

130. Bogaerts A.; Guenard, R.; Smith, B.W.; Winefordner J.D.; Harrison, W.W.; Gijbels, R. *Spectrochim. Acta Part B*. (submitted).

131. Riseberg, L.A.; Parks, W. F.; Schearer, L.D. *Phys. Rev. A*. **1973**, 8, 1962.

132. Bogaerts, A.; Gijbels, R. *J. Anal. Atom. Spectrom*. in press, **1996**.

133. Moore, C. E. *Atomic Energy Levels, Volume I-III*, Nat. Stand. Ref. Data Ser., Nat. Bur. Stand. (U.S.), **1971**.

134. Johansson, S.; Litzen, U. *J. Phys. B*. **1978**, 11, L703.

135. Danzmann, K.; Koch, M. *J. Phys. B*. **1981**, 14, 2989.

136. Farnsworth, P.B.; Walters, J. P. *Spectrochim. Acta.* **1982**, 37B, 773.

137. Hudson, R. S.; Skrumeda, L. L.; Whaling, W. *J. Quant. Spectrosc. Radiat. Transfer*. **1987**, 38, 1.

138. Steers, E. M. B.; Fielding, R. J. *J. Anal. Atom. Spectrom.* **1987**, 2, 239.

139. Steers, E. M. B.; Leis, F. *Spectrochim. Acta.* **1991**, 46B, 527.

140. Steers, E. M. B.; Thorne, A. P. *J. Anal. Atom. Spectrom.* **1993**, 8, 309.

141. Steers, E. M. B.; Thorne, A. P.; Weiss, Z. *12th European Sectional Conference on the Atomic and Molecular Physics of Ionized Gases, Eurphysics Conference Abstracts.* **1994**, 18E, 65.

142. Wagatsuma, K.; Hirokawa, K. *Spectrochim. Acta.* **1996**, 51B, 349.

143. Parsons, J. *Environ. Res.* **1992**, 57, 149.

144. *Preventing Lead Poisoning in Young Children-A Statement by the Centers for Disease Control;* October, **1991**, USDHHS/PHS, CDC, Atlanta, GA, USA.

145. Feldman, B. J.; D'Alessandro, A.; Osterloh, J. D.; Hata, B. H. *Clin. Chem.* **1995**, 41, 557.

146. Jagner, D; Wang, Y. D. *Electroanalysis*, **1995**, 7, 614.

147. Miller, D. T.; Paschal, D. C.; Gunter, E. W.; Stroud, P. E.; D'Angelo, J. *Analyst.* **1987**, 112, 1701.

148. Bannon, D. I.; Murashchik, C.; Zapf, C. R.; Farfel, M. R.; Chisolm, Jr., J. J. *Clin. Chem.* **1994**, 40, 1730.

149. Parsons, P. J.; Slavin, W. *Spectrochim. Acta.* **1993**, 48B, 925.

150. Jacobson, B. E.; Lockitch, G.; Quigley, G. *Clin. Chem.* **1991**, 37, 515.

151. Paschal, D. C; Caldwell, K. L.; Ting, B. G. *J. Anal. Atom. Spectrom.* **1995**, 10, 367.

152. Bowins, R. J.; McNutt, R. H. *J. Anal. Atom. Spectrom.* **1994**, 9, 1233.

153. Flegal, A. R.; Smith, D. R. *Enviro. Research*, **1992**, 58, 125.

154. Renner, R. *Enviro. Science and Tech.* **1995**, 29, 256A.

155. Neumann, S; Kriese, M. *Spectrochim. Acta.* **1974**, 29B, 127.

156. Vera, J. A.; Leong, M. B.; Omenetto, N.; Smith, B. W.; Womack, B.; Winefordner, J. D. *Spectrochim. Acta.* **1989**, 44B, 939.

157. Bolshov, M. A.; Zybin, A. V.; Smirenkina, I. I. *Spectrochim. Acta.* **1981**, 36B, 1143.

158. Cheam, V.; Lechner, J.; Sekerka, I.; Desrosiers, R.; Nriagu, J.; Lawson, G. *Anal. Chim. Acta.* **1992**, 269, 129.

159. Dougherty, J. P.; Preli, Jr., F. R.; Michel, R. G. *J. Anal. Atom. Spectrom.* **1987**, 2, 429.

160. Leong, M.; Vera, J.; Smith, B. W.; Omenetto, N; Winefordner, J. D. *Anal. Chem.* **1988**, 60, 1605.

161. Smith, B. W.; Farnesworth, P. B.; Cavalli, P.; Omenetto, N. *Spectrochim. Acta.* **1990**, 45B, 1369.

162. Omenetto, N.; Winefordner, J. D. *Prog. Analyt. Atom. Spectrsc.* **1979**, 2, 1.

163. Smith, B. W.; Womack, J. B.; Omenetto, N.; Wineforndner, J. D. *Appl. Spectrosc.* **1989**, 43, 873.

164. Alvarado, J.; Cavalli, P; Omenetto, N.; Rossi, G.; Ottaway, J. M.; Littlejohn, D. *Anal. Lett.* **1989**, 22, 2975.

BIOGRAPHICAL SKETCH

Eugene P. Wagner II was born in Elmhurst, Illinois, on January 16, 1966, and was raised in Winfield, Illinois. Both of these towns are suburbs of Chicago. He received his BS degree in industrial technology with a minor in chemistry from Illinois State University in May 1988. He worked in industry for two years in various positions and companies. He returned to ISU in 1990 to pursue a MS degree in physical chemistry under the supervision of Dr. Cheryl Stevenson. After completion of this degree in December of 1992, he worked at Harper Community College for one semester as a chemistry instructor before continuing his education. He entered the University of Florida in the fall of 1993 and joined Prof. Jim Winefordner's group to work on his doctoral degree in physical and analytical chemistry.

I certify that I have read this study and that in my opinion it conforms to acceptable standards of scholarly presentation and is fully adequate, in scope and quality, as a dissertation for the degree of Doctor of Philosophy.

James D Winefordner

James D. Winefordner, Chair
Graduate Research Professor of Chemistry

I certify that I have read this study and that in my opinion it conforms to acceptable standards of scholarly presentation and is fully adequate, in scope and quality, as a dissertation for the degree of Doctor of Philosophy.

Russell S Drago

Russell S. Drago
Graduate Research Professor of Chemistry

I certify that I have read this study and that in my opinion it conforms to acceptable standards of scholarly presentation and is fully adequate, in scope and quality, as a dissertation for the degree of Doctor of Philosophy.

Willis B. Person

Willis B. Person
Professor of Chemistry

I certify that I have read this study and that in my opinion it conforms to acceptable standards of scholarly presentation and is fully adequate, in scope and quality, as a dissertation for the degree of Doctor of Philosophy.

William Weltner

William Weltner
Professor of Chemistry

I certify that I have read this study and that in my opinion it conforms to acceptable standards of scholarly presentation and is fully adequate, in scope and quality, as a dissertation for the degree of Doctor of Philosophy.

Joseph J Delfino

Joseph J. Delfino
Professor of Environmental Engineering Sciences

This dissertation was submitted to the Graduate Faculty of the Department of Chemistry in the College of Liberal Arts and Sciences and to the Graduate School and was accepted as partial fulfillment of the requirements for the degree of Doctor of Philosophy.

August 1996

Dean, Graduate School